Scientific Excellence • Resource Protection & Conservation • Benefits for Canadians
Excellence scientifique • Protection et conservation des ressources • Bénéfices aux Canadiens

DRAFT AND MOVEMENT OF PACK ICE IN THE BEAUFORT SEA, April 1990 - March 1991

by

H. Melling and D.A. Riedel

Institute of Ocean Sciences
Department of Fisheries and Oceans
Sidney, B.C.

1993

CANADIAN TECHNICAL REPORT OF HYDROGRAPHY AND OCEAN SCIENCES NO. 151

Fisheries and Oceans Pêches et Océans

Canada

Canadian Technical Report of Hydrography and Ocean Sciences

Technical reports contain scientific and technical information that contributes to existing knowledge but which is not normally appropriate for primary literature. The subject matter is related generally to programs and interests of the Ocean Science and Surveys (OSS) sector of the Department of Fisheries and Oceans.

Technical reports may be cited as full publications. The correct citation appears above the abstract of each report. Each report is abstracted in *Aquatic Sciences and Fisheries Abstracts* and indexed in the Department's annual index to scientific and technical publications.

Technical reports are produced regionally but are numbered nationally. Requests for individual reports will be filled by the issuing establishment listed on the front cover and title page. Out of stock reports will be supplied for a fee by commercial agents.

Regional and headquarters establishments of Ocean Science and Surveys ceased publication of their various report series as of December 1981. A complete listing of these publications is published in the *Canadian Journal of Fisheries and Aquatic Sciences*, Volume 39: Index to Publications 1982. The current series, which begins with report number 1, was initiated in January 1982.

Rapport technique canadien sur l'hydrographie et les sciences océaniques

Les rapports techniques contiennent des renseignements scientifiques et techniques qui constituent une contribution aux connaissances actuelles, mais qui ne sont pas normalement appropriés pour la publication dans un journal scientifique. Le sujet est généralement lié aux programmes et intérêts du service des Sciences et levés océaniques (SLO) du ministère des Pêches et des Océans.

Les rapports techniques peuvent être cités comme des publications complètes. Le titre exact paraît au-dessus du résumé de chaque rapport. Les rapports techniques sont résumés dans la revue *Résumés des sciences aquatiques et halieutiques*, et ils sont classés dans l'index annuel des publications scientifiques et techniques du Ministère.

Les rapports techniques sont produits à l'échelon régional, mais numérotés à l'échelon national. Les demandes de rapports seront satisfaites par l'établissement auteur dont le nom figure sur la couverture et la page du titre. Les rapports épuisés seront fournis contre rétribution par des agents commerciaux.

Les établissements des Sciences et levés océaniques dans les régions et à l'administration centrale ont cessé de publier leurs diverses séries de rapports en décembre 1981. Une liste complète de ces publications figure dans le volume 39, Index des publications 1982 du *Journal canadien des sciences halieutiques et aquatiques*. La série actuelle a commencé avec la publication du rapport numéro 1 en janvier 1982.

Canadian Technical Report of Hydrography and Ocean Sciences No. 151

1993

DRAFT AND MOVEMENT OF PACK ICE IN THE BEAUFORT SEA, APRIL 1990 - MARCH 1991

by

H. Melling and D. A. Riedel

Institute of Ocean Sciences
Department of Fisheries and Oceans
Sidney. B.C.

Cat. No. Fs 97-18/151 ISSN 0711-6764

Correct Citation for this publication:
Melling, H. and D.A. Riedel. 1993. **Draft and Movement of Pack Ice in the Beaufort Sea, April 1990 - March 1991**. *Can. Tech. Rep. Hydrogr. Ocean Sci. No. 151*. 79 pp.

Table of Contents

Abstract 2

Acknowledgements 3

1. Introduction 4

2. Observational Programme 6

3. Instrumentation 11

    a. Ice Movement 11

    b. Ice Draft 11

4. Calibration 15

    a. Ice Movement 15

    b. Ice Draft 16

5. Data Processing 24

    a. Ice Movement 24

    b. Ice Draft 25

6. Observations 33

7. Statistical Summaries 40

    a. Ice Movement 40

    b. Ice Draft 40

    c. Ice Thickness 46

References 60

Appendix: Continuous Record of Sea Ice Draft 61

Abstract

Melling, H. and D.A. Riedel. 1993. **Draft and Movement of Pack Ice in the Beaufort Sea, April 1990 - March 1991**. *Can. Tech. Rep. Hydrogr. Ocean Sci. No. 151.* 79 pp.

The Ice Subsurface Characterization Project, a multi-year study of the motion and thickness of sea ice in the Beaufort Sea, was initiated in April 1990. This report presents and discusses the measurements made during the first field year of the project, between April 1990 and March 1991. Observations were made using two types of self-contained sonar moored at the seafloor. A four-beam doppler sonar was used to measure the velocity of ice movement over the mooring, while a narrow-beam ice profiling sonar was used to measure ice draft. Two sites on the Mackenzie continental shelf north of Tuktoyaktuk were instrumented. One was situated near the middle of the shelf, and the other near the shelf edge. Ice motion measurements were obtained at both sites at all times during the twelve-month deployment when sea ice was present. Measurements of ice draft were obtained only at the northern site during April and May of 1990. From this location a topographic profile across almost 350 km of sea ice was surveyed at 1 m intervals. This profile and a variety of statistical measures of the thickness, topography and motion of the ice field are presented.

Key words: arctic, sea ice, ice thickness, ice drift, sonar

Résumé

Melling, H. and D.A. Riedel. 1993. **Draft and Movement of Pack Ice in the Beaufort Sea, April 1990 - March 1991**. *Can. Tech. Rep. Hydrogr. Ocean Sci. No. 151.* 79 pp.

Le projet de caractérisation de la surface submergée de la glace, une étude à long terme du mouvement et de l'épaisseur de la glace dans la mer de Beaufort, a été inauguré en avril 1990. Ce rapport présente et discute les mesures prises durant la première année expérimentale du projet, entre avril 1990 et mars 1991. Les observations ont été faites en utilisant deux types de sonars indépendants amarrés au fond de la mer. Un sonar Doppler à quatre faisceaux a été utilisé pour mesurer la vitesse et la direction de la glace se déplaçant au-dessus de l'ancrage, alors qu'un sonar de profil de glace à faisceau mince a été utilisé pour mesurer le tirant d'eau de la glace. Les instruments ont été installés en deux sites sur la plate-forme continentale du Mackenzie, au nord de Tuktoyaktuk. Un premier site était situé près du milieu de la plate-forme, alors que le deuxième était situé près de la bordure de la plate-forme. Les mesures du mouvement de la glace ont été continuellement obtenues aux deux sites durant les 12 mois du déploiement, lorsque la glace était présente. Les mesures du tirant d'eau de la glace ont été obtenues seulement au site le plus au nord, durant avril et mai 1990. A partir de cet endroit, un profil topographique a été levé sur une distance de presque 350 km de glace de mer, à intervalle de 1 m. Ce profil ainsi qu'une variété de mesures statistiques de l'épaisseur, de la topographie, et du mouvement de la glace sont présentés.

Mot clés: arctique, glace de mer, épaisseur de la glace, dérive de la glace, sonar

Acknowledgements

This work was funded by the Federal Panel on Energy Research and Development under projects 67114 and 67160, and supported by the Department of Fisheries and Oceans Canada. We acknowledge the essential role of the Polar Continental Shelf Project of Energy Mines and Resources Canada in the provision, for our wintertime operations, of chartered aircraft, accomodations and support facilities at its Tuktoyaktuk base. Air crews of Aklak Air Ltd. and Canadian Helicopters Ltd. are thanked for their capable flight support for these activities. Appreciation is also expressed to the Canadian Coast Guard, and to Captain Gomes and the officers and crew of the **CCGS *Henry Larsen***, for their contribution to our ship-based work in September 1990. Technical expertise and competent laboratory and field services were provided by Ron Cooke, Peter Gamble, Paul Johnston and Syd Moorhouse. Paul Johnston and Todd Warnes are credited with the successful development of the ice profiling sonar. Edmand Fok is thanked for his programming support to the processing of project data.

1. Introduction

In the absence of large-scale horizontal movements, sea ice grows in vast featureless sheets of uniform thickness. An equilibrium thickness is attained when the heat conducted up through the ice from the ocean is adequate to balance the energy budget at the atmospheric interface. As this budget varies seasonally, so does the equilibrium thickness. Calculations show that the annually averaged thickness of arctic sea ice, when subject only to thermodynamic forcing, is about 3 m (MAYKUT and UNTERSTEINER, 1971).

The constant movement of sea ice in response to winds and currents generates stresses which cause ice sheets to break apart into floes, separated by leads of open water. Under cold conditions, these leads develop a new cover of thinner ice. Where moving floes collide, ice is broken into fragments and piled into sinuous mounds called ridges. By these processes, the ice pack is quickly deformed into a rough and geometrically complex *landscape* both above and below the sea surface. In the southern Beaufort Sea in late winter, first-year sea ice typically ranges in thickness from zero to about 2 metres. However, ridges accumulate to very much greater total thickness. The deepest free-floating ridge keel recorded to date extended to almost 50 m depth (KOVACS *et al.*, 1973).

Sea ice is conveniently described by its thickness density function, $g(h)$ (THORNDIKE *et al.*, 1975). Consider a region of ice of area R large relative to that of recognizeable features in the ice pack. This area is not well defined, but might, in the Arctic Ocean, be characterized by a scale greater than one hundred kilometres. If $dA(h, h+dh)$ is the area within R covered by ice having thickness in the range $(h, h+dh)$, then:

$$g(h)\, dh = \frac{1}{R} dA(h, h+dh).$$

Note that $g(h)$ includes open water area as ice of zero thickness. In this representation, the mean ice thickness in R is given by the first moment of $g(h)$:

$$\bar{h} = \int_0^\infty h\, g(h)\, dh.$$

In general, $g(h)$ will be a function of both space and time. It is recognized that the thermodynamic processes of freezing and melting tend over time to narrow $g(h)$ to a small band of ice thicknesses about the equilibrium thickness for the region. Conversely, the dynamic processes of lead opening and ridging broaden the function by creating open water (zero ice thickness) at one end of its range and by creating thick ridged ice at the other.

Pressure ridges present the most severe commonplace ice hazard to offshore structures and shipping in the Beaufort Sea. Icebreaking ships and drilling platforms reach their design limits when encountering pressure ridges, long before they are threatened by the level ice between the ridges. Grounded ridges have been the cause of the heavy scouring of the seafloor to depths of 70-80 m in the Beaufort Sea, and therefore pose a major hazard to subsea well completions and oil pipelines. Very few data are available at the present time to characterize the population of pressure-ridge keels in the Beaufort Sea and its interannual fluctuations.

Data acquired by upward-looking sonars mounted on nuclear submarines have been used for several decades to determine the draft and ridging characteristics of sea ice in the basins of the Arctic Ocean (BOURKE and GARRETT, 1987). Over the shallow arctic continental shelves, however, the acquisition of data by submarine has not been practical. Moreover, military security regulations have allowed the release of only a small fraction of the data which have been acquired. Over the Alaskan continental shelf of the Beaufort Sea, observations using aircraft-mounted laser profilometers have revealed dramatical increases in both the frequency and height of ridges with

approach to the coast (TUCKER *et al.*, 1979).

Moored self-contained upward-looking sonars now provide the capability to acquire excellent underside topographic measurements of sea ice in shallow arctic seas. This method, based on measurements at a fixed location, relies on the natural movement of the ice pack to bring new ice into the sonar's field of view. In the southern Beaufort Sea, approximately 2000 kilometres of ice can be profiled annually in this way. Observations of this type were acquired in the Beaufort Sea with prototype instruments in the late 1970's and early 1980's (HUDSON, 1990; PILKINGTON and WRIGHT, 1991). In this report, observations made in the same area with second-generation instruments are reported.

2. Observational Programme

This project is named the Ice Subsurface Characterization Project, and the work of the 1990-91 field year is identified by the acronym ISC90.

Between April 1990 and March 1991 (the 1990-91 field year), moorings bearing instruments to measure ice draft and movement were maintained at two sites in the Kugmallit Valley of the Beaufort Sea, north of Tuktoyaktuk. The geography of the area, and the mooring sites, are shown in Figure 1. Moorings were deployed from the ice surface using aircraft logistics in April 1990, were recovered, serviced and re-deployed from the **CCGS *Henry Larsen*** in September 1990, and recovered again, this time through the ice in April 1991. Wintertime aircraft operations were based at the Tuktoyaktuk base camp of the Polar Continental Shelf Project of Energy, Mines and Resources, Canada.

The plan required the positioning at each site of an Ice Profiling Sonar (IPS), for the measurement of variations in ice draft, and an Acoustic Doppler Current Profiler (ADCP), for the measurement of ice motion. In April 1990, only one of the ice profilers (IPS2) was serviceable, and this was deployed at the northern site, ISC90-2A. At the southern site, only ice motion was measured over the first deployment. In September 1990, both an ADCP and an IPS were deployed at each site. Unfortunately, during the period from September 1990 to March 1991, no ice profile data were recorded. The ice profiler at ISC90-1B (IPS1) developed a leak and became non-functional shortly after it turned on in mid-October, while that at ISC90-2B failed to turn on because of a flaw in the instrument firmware.

Tables 1 and 2 summarize the details of the two deployments. Positions were determined using a Trimble Transpack GPS receiver, and are reported in the NAD83 datum. Soundings were estimated from the National Resource Series Chart No 26602. Note that the period of data recovery from functioning instruments is shorter than the deployment period because ice was not present at the mooring site at all times.

It is noted that the ADCP's were configured to measure range to the ice, thereby providing a time averaged and rather imprecise (uncertainty $\approx$ 1 m) version of the IPS draft record. They also measured ocean current and acoustic scattering cross-section at 4 m increments between 4 m above the transducer head and about 10 m below the ice. These complementary ADCP-derived observations are not discussed in this report.

The design of the ADCP mooring is depicted in Figure 2. It is a short taut-line configuration, with buoyancy sufficient to maintain a zenithal orientation within $\pm 1.5°$ in currents up to 30 cm/s. A short vane was attached to the ADCP mooring frame to reduce azimuthal oscillations of the instrument. Large azimuthal oscillations complicate the correction of the time-averaged ADCP headings for compass non-linearity. In this first year of the ISC project, three different IPS moorings were used. The mooring used for the successful deployment of IPS2 at ISC90-2A was built around a rigid, bottom-penetrating lance which held IPS2 in a fixed orientation regardless of current drag forces. The IPS1 mooring used for both deployments was similar, with the difference that ISP1 was suspended in a gimballed mount. The mooring for the second deployment of IPS2 at ISC90-2B is illustrated in Figure 3. This is the design of IPS mooring which has been adopted for subsequent use in the ISC research programme.

Additional environmental observations are required for the calibration and analysis of the subsea sonar data. Sound speed, which is used to convert measured echo times to ranges, is calculated from water-column profiles of temperature and salinity. Profiles were measured by CTD at locations shown in Figure 1 in March and in September of 1990. The CTD profiles also were used

to convert hydrostatic pressure measured at the IPS to depth, via a calculated profile of density.

Sea-level atmospheric pressure observations are required to correct the total pressure measured by the IPS for variations in atmospheric pressure. Routine sea-level pressure observations made at Tuktoyaktuk were acquired from the Arctic Weather Centre of Environment Canada.

Two Argos PTT's were deployed in March 1990 at locations on the sea ice to the east of the mooring sites shown in Figure 1. The tracks followed by these buoys during the time that pack ice overlay the mooring sites are also shown in the figure. The buoys, manufactured by Hermes Electronics Ltd. of Dartmouth, N.S., used the HT101A transmitter and were tracked by Service Argos. Approximately 18 positions were obtained per day, with a typical error of 350 m.

Table 1: Moorings for Ice Subsurface Characterization: First Deployment 1990

Site	ISC90-1A		ISC90-2A	
Sounding	56 m		76 m	
Mooring Separation	-		240 m	
Instrument Type	ADCP	-	ADCP	IPS2
Serial No	179	-	318	1
Acoustic Frequency	614.4 Khz	-	307.2 kHz	200 kHz
Latitude	70° 18.30' N	-	70° 48.66' N	70° 48.62' N
Longitude	133° 36.62' W	-	133° 43.25' W	133° 43.41' W
Transducer Depth	50 m	-	70 m	74 m
Sample Interval	31' 33.58"	-	30' 25.08"	15 s
Deployment (GMT)	22:23 30 Mar 1990	-	21:05 4 Apr 1990	23:16 4 Apr 1990
Recovery (GMT)	02:22 30 Aug 1990	-	14:44 30 Aug 1990	15:06 30 Aug 1990
Start Time (GMT)	08:55 31 Mar 1990	-	05:55 5 Apr 1990	23:16 4 Apr 1990
End Time (GMT)	18:51 21 May 1990	-	16:30 31 May 1990	16:41 31 May 1990
Duration	51.4 days	-	56.4 days	56.7 days

Table 2: Moorings for Ice Subsurface Characterization: Second Deployment 1990

Site	ISC90-1B		ISC90-2B	
Sounding	56 m		82 m	
Mooring Separation	ADCP 340 m along 21°		ADCP 260 m along 78°	
Instrument Type	ADCP	IPS1	ADCP	IPS2
Serial No	179	1	318	1
Acoustic Frequency	614.4 kHz	200 kHz	307.2 kHz	200 kHz
Latitude	70° 20.83' N	70° 20.66' N	70° 58.12' N	70° 58.09' N
Longitude	133° 43.96' W	133° 44.16'W	133° 41.09' W	133° 41.50' W
Transducer Depth	50 m	54 m	76 m	76 m
Sample Interval	30 min	15 s	30 min	15 s
Deployment (GMT)	15:23 8 Sep 1990	15:13 8 Sep 1990	22:38 7 Sep 1990	22:23 7 Sep 1990
Recovery (GMT)	21:30 12 Mar 1991	19:14 12 Mar 1991	22:40 13 Mar 1991	23:48 13 Mar 1991
Start Time (GMT)	11:00 21 Oct 1990	-	00:30 9 Sep 1990	-
End Time (GMT)	21:27 12 Mar 1991	-	21:54 13 Mar 1990	-
Duration	142.4 days	No data	185.9 days	No data

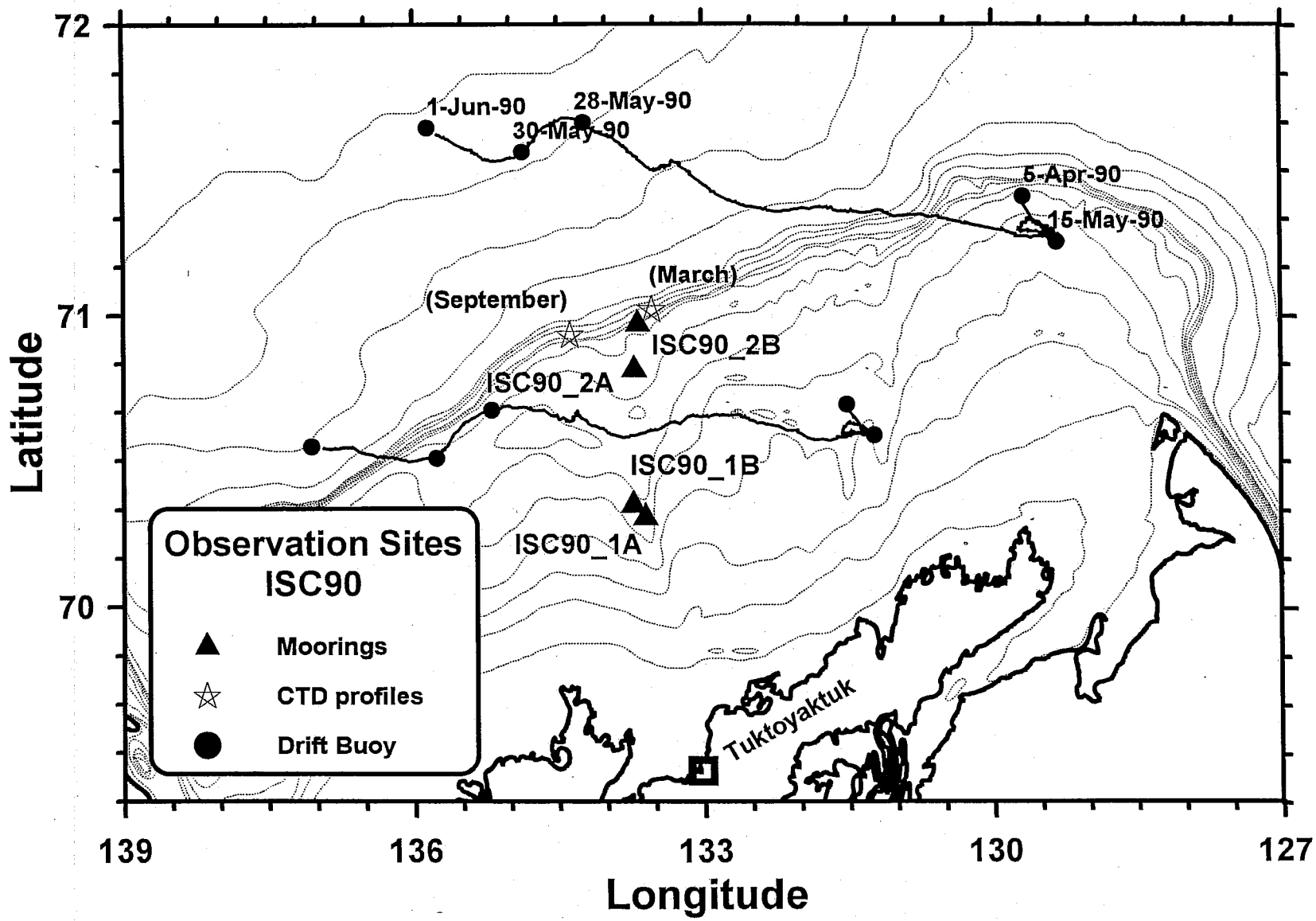

Figure 1: *Map of the Beaufort Sea showing the locations of sonar moorings in 1990-91. Locations of CTD profiles, and drift tracks of satellite-tracked buoys are also shown. Isobaths are at 10 m intervals over the continental shelf.*

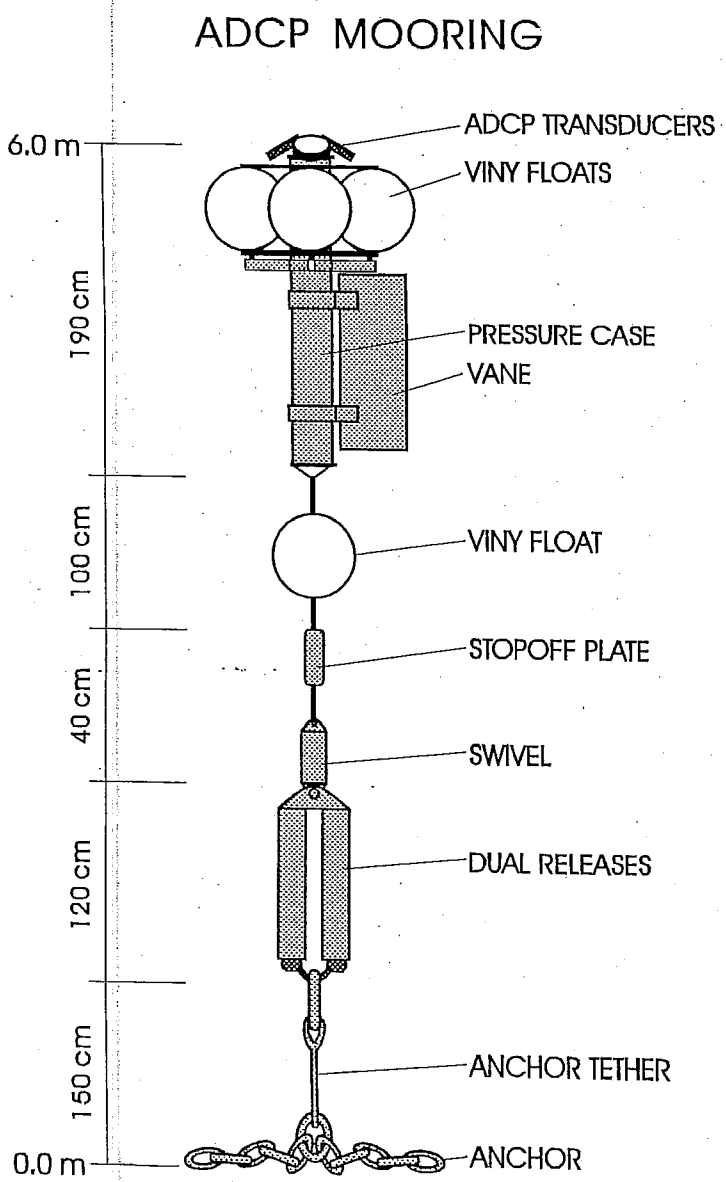

Figure 2: Mooring design for the ADCP deployed at both sites.

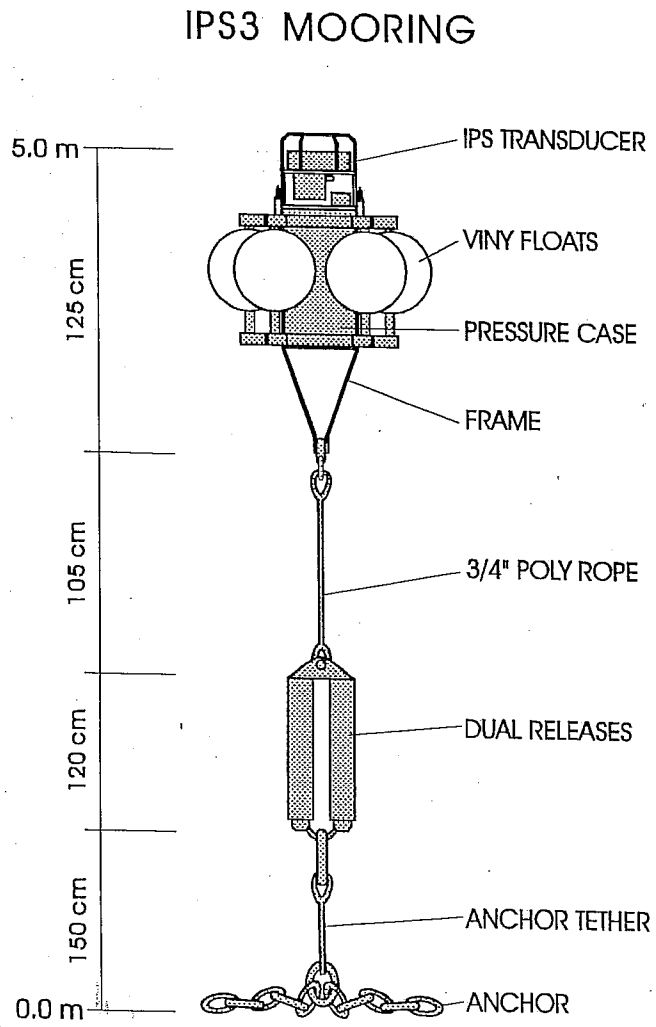

Figure 3: Mooring design for the IPS deployed at ISC90_2B.

3. Instrumentation

a. Ice Movement

A time series of ice motion at each site is both a variable of interest in this project, and the means by which the time series of ice draft observed by the IPS is mapped to a spatial coordinate. Temporal integration of the ice velocity generates a curve of ice displacement which represents the IPS survey track across the bottom of the ice field.

The instruments used in this project to measure ice motion were ADCP's manufactured by RD Instruments of San Diego, California. The ADCP is a complex, microprocessor-controlled echo sounder which determines the motion of an underwater acoustic target by measuring the doppler shift of the echo returned from it. The instrument has four separate beams inclined at 30° to the vertical orientation of the instrument and separated in azimuth by 90°. Determination of radial velocities along each beam by application of the doppler principle allows calculation of the three velocity components of the target at a particular range, under the assumption that the target velocity is uniform over the spread of the beams. The use of four beams provides an extra degree of freedom which allows assessment of the validity of the basic assumption. In the water column, sound is backscattered to the instrument strongly from planktonic organisms within the directional beam, and weakly from turbulent microstructure.

The ice-water interface presents a very strong target to the sonar, but in general, because of instrument tilt and irregularity in the ice surface, this interface is not at the same range in each of the sonar beams. Therefore, the ADCP has a separate mode of operation and tracking algorithm to determine the motion of ice (the more common application of this algorithm is for tracking the seafloor from a ship, where the instrument is pointing downward). Firmware within the instrument scans the received echoes in each beam and identifies the strong echo from the ice-water interface. It then measures the doppler shift of this echo, regardless of its range, and computes the velocity of the scattering interface by combining the doppler information from appropriate range in each of the four sonar beams.

Because of the pulsed character of the sonar operation, the returned echo has a wide bandwidth, which in single echoes masks the small doppler shift. Results from the processing of many separate pings are averaged to produce a velocity estimate sufficiently accurate for oceanographic applications. The nominal accuracy of doppler velocities obtained during the present deployments is ±0.7 cm/s. Parameters used in the setup of the ADCP are listed in Table 3.

b. Ice Draft

The Ice Profiling Sonar (or IPS2) is an instrument developed at Institute of Ocean Sciences to measure precise ranges to the ice-water interface (MELLING *et al.*, 1992). The unit is deployed 30-100 m beneath the surface, looking upward. It transmits an acoustic pulse of selectable duration, and then identifies the echo from the bottom of the ice. IPS2 examines the returned echoes and decides which part of the signal is returned from the bottom of the sea ice, or in the absence of ice, from the sea surface. The interval between transmission and receipt of this echo is the Travel Time. It is the main parameter measured and recorded internally in the IPS's EPROM memory. IPS2 may be programmed to record also the maximum Amplitude, and the Persistence of the selected echo.

Table 3: Setup Parameters Used for ADCP's

Deployment A	Water-Column Mode		Ice-Track Mode	
Serial Number	**179**	**318**	**179**	**318**
Ping Length	2 m	4 m	10 m	20 m
Cell Size	2 m	4 m	4 m	8 m
No of Cells	30	20	20	14
Pings per Ensemble	300	320	50	40
Ping Interval	5.42 s	5.08 s	30.48 s	40.64 s
Uncertainty	0.76 cm/s	0.74 cm/s	0.9 cm/s	1.0 cm/s

Deployment B	Water-Column Mode		Ice-Track Mode	
Serial Number	**179**	**318**	**179**	**318**
Ping Length	2 m	2 m	8 m	12 m
Cell Size	2 m	4 m	2 m	1 m
No of Cells	30	20	35	128
Pings per Ensemble	360	350	60	50
Ping Interval	4 s	4 s	24 s	28 s
Uncertainty	0.70 cm/s	0.71 cm/s	0.4 cm/s	0.5 cm/s

IPS2 contains pendulum sensors for measuring the tilt of the sonar beam from vertical on two orthogonal axes, a sensor for measuring pressure and temperature, and a real time clock. The frequency of the recording of these auxilliary variables may be controlled by the user. The tilt data allow the calculation of zenith distance from echo range. The pressure sensor allows for calculation of the actual depth of the IPS2 beneath (unseen) sea level, as the instrument's depth below sea level changes in response to storms, tides and mooring motions. Atmospheric pressure must be obtained by means of independent instrumentation at the surface. Temperature values are used in the precise calibration of pressure data.

IPS2 views a spot of approximately 1 m diameter at the surface. It relies on the motion of the sea ice to bring new ice into this target area for measurement. Thus IPS2 can record the draft profile of pack ice as it moves through the sonar's field of view. If the motion of the ice between pings is less than 1-2 m, then the ice profile will be over-sampled, and some of the measurements redundant. If, however, the ice motion between pings exceeds 1 m, then the ice profile will be under-sampled, and small-scale features of the profile may be misinterpreted as features of larger scale (aliasing). Although high drift speeds are relatively rare, the IPS2 measures a large fraction of all the ice which it surveys when ice drift is rapid. The general specifications of the instrument are summarized in Table 4.

IPS2 has five parameters which the operator may adjust to reduce uncertainties in the identification of the ice-water interface. These are Minimum Acceptable Range, Maximum Acceptable Range, Echo Start Amplitude, Echo Stop Amplitude and Minimum Persistence. The parameter values used for the ISC90-2A deployment are summarized in Table 5.

- Minimum Acceptable Range is the distance above the transducer within which IPS2 will ignore all echoes. This parameter is useful for controlling the rejection of potentially large echoes from scatterers near the instrument.
- Maximum Acceptable Range is the distance above the transducer beyond which IPS2 will ignore all echoes. IPS2 permits only a coarse selection of this parameter, with increments of

approximately 24 m.

- Echo Start Amplitude is the amplitude in percent of saturation that an echo must exceed before IPS2 will start the Minimum Persistence check.
- Echo Stop Amplitude is the amplitude in percent of saturation below which an echo must drop, after that echo has exceeded the Echo Start Amplitude, before the end of the echo is identified. This value must always be less than Echo Start Amplitude.
- Minimum Persistence is the minimum duration of the returned echo selected by Start and Stop Amplitude that IPS2 will consider as a surface echo. This parameter is useful for rejecting strong, short-lived echoes from point scatterers. To accomplish this function, the Minimum Persistence must exceed the length of the transmitted pulse.

IPS2 timing is based on a 2 MHz clock, whose frequency decreases with increasing temperature. For the ISC90-2A deployment, the clock frequency of IPS2 at the operating temperature of -1.5°C was 2,000,087.6 Hz.

Table 4: Specifications of the IPS2 Instrument

General

Measured Parameter	Range in Value	Precision
Range	1 - 350 m	1.5 cm
Amplitude	0 - 100 % Saturation	0.4 %
Persistence	0 - 49 m	1.5 cm
Tilts	± 20 °	0.16 °
Temperature	-10° to 30° C	0.05° C
Pressure	0 - 280 db	0.005 db

Echo Sounder

Power Output	30 watts (rms) into transducer equivalent	
Receiver Sensitivity	8 μV (rms) in = 2.5 Vdc out	[110 dB gain]
Receiver Bandwidth	8 kHz @ -3 dB	
Receiver Signal/Noise	50 dB	
Depth	< 140 m	[housing limitiation]
Transducer Beam Width	2° @ -3 dB	5° @ -10 dB

Sampling

Travel Time, Amplitude Persistence	2, 3, 4, 5, 6, 10, 15, 20, 30 or 60 s	
Tilt-A, Tilt-B Pressure	Multiples of the TT sample interval up to 25	
Calendar Time, Temperature Battery voltage	Powers of 2 of the memory address	[28 to 215]
Data Storage	16 megabytes	

Table 5: Setup Parameters Used for IPS2 at ISC90_2A

Ping Length	50 cm
Minimum Persistence	150 cm
Minimum Acceptable Range	25 m
Maximum Acceptable Range	95 m
Echo Start Amplitude	49.8%
Echo Stop Amplitude	5.1%
Ping Interval	15 s
Block Interval	24 pings
Paragraph Bounds	16 [4096-byte paragraphs]
Optional Parameters	Amplitude, Persistence, Pressure, Tilt, Temperature

4. Calibration

a. Ice Movement

Uncertainty in the ice velocity vector derived by the ADCP arises from the following sources:

i. sampling error in the determination of the mean doppler frequency shift.
ii. uncertainty in the oceanic sound speed used to convert doppler frequency shift to doppler velocity.
iii. uncertainty in ADCP heading, pitch and roll.

The sampling error is random and a function of the acoustic frequency and pulse length used by the ADCP, and of the signal-to-noise ratio achieved and the number of pings averaged in each estimate. For the setup used in these deployments, the sampling error was 0.7 cm/s in each velocity component. However, when an ADCP is tracking first-year ice floes, which have a very smooth lower surface, much of the transmitted pulse, incident at 30°, is reflected in a specular fashion from the ice, and the signal-to-noise ratio at the receiver is very poor. In this instance, the sampling error, estimated from the root-mean-square value of the vertical velocity component, can increase to several cm/s. Fortunately, extensive areas of very smooth ice are rare in the Beaufort Sea. This situation of poor signal-to-noise ratio is only problematic when a flat first-year floe is stationary over the sonar.

The calculated ice velocity is linearly dependent on the speed of sound at the ice-water interface. Sound speed beneath ice varies little over the course of the year, because the temperature at the ice-water interface is always close to freezing. A systematic error of no more than 1% may be present.

The conversion of velocity components from a beam-referenced coordinate system to an Earth-referenced system is based on measurements of tilt and heading by the ADCP. The accuracy of the tilt measurement is not critical, since a (large) error of 5° in tilt generates an error of only 3% in a velocity component. Errors in the compass measurement of instrument heading, however, translate directly into errors in the direction of ice drift. The ADCP compass is a magnetic flux-gate compass. Because the strength of the horizontal component of the Earth's magnetic field is only 7000 nT in the Beaufort Sea, the sensitivity of the ADCP compass to small direction changes is less than at lower latitudes, and the response time and non-linearity of response are greater.

To determine the non-linearity in response at high latitude, the ADCP compass output was measured at 11.25° increments in orientation in a non-magnetic enclosure located near the PCSP base at Tuktoyaktuk. Corrections for the observed non-linearity were entered into an EPROM look-up table within the instrument, and the ADCP rotation was repeated. The residual non-linearity in the compass of ADCP-318 (KVH-manufactured) was about ±2°, but that in the compass of ADCP-179 (EG&G-manufactured) was very much larger, ±12°. Correction of ADCP-recorded headings for residual non-linearity was made during data processing. To permit assignment of a unique value of heading correction for each ensemble, the ADCP mooring was equipped with a vane and swivel to discourage fluctuations in ADCP heading during the course of an ensemble. Following calibration, remnant errors in ice-drift direction which originate as errors in instrument heading are estimated to be random and of magnitude ±2°.

Because the ADCP measures components of ice velocity directly, uncertainty in the direction of ice drift is poor at low drift speeds. At a speed of 5 cm/s, the uncertainty in each component (±0.7 cm/s) corresponds to an uncertainty in direction of about ±8°.

In order to gauge the accuracy of the ice drift measurements by ADCP, the Eulerian measurements of ice velocity were integrated to produce a progressive vector for comparison with the Lagrangian drift trajectories of the two satellite-tracked drift buoys. This comparison is depicted in Figure 4. Bearing in mind the existence of spatial gradients in velocity within the pack ice, the correspondence between the drift paths derived from the two drift-buoys and the two ADCP's is very reasonable.

b. Ice Draft

The target value for the error in individual draft determinations by IPS2 is ±5 cm. Attainment of this target requires a careful approach to calibration. Both of the two primary parameters measured by the IPS2 are surrogates for distance. These are the total hydrostatic pressure measured at the pressure transducer (related to the depth of IPS2) and the round-trip travel time between the ice-water interface and the sonar transducer (related to the range to the ice-water interface). The sonar transducer is located 0.26 m above the pressure transducer on IPS2. Figure 5 illustrates that, during the first 40 days of the deployment at ISC90-2A, the depth of the sonar varied over a range of 65 cm because of changes in sea level generated by tide, changes in air pressure and wind.

The hydrostatic pressure of the ocean on the IPS2, $p(t)$, is the product of the gravitational acceleration, g, and the integral of *in situ* seawater density, $\rho(z,t)$, over the water column above the instrument. If the pressure calibration is accurate, then seawater density, calculated from CTD profiles, can be integrated to the pressure at IPS to determine instrument depth $D(t)$:

$$D(t) = \frac{1}{g} \int_0^{p(t)} \frac{dp}{\rho(z,t)}$$

Note that all parameters vary with time.

The round-trip travel time $T(t)$ is related to the range to the reflecting surface $R(t)$ by,

$$T(t) = 2 \int_0^{R(t)} \frac{dr}{c(D-r,\ t)}$$

Here $c(z,t)$ is the sound-speed profile as a function of depth and time. The range to a target may be determined by evaluating this integral upward from the location of the IPS to the value R which yields the observed travel time. Note that parameters vary with depth and time.

The pressure measured by IPS is the total hydrostatic pressure. To determine the oceanic component of hydrostatic pressure, it is necessary to subtract the contribution to total pressure made by the atmosphere. Continuous local measurements of atmospheric pressure on moving sea ice are not practical. Therefore, for this project, routine air pressure measurements at nearby coastal observational sites were used. Observations made at hourly intervals between 7 am and 11 pm local time at Tuktoyaktuk airport, and at 00, 06, 12, and 18 GMT at the Tuktoyaktuk DEW station were acquired from the Arctic Weather Centre of Environment Canada. The two series of observations were merged, and missing data were interpolated to produce a regular series at hourly intervals.

The air pressure measured at Tuktoyaktuk does not in general equal the air pressure measured at site ISC90-2A, 140 km to the north. In Table 6, values of air pressures measured at Cape Parry, at Sachs Harbour (200 km to the north of Cape Parry) and at Tuktoyaktuk (340 km to the west of Cape Parry) during 1991-92 are compared. Typical pressure differences between stations

Table 6: Comparison of Air Pressure Values Measured Simultaneously at Separations of Several Hundred km in the Beaufort Area

	Sachs re Parry	Tuktoyaktuk re Parry
Mean Difference (db)	0.003	0.000
Standard Deviation of Difference (db)	0.022	0.039
Range of Difference (db)	(-0.11, 0.07)	(-0.12, 0.16)

separated by less than 200 km are estimated from this table to be in the range 0.01-0.02 db, equivalent to 1-2 cm in sea level. On average the air pressure differences anticipated between Tuktoyaktuk and Site ISC90-2A are not important in the context of this work.

For the deployment of IPS2 at ISC90-2A, the required absolute accuracy of ± 0.01 db for the pressure sensor was not attained in the laboratory calibration. The zero correction to pressure measurements was determined by the following procedure:

i. echoes from an ice-free water surface, at times close to that of CTD-profile measurement, were identified in the range record.
ii. the range to the air-water interface at these times was calculated using CTD profile data and the integral equation for ***T(t)*** above. This is the depth of the vertically pointing sonar transducer.
iii. the oceanic hydrostatic pressure at the pressure transducer was calculated by integrating the CTD-derived *in situ* density from the surface to a depth equal to that derived in (ii) plus 0.26 m.
iv. the zero correction to pressure equals this calculated pressure *minus* the total pressure measured at these times corrected for the effect of atmospheric pressure.

By this method, the actual depth and the actual pressure at the IPS at one or more specific times during the deployment were determined.

Unfortunately, as the density and sound speed profiles within the water column above the instrument evolve, particularly with seasonal changes in the oceanography, the relationships between pressure and depth, and between echo time and target range change. Because frequent CTD profiling at the mooring site to monitor these changes is not practical, a pragmatic approach is required.

First, it is informative to examine the nature and magnitude of seasonal changes in hydrographic profiles. Data from the CTD drops in March and September 1990, at the locations mapped in Figure 1, are illustrated in the plots of Figure 6. In general waters below 40 m depth change little with season, while those above this depth become warmer and less saline in summer. As a result the average density decreases in summer, and the average sound speed increases. The change in sound speed is almost entirely a result of the change in temperature.

For an instrument at the depth of IPS2 (72 m), the apparent change in depth caused by the decrease in near-surface density between winter and summer (Figure 7, left) is small (≈0.03 m). Thus, after an offset to convert pressure in decibars to the numeric value of depth in metres has been applied, measured pressure is an acceptable indicator of instrument depth in this area throughout the year.

The apparent change in distance to the surface associated with the increase in near-surface sound speed is more dramatic (Figure 7, right). The change of 0.15-0.20 m cannot be ignored. The only feasible method to correct echo ranges for changes in sound speed is to use corrections derived from the apparent draft of open-water areas[1] which pass through the sonar beam. This

[1]The identification of areas of open water in IPS records will discussed below.

apparent draft is calculated from the target range, derived using the reference sound speed profile, and from the sonar depth, derived from pressure. A correction continuous in time is obtained by fitting a line to the available open-water corrections (see Figure 8). This time-dependent function may be used to correct ranges to the ocean surface. The fitting error of this curve (± 2 cm) is a measure of the observational uncertainty in the draft of level ice surfaces.

The speed of sound is not uniform with depth. Therefore, the value of the range correction depends on the range to the target. Since no targets of known draft are available below the surface, the surface range correction has been used at all ranges. Thus the best accuracy in range is obtained for the critical, thin-ice targets near the surface. From inspection of Figure 7, it can be seen that if all ranges are adjusted by the offset which corrects ranges to the surface, then the sound-speed-related error in the draft of thicker ice will increase to a value of approximately 0.10 m at 25 m draft.

Under rough ice, as a result of the finite angular width of the sonar beam, the first contact of the transmitted sound pulse with the ice may not be on the axis of the sonar beam. The local draft of the ice will thus be overestimated. The magnitude of the overestimate depends not only on the beam pattern of the sonar, but also on its gain, on the sensitivity of its threshold detector, and on the geometry, reflection coefficient and range of the ice, A definitive discussion of this draft error is not feasible. However, the narrow beam pattern and high system gain of IPS2 have reduced the error to a practical minimum.

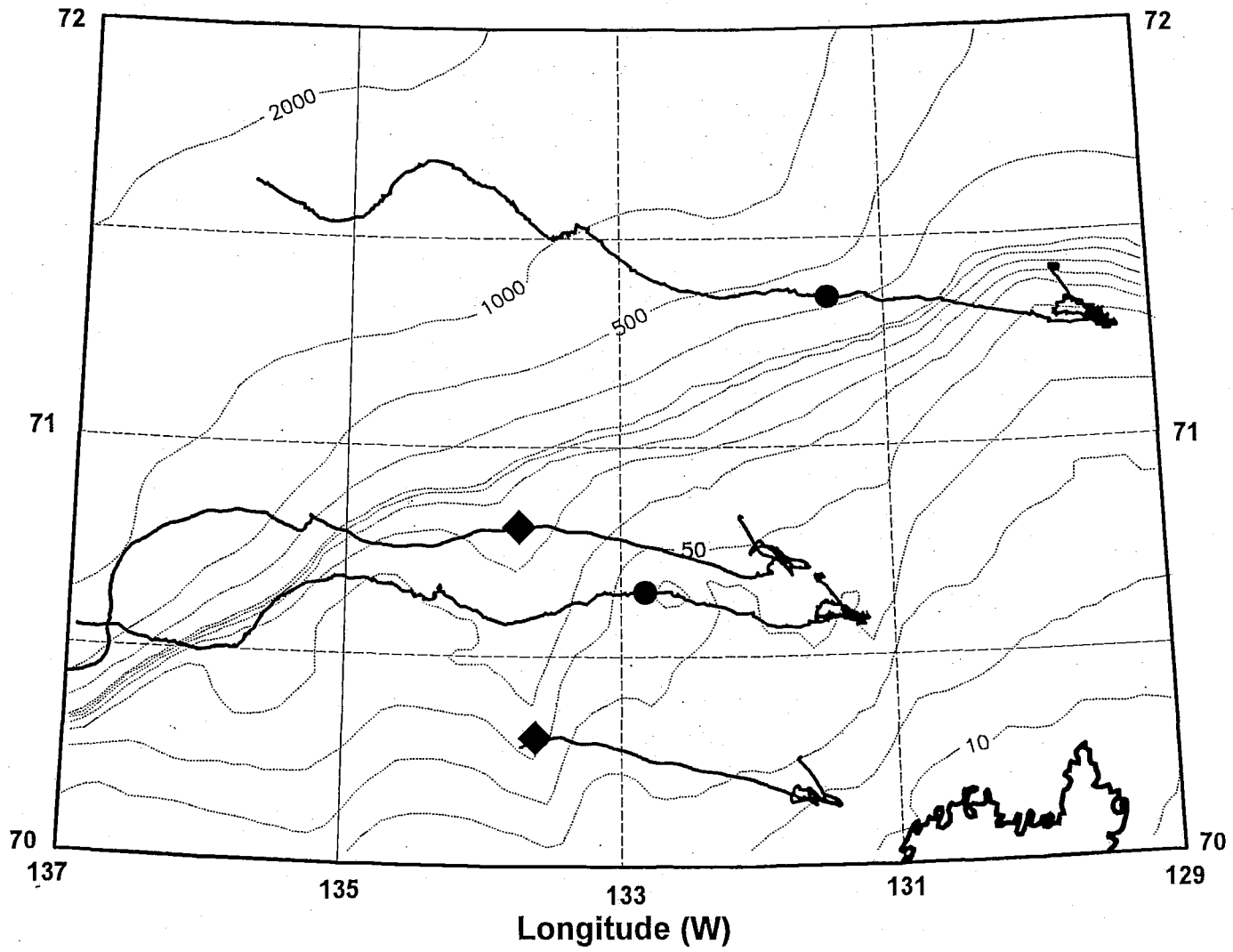

Figure 4: *Comparison of Lagrangian drift tracks of satellite-tracked buoys and Eulerian progressive vectors from ice-velocity measurements made by ADCP. Buoy tracks are shown only for the period when pack ice overlay the ADCP's. Tracks are positioned at the locations of the ADCP's (◆) and buoys (●) at 1200 GMT on 21 May 1990.*

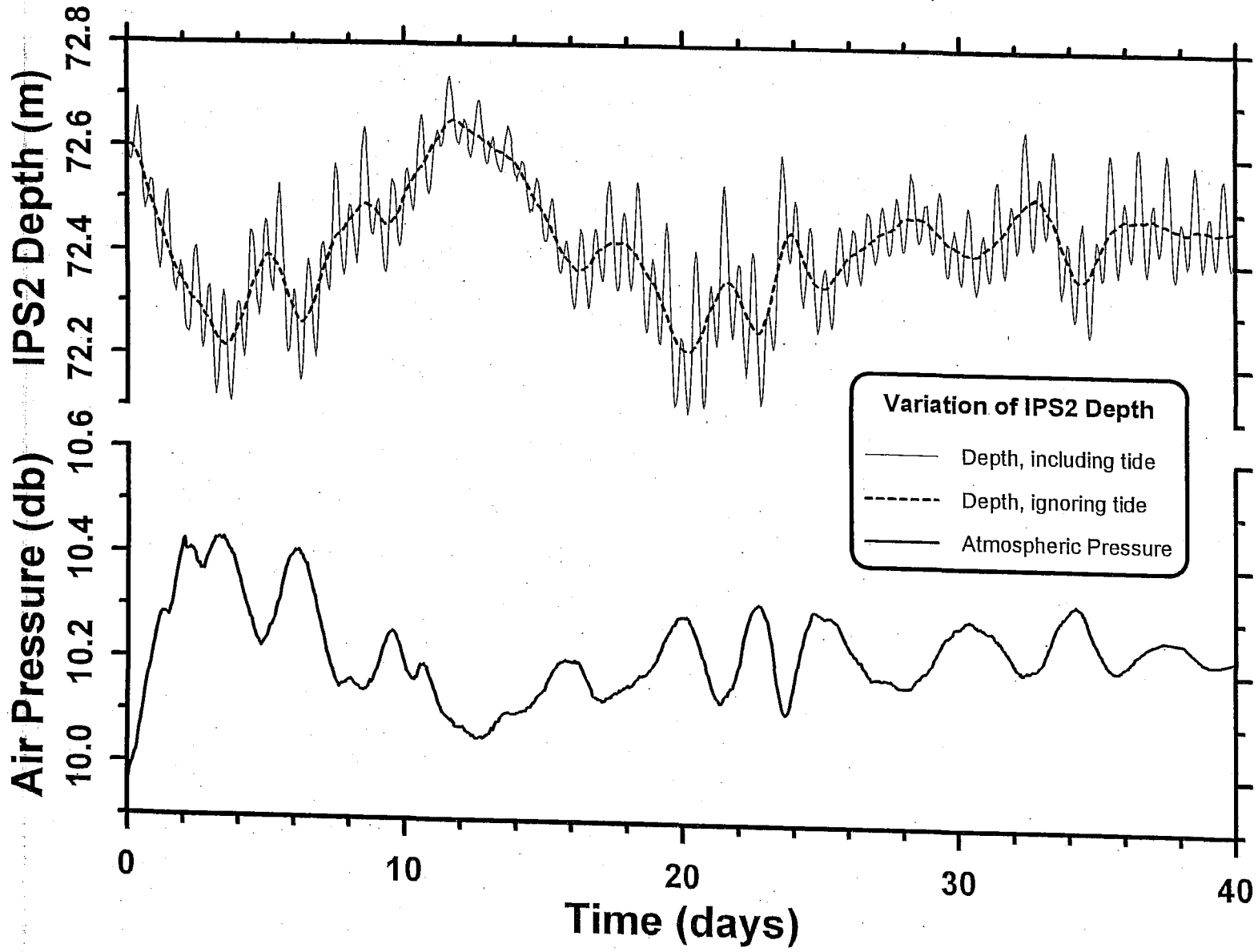

Figure 5: Changes in the depth of IPS2 over a 40-day period, showing changes in response to tidal and meteorological forcing

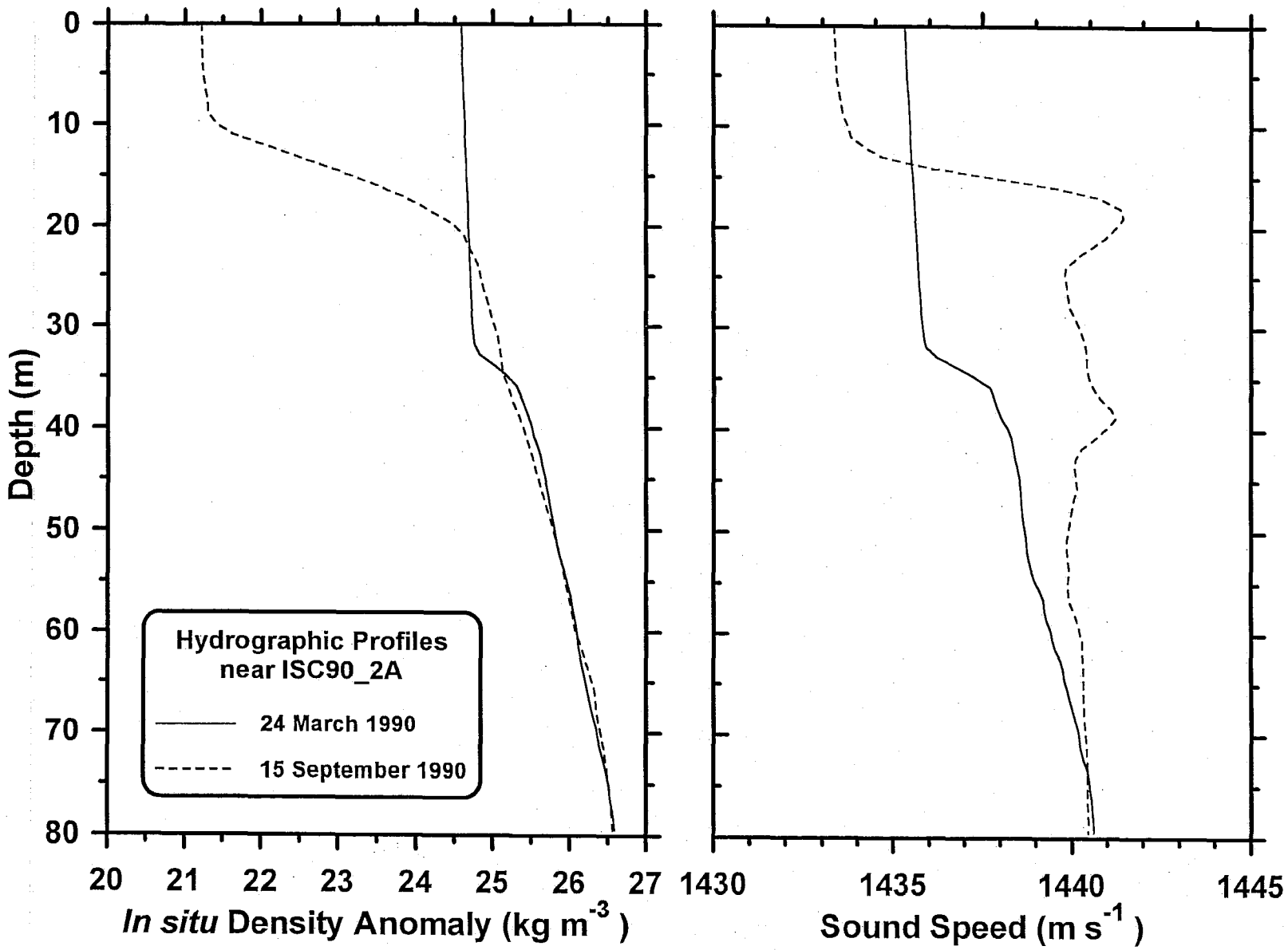

Figure 6: Hydrographic profiles at locations near ISC90_2A illustrate oceanic conditions in winter and summer.

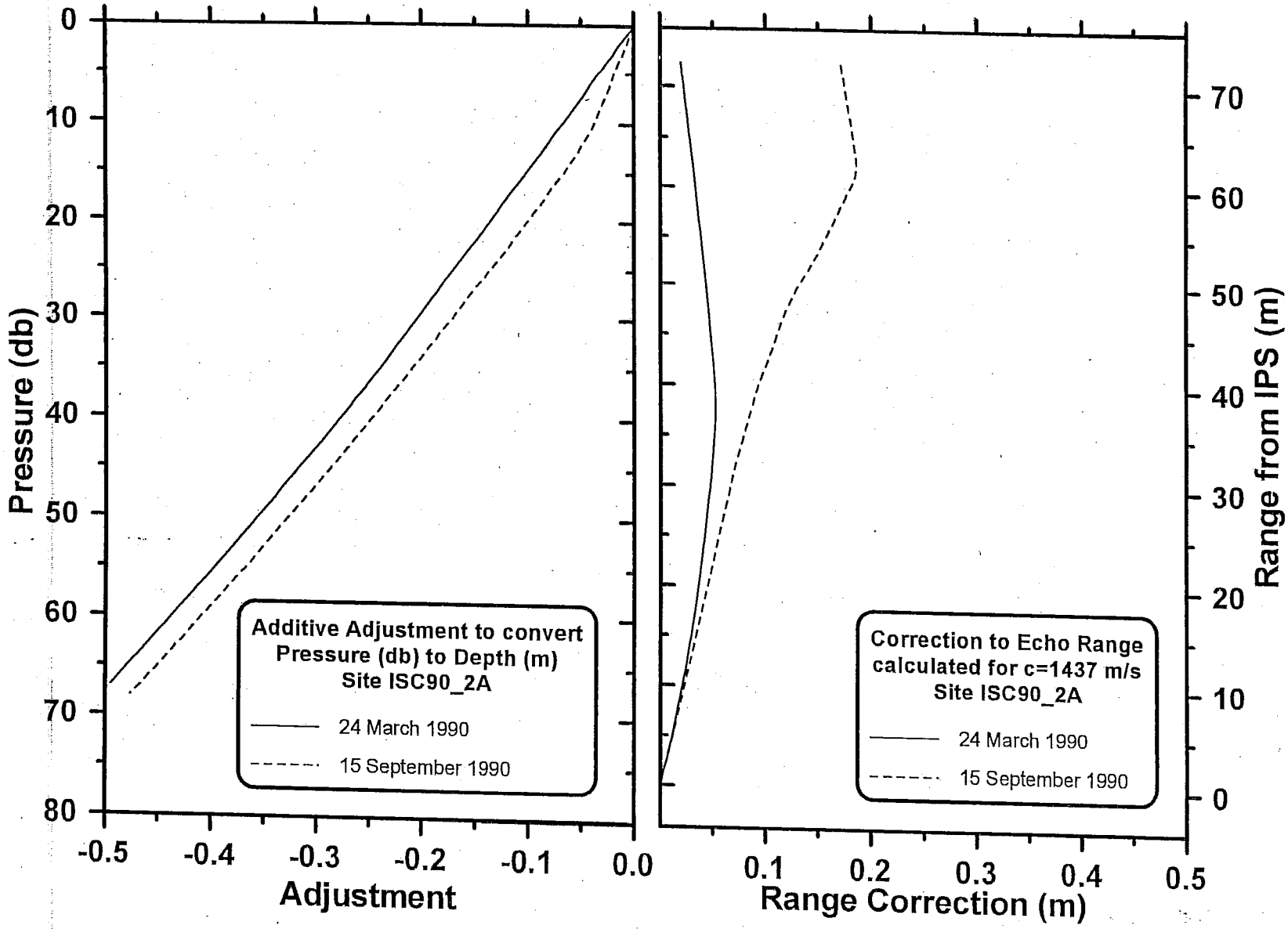

Figure 7: The numerical difference between depth in metres and pressure in dbar (left), and the correction to ranges based on a sound speed of 1437 m s^{-1} (right). The curves are based on hydrographic data in March and in September.

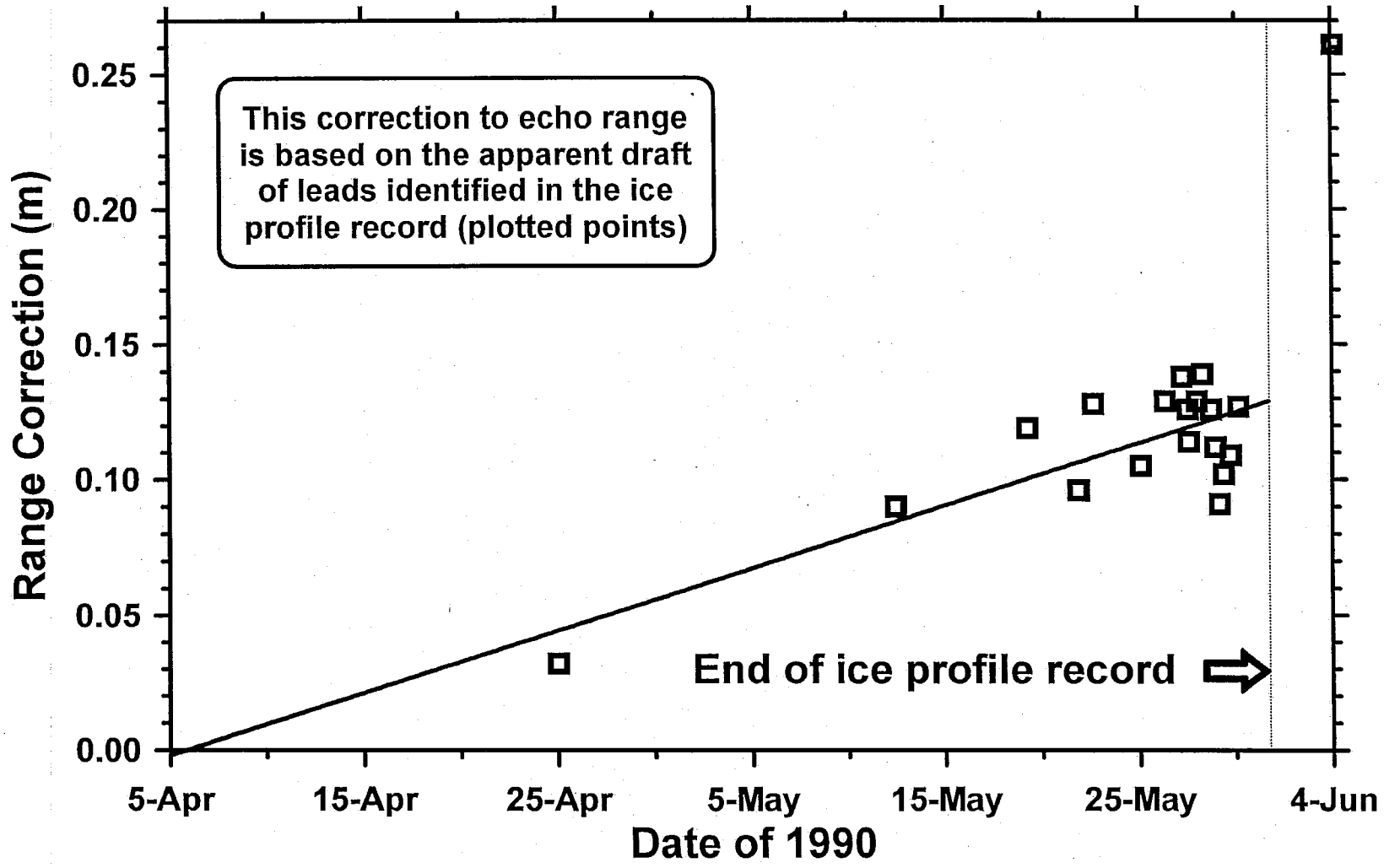

Figure 8: *Corrections to ice draft which compensate for variations in oceanic sound speed over time. Corrections are computed from sonar ranges to open-water areas within the ice pack. The straight line is the empirical fit used in the calibration of IPS2 data.*

5. Data Processing

a. Ice Movement

i. Elimination of the Open-Water Period

Except under very calm conditions, sound is backscattered strongly from the sea surface. However, because of the high and spatially incoherent velocities associated with the surface wave field, the doppler velocities derived from the surface echo are large and rapidly fluctuating. The error velocity, which is the difference between two independent estimates of the vertical component of velocity, is also large. Thus, open-water conditions are easily identified in the doppler record (BELLIVEAU *et al.* 1990). During the summer and early autumn of 1990, the mooring sites were in open water. Data acquired during this period were deleted from the ice velocity record.

An example of the change in the character of the doppler signal during a transition from ice-covered to ice-free conditions at the ADCP site is presented in Figure 9.

ii. Editing for Leads

Shorter intervals of open-water over the ADCP, caused by leads in the ice cover, were also easily detected in the ice velocity record. For small leads, remaining over the sonar for no more than a few hours, the erroneous doppler velocities over the interval were replaced by values interpolated linearly between valid velocities of the ice floes on either side of the lead. Occasionally, open-water conditions prevailed over the moorings for many hours. In such instances, linear interpolation of velocity across the lead was inappropriate. Instead, ocean current determined by the ADCP close to the sea surface (about 8-10 m depth), over the same interval, was patched into the ice velocity record.

iii. Editing for Stationary Smooth Ice

As mentioned earlier, backscatter into the inclined ADCP beams from smooth ice is often very weak. As a result of poor signal-to-noise ratio, the echo bandwidth and the uncertainty in ice velocity are large for such a target. This is a significant problem if the ice is not moving. First, the errors in ice velocity dominate the small ice velocity. Second, with little or no movement of the ice cover, the same (poor) target stays over the sonar for prolonged periods.

Such periods in the ice velocity records were identified by the large values of error velocity, despite modest values of ice velocity (see Figure 10). For ADCP-318, the identifications were confirmed by the very steady ice draft detected at the adjacent IPS2 mooring. Editing of doppler velocity was accomplished in these instances in the following manner. Positions of the Argos buoys over these periods were extracted from the buoy record, and an average velocity (generally very small) was computed from a least-squares linear fit to the positions versus time. This average velocity was used in the ADCP ice velocity record to replace each noisy value in the interval.

iv. De-Spiking

Plotted velocity components were examined subjectively, and isolated objectionable values were replaced by linear interpolation between neighbouring points.

v. Calibration

Ice velocities were corrected for the sound speed appropriate to surface waters during the deployment (1437 m/s). Drift directions were corrected for non-linearity in the compass response

measured at high latitude during tests at the Tuktoyaktuk base camp.

vi. Integration to Displacement

For use in conjunction with the ice-profile data, the components of ice velocity were transformed into the UTM (Universal Transverse Mercator) coordinate system and integrated to displacement.

$$x(t_{N+1}) = -\tau \times \sum_{i=1}^{N} u(t_i)$$

$$y(t_{N+1}) = -\tau \times \sum_{i=1}^{N} v(t_i)$$

$$s(t_{N+1}) = \tau \times \sum_{i=1}^{N} \sqrt{u^2(t_i) + v^2(t_i)}$$

Here $(u(t),v(t))$ is the velocity vector $(x(t),y(t))$ is the displacement vector, τ is the ensemble interval, and $s(t)$ is the curvilinear coordinate along the path. Note that in the ADCP file, the time associated with each record is the time at which each velocity-averaging period is initiated. The time reference is the start time of the record and position reference (0,0) is the location of the mooring. The minus signs in the equations for (x,y) reverse the displacement vector, so that it represents the locus of points in the ice pack at $t=0$ which will drift over the mooring during the course of deployment. Underlying this interpretation is the assumption that the ice pack moves as a rigid plate. In reality, this is not so, but this interpretation will likely be good over small time intervals and small distances along the path.

b. Ice Draft

i. Discrimination of Open Water from Ice

Under rare calm conditions, consecutive echoes from an ice-free water surface are consistent in range and amplitude, and of very short persistence. These properties correspond to specular reflection from a very smooth air-water interface. Ice draft deduced from the IPS record under these conditions is close to zero, and no problems are encountered.

More typically, the water surface is roughened by capillary and/or gravity waves. These cause the air-water interface to vary in range. They also inject to depths of several metres clouds of air bubbles which scatter sound very effectively. Under these conditions consecutive echoes, which fluctuate dramatically in range and amplitude, give the impression, particularly at long ping intervals, that ice up to several metres in thickness is present. An example of an IPS record during rough open-water conditions is shown in Figure 11.

Fortunately, because part of their origin is in volume backscatter, these echoes are more persistent than echoes would be from ice at a similar range. By exploiting the range and persistence properties of the IPS echo, periods of open water can be effectively discriminated from periods when the IPS is overlain by ice of thickness in the 0-2 m range.

Examples of the range and persistence properties of surface echoes under different surface conditions are illustrated in Figures 11, 12 and 13. In these figures, range has been converted to draft, and reverberation has been substituted for persistence. Reverberation (here defined as the difference between the 25th and 75th percentiles of the persistence distribution) has proven a more

sensitive discrimination parameter.

In the processing of the IPS2 data, periods of open-water were identified through automated inspection of the entire IPS record. Rough lead areas were flagged for future treatment. The prolonged summertime open-water period was deleted from the file.

ii. Echo Loss under Smooth Ice

In the setup of IPS2 for deployment (Table 5), the minimum persistence of an echo considered by the IPS2 firmware as a possible ice echo was chosen to be three times the length of the transmitted pulse. The intent in using a factor of three was to reduce the possibility of identifying a strong point scatterer in the water column as the ice-water interface. Unfortunately, because of the narrow beamwidth of the IPS, and because the underside of level first-year sea ice is very smooth, such ice sometimes returned a pulse which was shorter than the minimum persistence which had been chosen. As a result, the firmware discarded the ice echo, and recorded a zero range, zero amplitude and zero persistence to memory.

In the processing of IPS2 data, this situation was easily identified, and values for echo range were interpolated linearly from adjacent valid data by an automated procedure.

iii. De-Spiking

The IPS2 record contained occasional echoes at short range. These originated either because IPS2 erroneously identified a scatterer in the water column as the ice-water interface, or because, for reasons unknown, a value of 8192 (2^{13}) was recorded to memory. In the processing of IPS2 data, such erroneous data were identified by application of a rejection threshold for range, and values for echo range were interpolated linearly from adjacent valid data by an automated procedure.

iv. Interpolation and Merging of Pressure Data

Values of both atmospheric and total hydrostatic pressure were required at the time of each ping for the purpose of deducing ice draft from echo range. Ping data were acquired at 15-second intervals, total pressure at 4-minute intervals, and air pressure at hourly intervals. Time-series files of pressure data were expanded by linear interpolation to the IPS2 ping interval, and then merged with the ping data to form a single file.

v. Calibration

At this stage, ice-draft values were calculated from the range and pressure data in the merged file using a generalized calibration programme. The calibration involved the following steps:

1) Calculation of the depth of the IPS2 sonar transducer from the approximate total pressure measurement by:
   - subtracting air pressure to obtain approximate oceanic hydrostatic pressure,
   - adding a zero correction to calibrate hydrostatic pressure,
   - adding an empirical correction, based on observed oceanic density profiles, to convert pressure in dbars to depth of the pressure transducer in metres,
   - subtracting the vertical separation of the pressure and sonar transducers (0.26 m).
2) Calibration of the range from the sonar transducer to the lower surface of the ice by:
   - multiplying approximate ranges by the factor c/c_{ref}, where c_{ref} is the reference sound speed used in decoding the IPS2 binary data file (1437 m s^{-1}) and c is the depth-average sound speed computed from CTD data at the start of the deployment,

- adding a time-dependent correction (of value zero at the time of the CTD profile) to compensate for the variations in depth-averaged sound speed at the mooring throughout the deployment (see Figure 8).

3) Calculation of the ice draft by subtracting the calibrated range from the depth of the sonar transducer.

vi. Editing for Rough-water Leads

Rough-water leads were identified in stage (i) of the data processing. In the current step, the apparent drafts determined by IPS2 within these leads were replaced by zero values. The exact boundaries of the leads, specified by ping number, were determined through detailed subjective evaluation of the draft record.

vii. Interpolation and Merging of Displacement Data

The outcome of stage (vi) is an edited and calibrated file of ice drafts at regularly spaced time increments. For mapping of the ice profile data, it is necessary that this file be combined with the ice displacement data derived from the ADCP. To accomplish this, the displacement data were interpolated from the roughly 30-minute original sampling interval to the 15 s sampling interval of IPS2. A linear interpolation function was used.

The displacement file was then merged with the draft file. The result permits the examination of the ice draft profiles as a function of an irregularly incrementing spatial coordinate, $s(t)$.

The outcome from this stage of processing is suitable for many applications of the ice profile data.

viii. Interpolation to Regular Spatial Increments

For the preparation of statistical summaries of ice draft data, such as draft distributions, spatial spectra and spatial auto-correlation functions, it is necessary to interpolate ice draft to regular increments in the curvilinear coordinate $s(t)$.

For the ISC90 IPS2 data, a linear interpolation function, working with a minimum of 2 points within a window of 1 m minimum length, was used. Since the average ice speed over the record and the IPS2 sample interval were 7.9 cm/s and 15 s, respectively, interpolation of ice draft, time and (x,y) coordinates of the path at intervals of 1 m was a reasonable compromise between the close spacing of data where drift speed was low and the wide (3-4 m) spacing where drift speed was high.

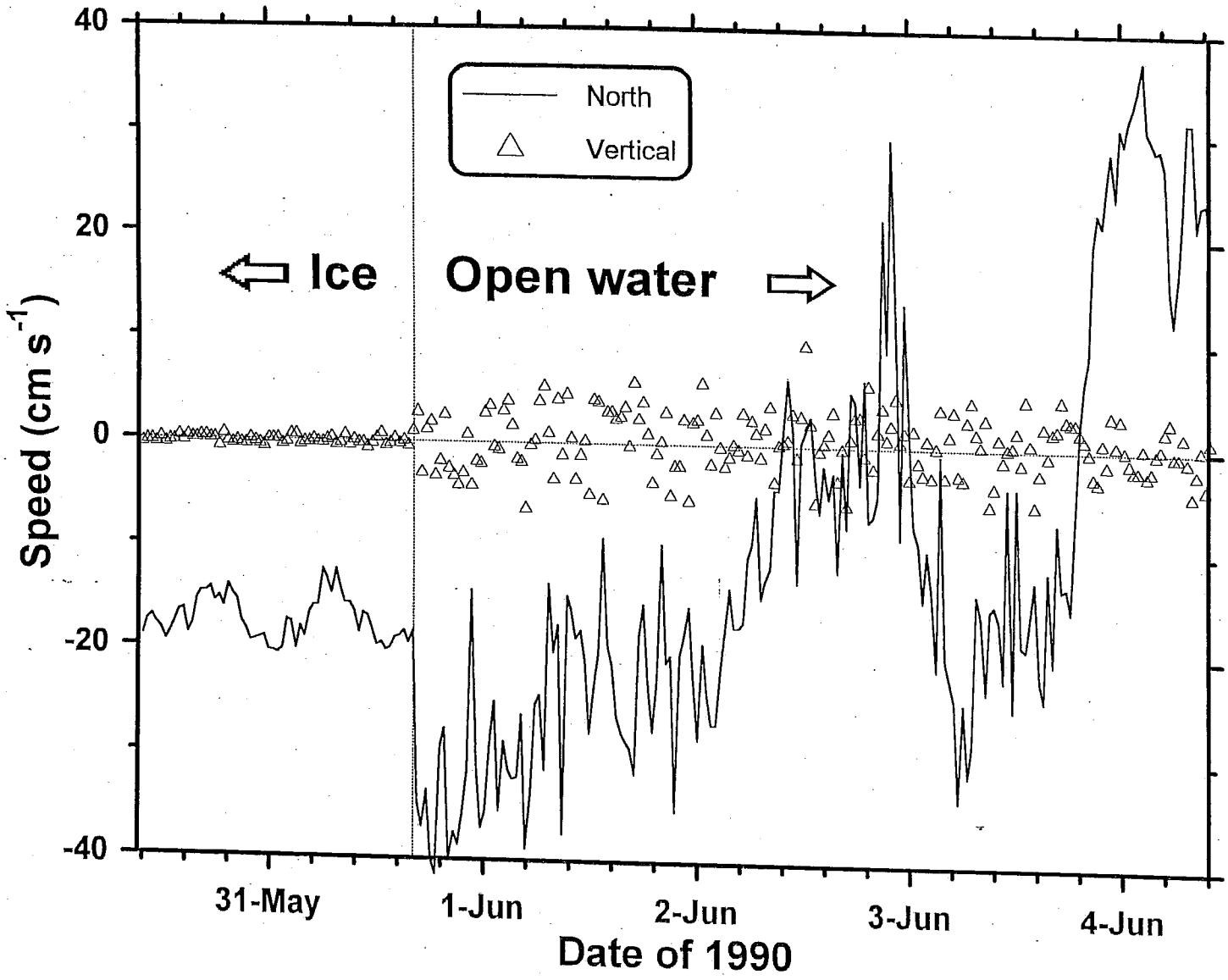

Figure 9: Example of the change in doppler velocity which accompanies the transition from ice-covered to open-water surface conditions. Two components of the ADCP-derived signal are shown.

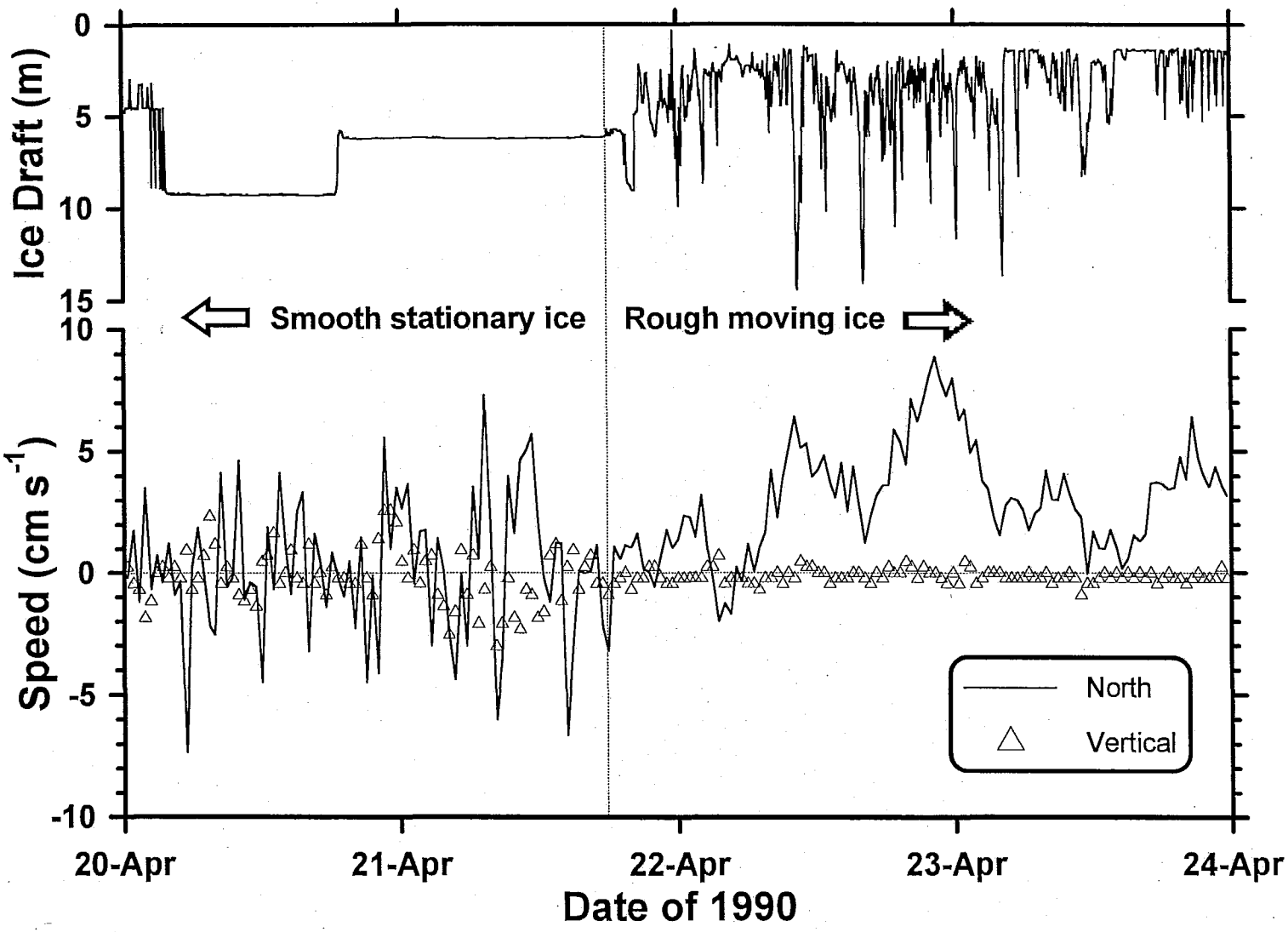

Figure 10: *Comparison of the doppler signal received by the ADCP from smooth first-year ice (left) and from ridged ice. Note the abrupt reduction in data scatter which accompanies the transition from smooth to rough ice conditions.*

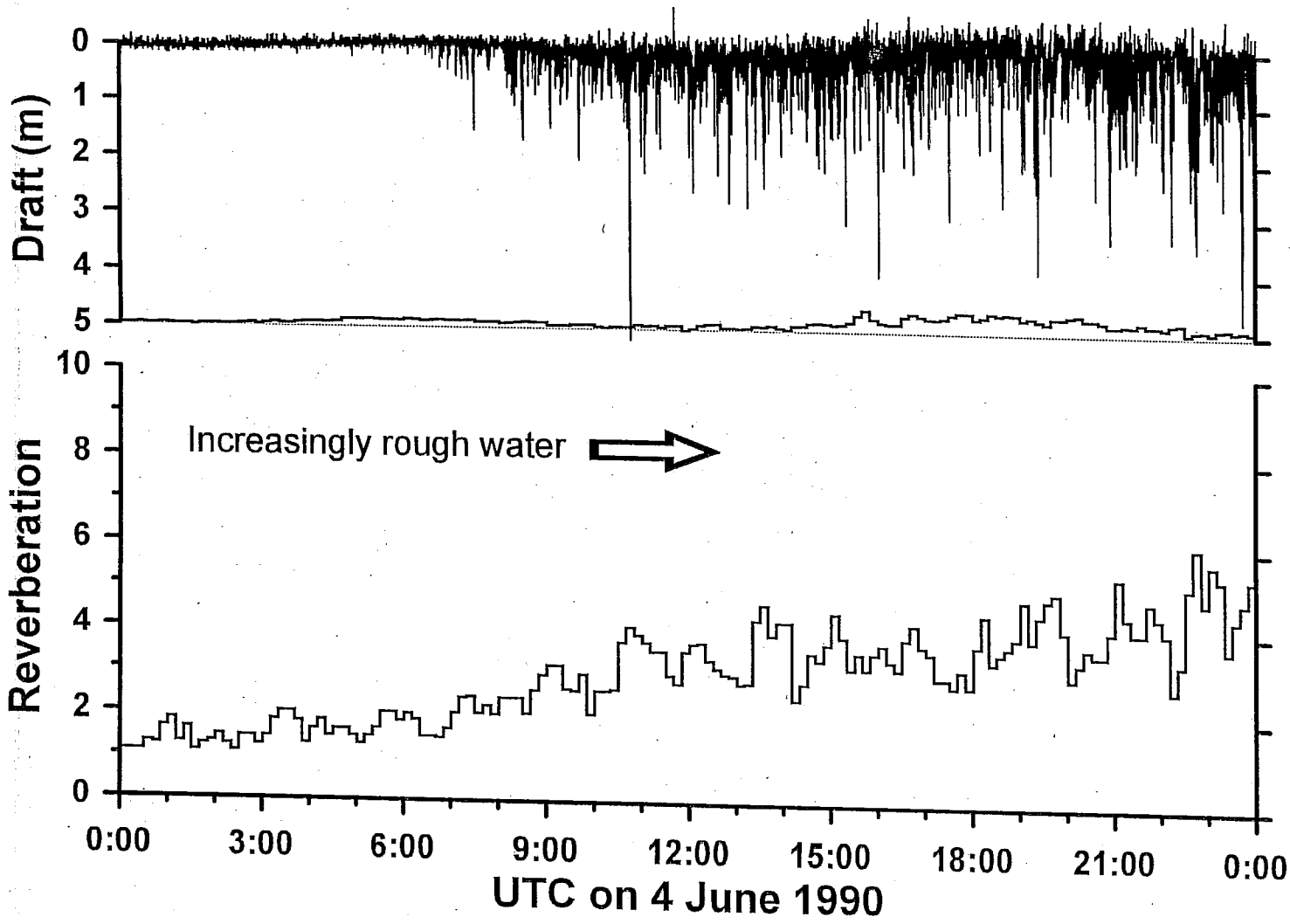

Figure 11: Example of the IPS record (draft and reverberation) during steadily roughening open-water conditions. The upper stepped curve, displaced to the base of the draft axis for clarity, is a statistic based on the 15th percentile of the draft distribution. The reverberation, expressed in multiples of the length of the transmitted sound pulse, is the distance between the 25th and 75th percentiles of the distribution of echo persistence values. Statistics are computed for 15-minute periods.

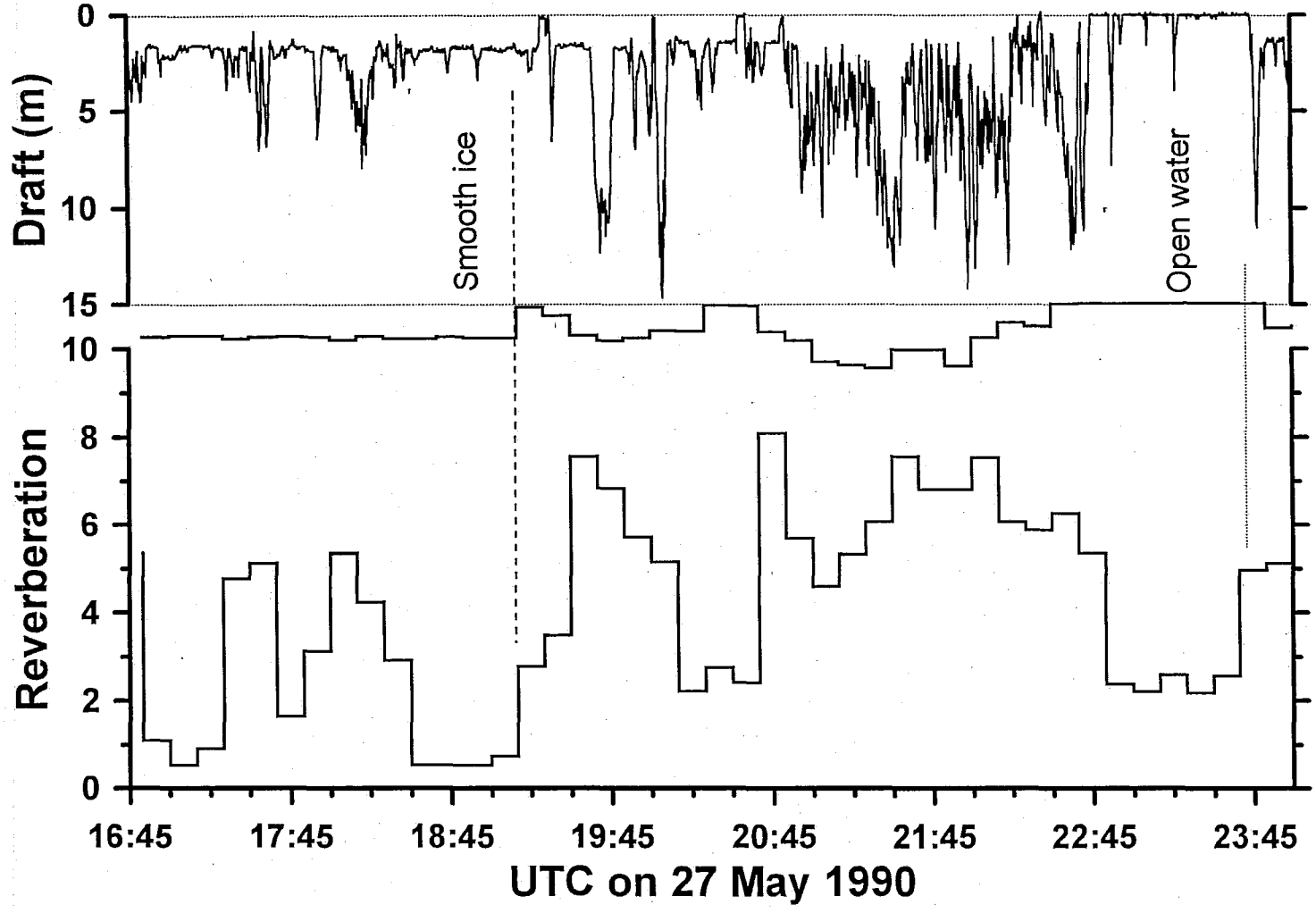

Figure 12: *Sequences of the IPS parameters draft and reverberation for a variety of surface conditions. Note the very brief reverberation time of echoes from smooth ice, which demonstrates the near-specular character of the reflection. Calm open water (right) is significantly rougher. See preceding figure for details.*

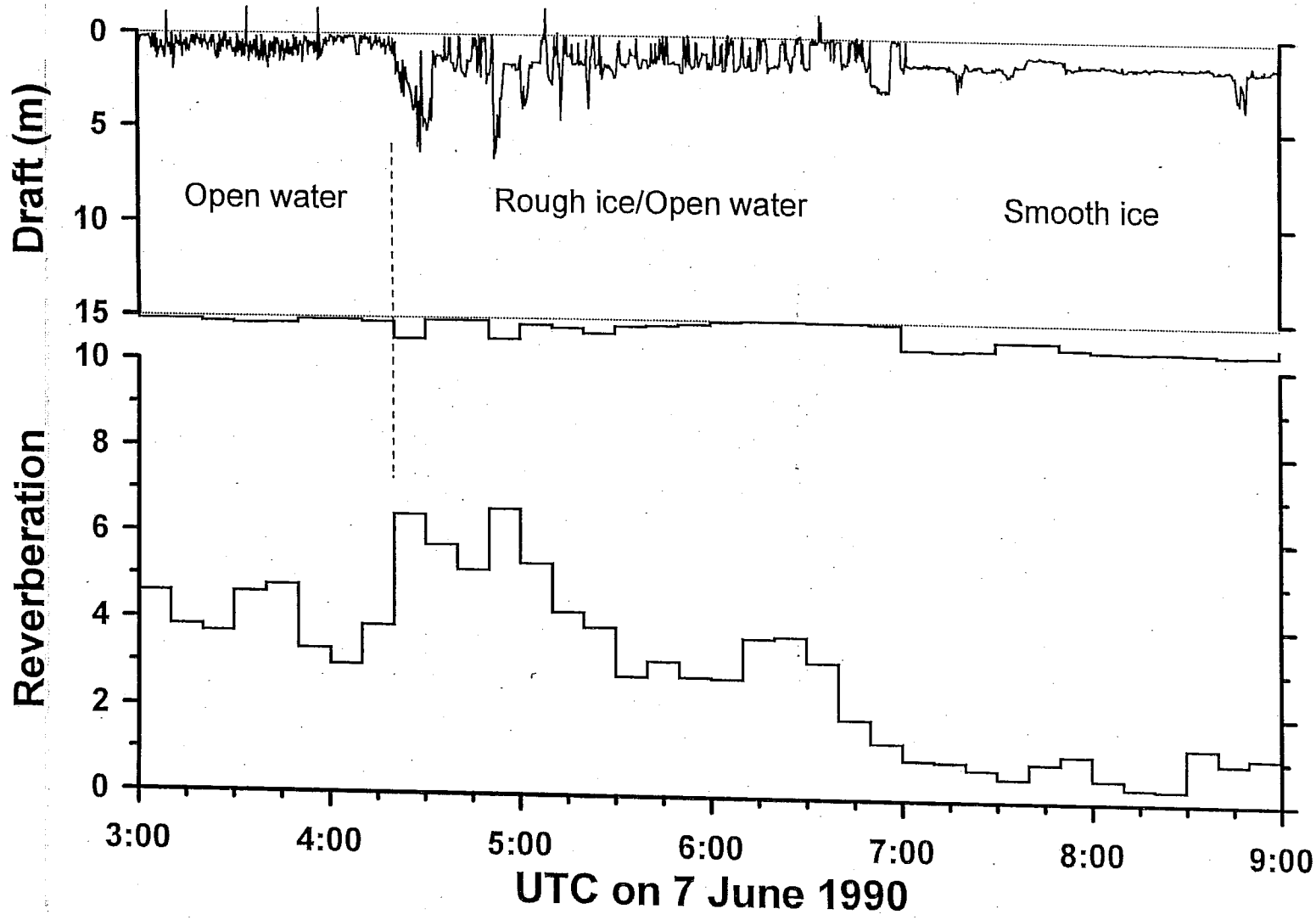

Figure 13: Example of the IPS record (draft and reverberation) illustrating both rough water and rough ice conditions. Note that a discrimination between rough water and rough ice is possible through a combination of range and reverberation criteria. See preceding figure for details.

6. Observations

The IPS2 record of ice draft was acquired between 4 April and 31 May 1990. During this time, the pack ice of the Beaufort Sea experienced four phases of movement:

- an oscillatory northwest-southeast motion between 4 April and 16 May, during which the first 110 km of ice were surveyed.
- a rapid westerly movement between 16 and 28 May, during which 175 km of ice (110 km < s < 285 km) were surveyed.
- a more leisurely southward movement between 28 and 30 May, during which 40 km of ice (285 km < s < 325 km) were surveyed.
- a rapid westward movement which moved the ice edge past the mooring on 31 May (the final 23 km of the record).

Figures 14-18 include maps which display for specific dates the position of the survey line explored by IPS2 during the deployment at ISC90_2A. Annotation on the track is the curvilinear path coordinate, s, in kilometres. Beneath the maps are AVHRR satellite scenes of the Beaufort Sea ice cover, on the same scale and map projection. Figure 19 is the satellite view on 12 June 1990, when only scattered ice was present over the sonars. The projection of maps and satellite views is conical, tangent at 72°N, with the central meridian at 133° 30' W.

In the Appendix, the entire IPS2 record of ice draft is displayed as a function of the curvilinear coordinate, s. The scales are distorted such that the draft is amplified by a factor of 27 relative to the horizontal coordinate.

Table 7: Details of the AVHRR satellite views available for the deployment period

Date	Time (gmt)	Day of 1990
24 April 1990	20:52	114.8694
11 May 1990	21:20	131.8889
23 May 1990	20:49	143.8674
26 May 1990	20:06	146.8375
31 May 1990	20:52	151.8694
12 June 1990	20:20	163.8472

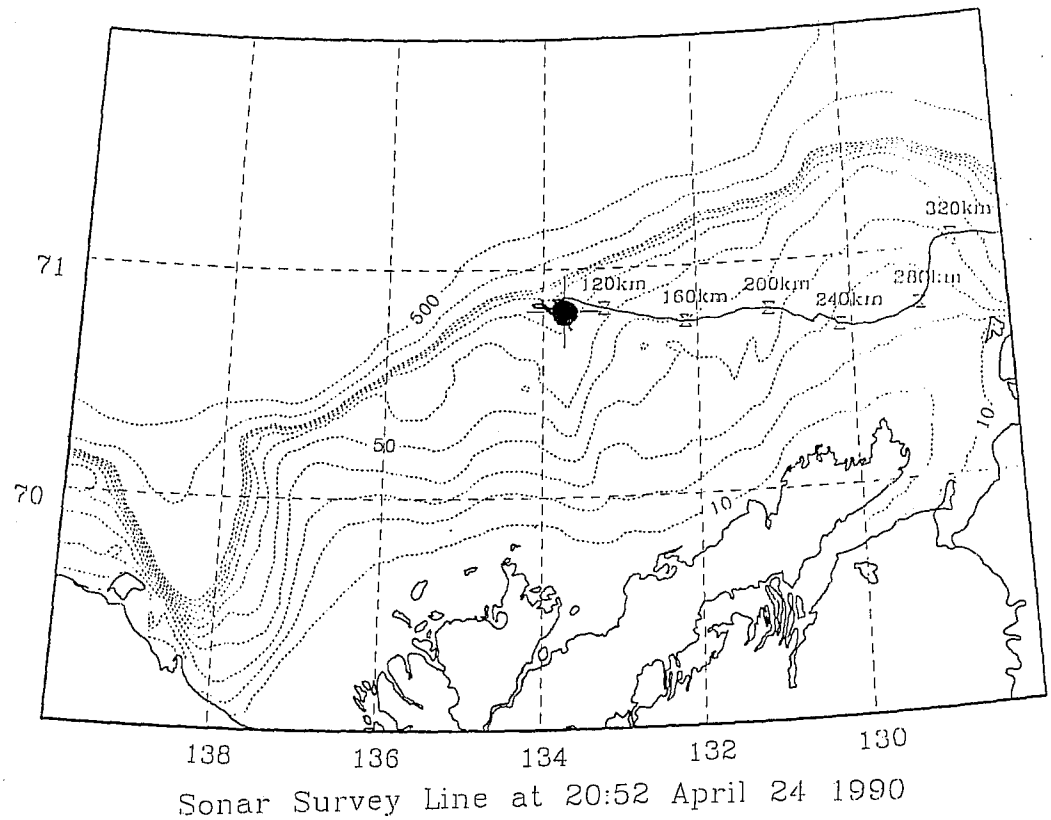

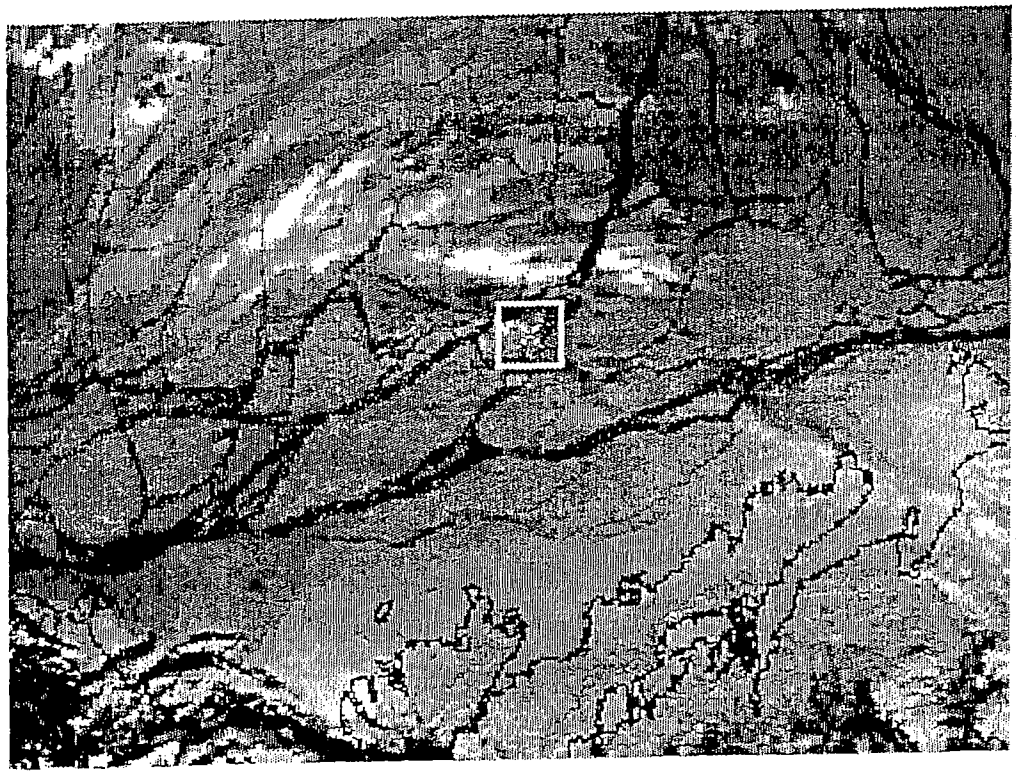

Figure 14: *Position at 2052 GMT on 24 April 1990 of the survey line explored by IPS2 during the course of the deployment (top), and the simultaneous AVHRR satellite view of the ice cover (bottom). Both frames are mapped in a conical projection with a centre meridian at 133° 30' W, and tangent at 72 °N. Annotation on the track is the curvilinear path coordinate, s.*

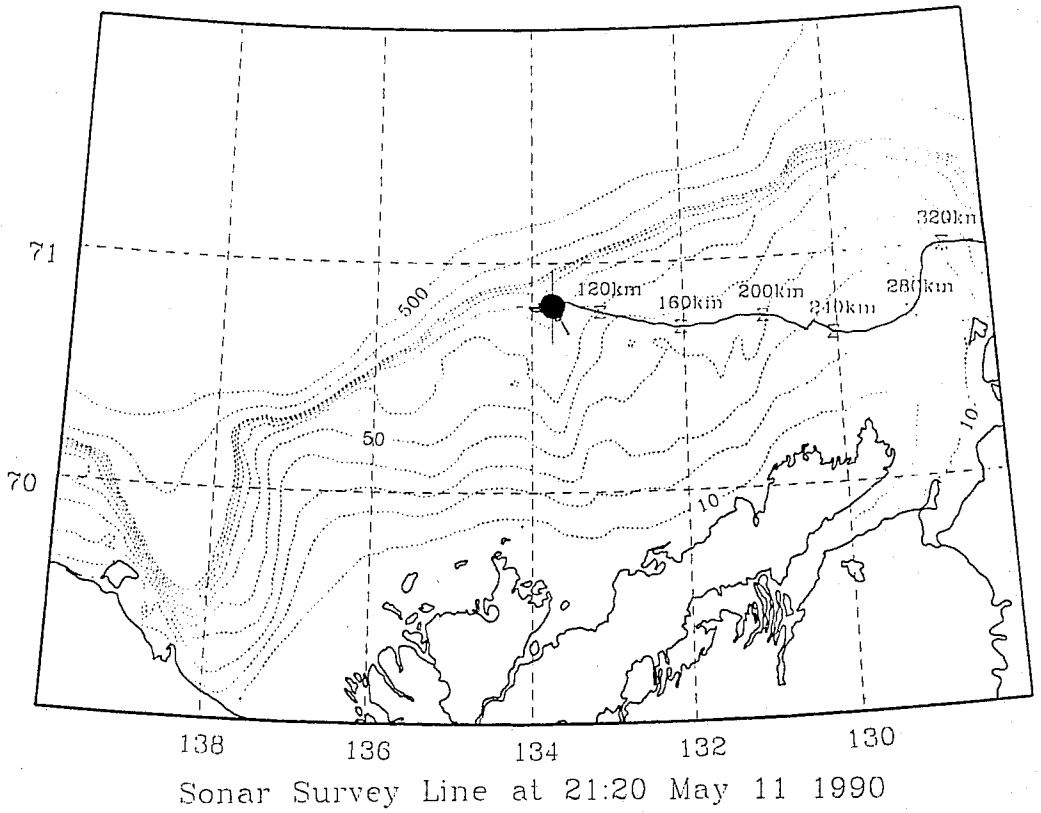

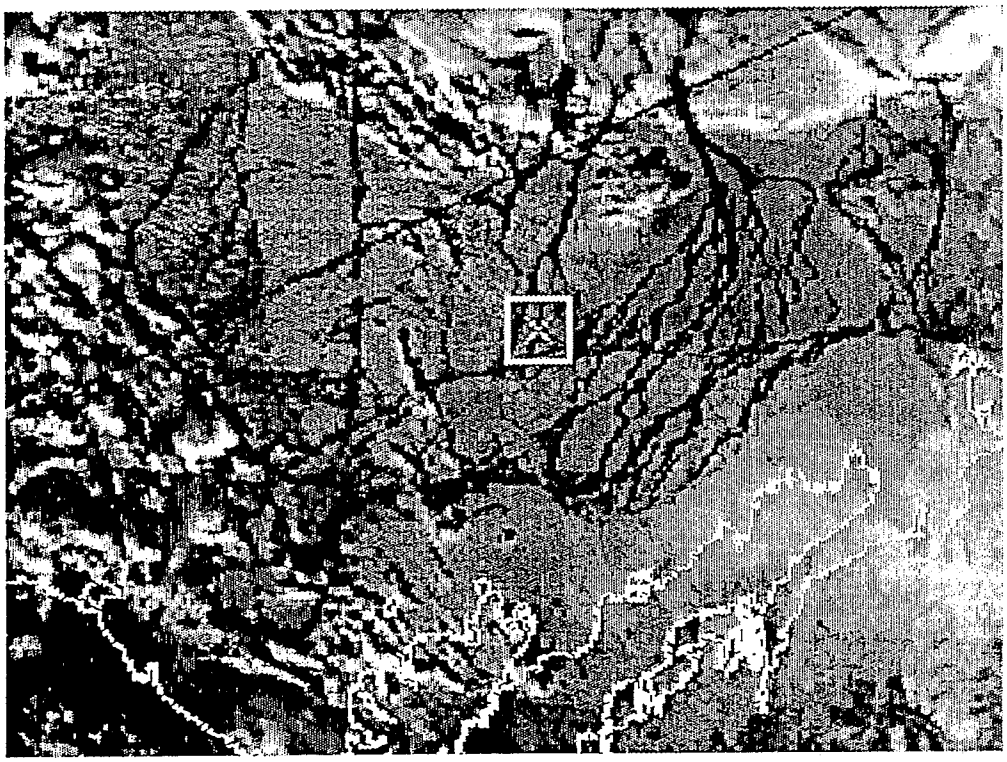

Figure 15: *Position at 2120 GMT on 11 May 1990 of the survey line explored by IPS2 during the course of the deployment (top), and the simultaneous AVHRR satellite view of the ice cover (bottom). Both frames are mapped in a conical projection with a centre meridian at 133° 30' W, and tangent at 72 °N. Annotation on the track is the curvilinear path coordinate, s.*

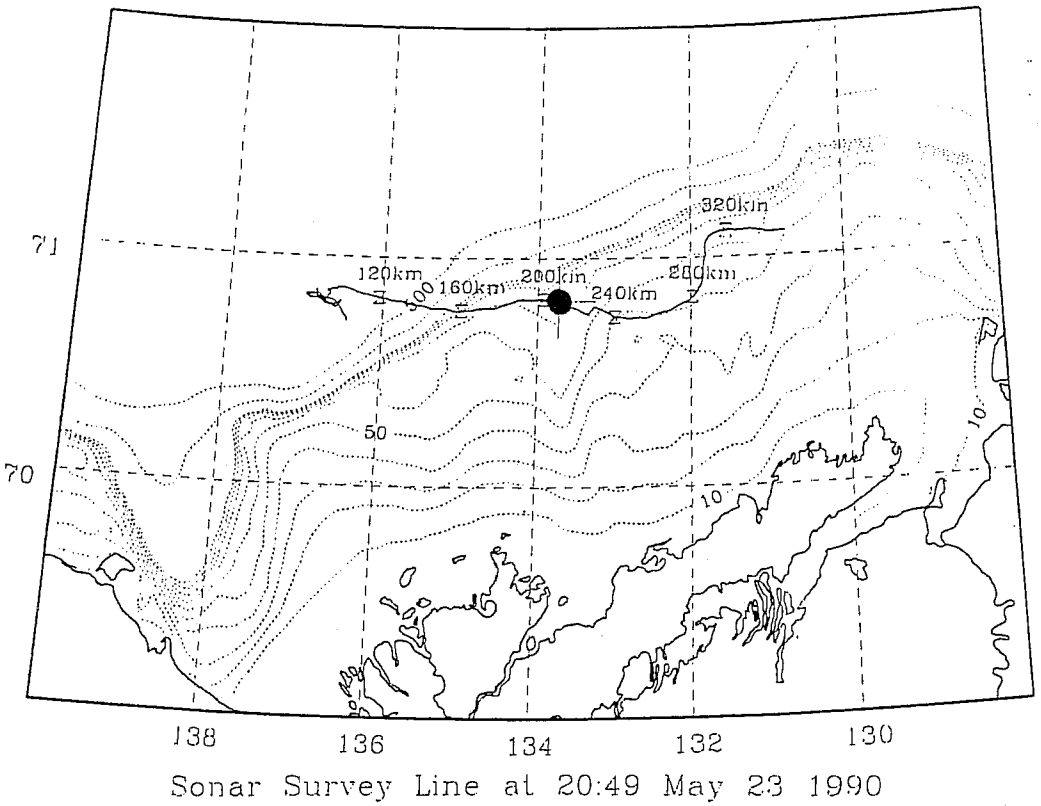

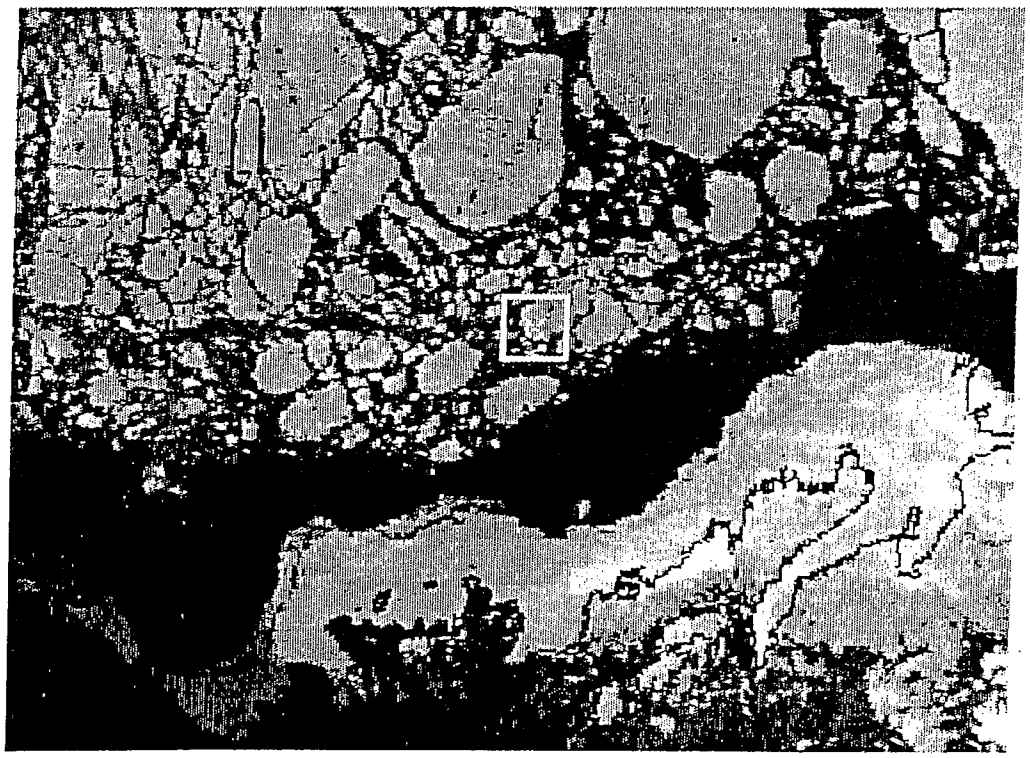

Figure 16: Position at 2049 GMT on 23 May 1990 of the survey line explored by IPS2 during the course of the deployment (top), and the simultaneous AVHRR satellite view of the ice cover (bottom). Both frames are mapped in a conical projection with a centre meridian at 133° 30' W, and tangent at 72°N. Annotation on the track is the curvilinear path coordinate, s.

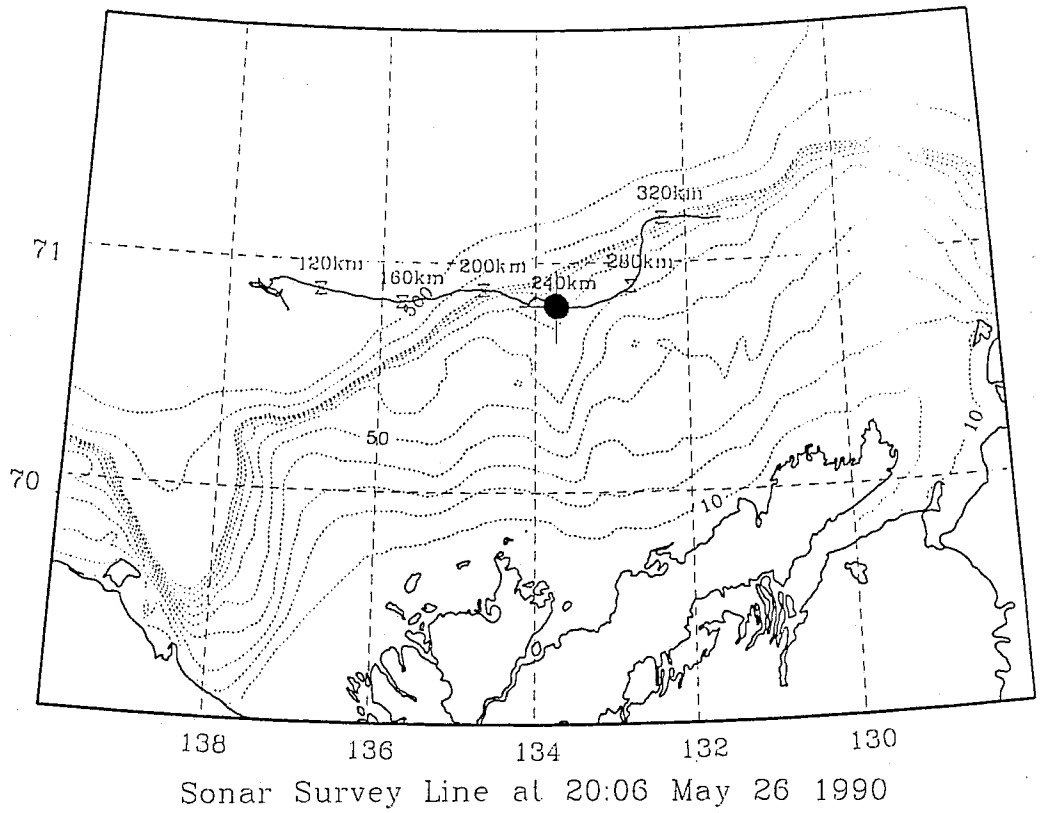

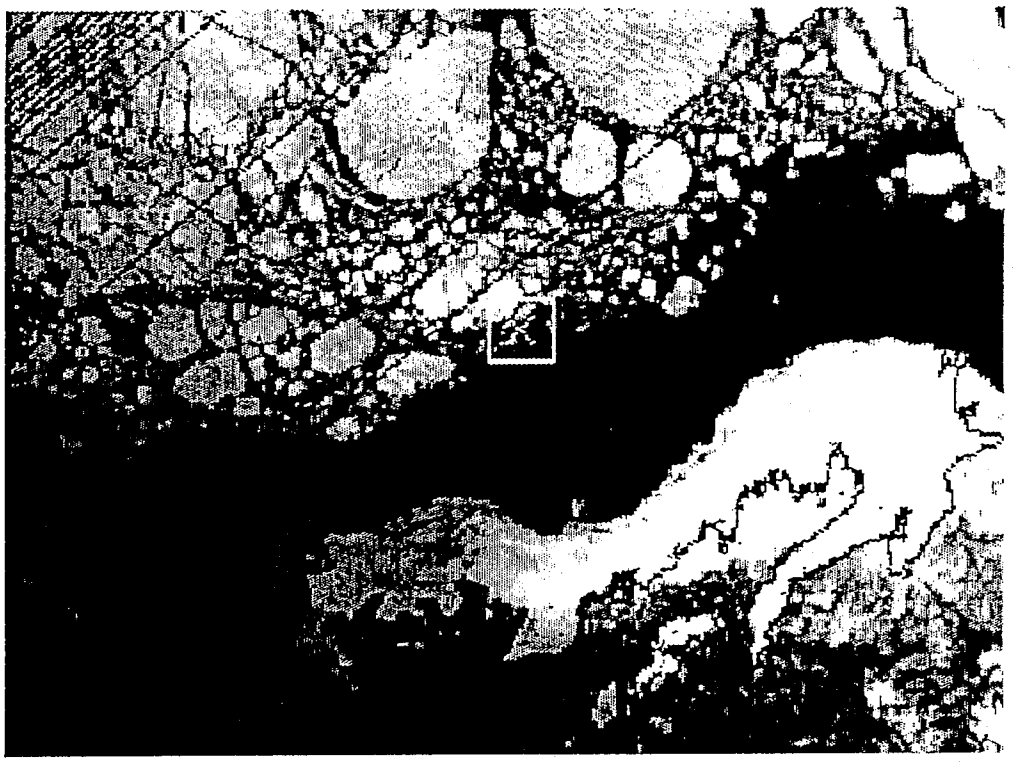

Figure 17: *Position at 2006 GMT on 26 May 1990 of the survey line explored by IPS2 during the course of the deployment (top), and the simultaneous AVHRR satellite view of the ice cover (bottom). Both frames are mapped in a conical projection with a centre meridian at 133° 30' W, and tangent at 72 °N. Annotation on the track is the curvilinear path coordinate,* ***s****.*

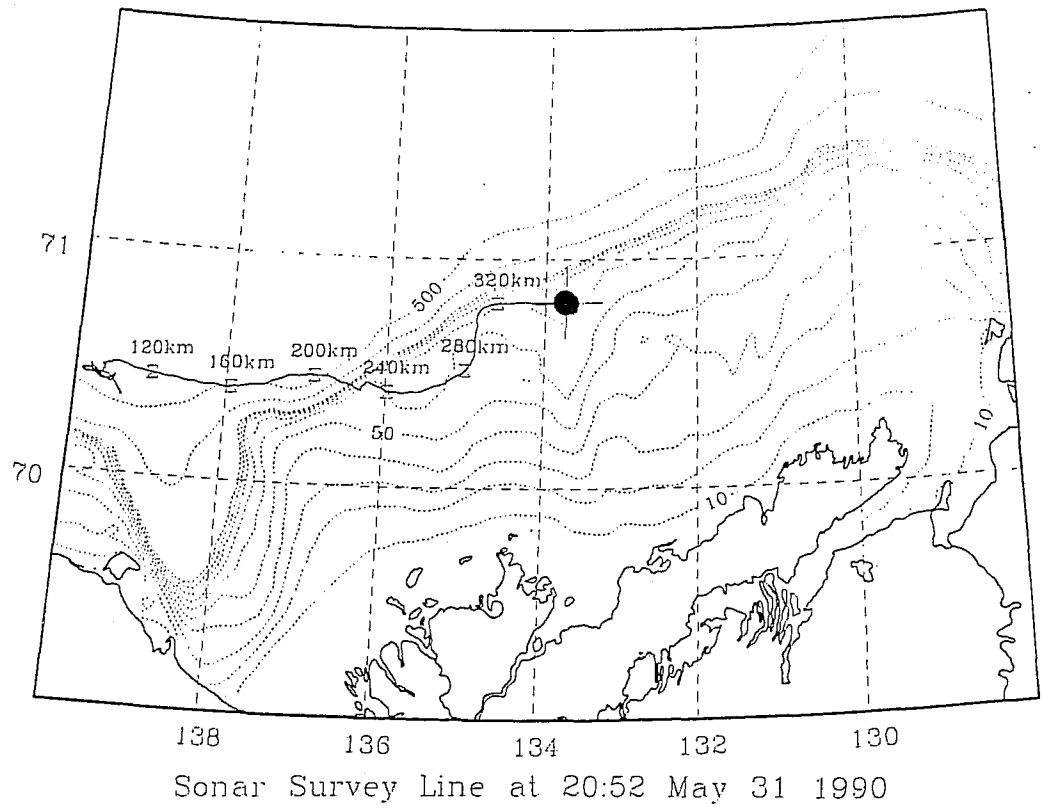

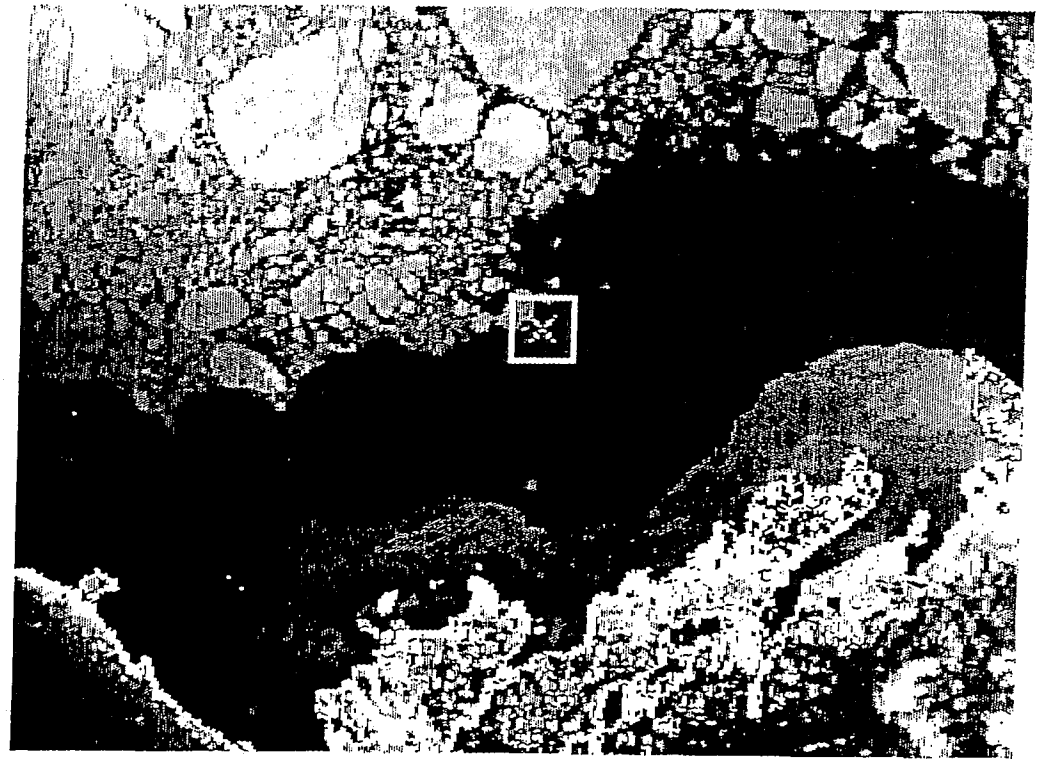

Figure 18: *Position at 2052 GMT on 31 May 1990 of the survey line explored by IPS2 during the course of the deployment (top), and the simultaneous AVHRR satellite view of the ice cover (bottom). Both frames are mapped in a conical projection with a centre meridian at 133° 30' W, and tangent at 72°N. Annotation on the track is the curvilinear path coordinate, s.*

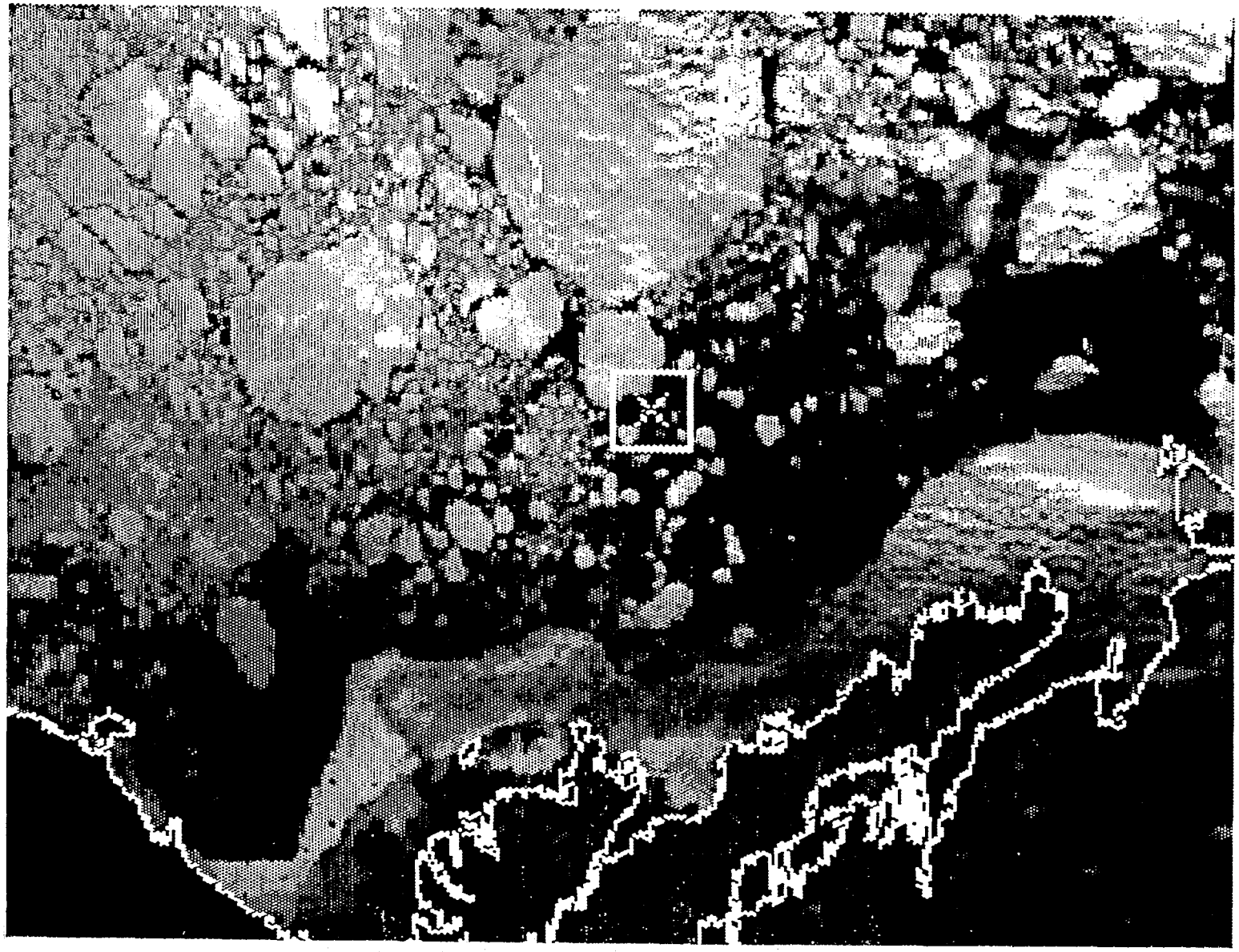

Figure 19: *AVHRR satellite view at 2020 GMT on 12 June 1990. By this time only scattered ice floes existed at ISC90_2A* (X).

7. Statistical Summaries

a. Ice Movement

Statistics of ice movement are presented in Tables 8 and 9 for the two sites separately, although apparent differences between sites may not be statistically significant. The confidence limits on the means are computed from the observed variance in speed and the estimated number of degress of freedom. The number of degrees of freedom equals the ratio of the length of the time series to its integral time scale. This time scale in turn is the asymptotic result of integrating the autocorrelation function of ice speed over lag time (see Table 8). Drift speeds are highly variable: the standard deviation exceeds the mean in all cases. Most rapid drift occurs in the stormy months of autumn and early winter. Speeds as high as 1 m s^{-1} were observed. Motions of the ice cover are least energetic in the mid-winter months.

Probability density functions of ice speed are shown in Figures 20 and 21. Figure 20 displays variations with season at Site 2. During all seasons, the ice pack was frequently stationary. In the mid-winter (January-March), the ice was in motion only 40% of the time, and even during the September-December period, there was no significant movement almost 20% of the time. Speeds greater than 40 cm s^{-1} were observed only during freeze-up. Figure 21 compares the conditions at the two sites averaged over the 3 seasons for which data were obtained. Presumably because the meteorological forcing is very similar at the two sites, so are the probability density functions of ice speed. The observations of the highest speeds (an early-winter occurrence) at Site 1 is probably an indication that oceanic stratification is stronger and ice thinner at Site 1 than at Site 2 at this time of year.

Figure 22 is a contour plot of the probability density function derived from the observations of ice velocity from both sites combined. The huge peak at speeds less than 4 cm s^{-1} has, for clarity, not been contoured[2]. The approximately east-west orientation of the variance ellipse is clear. There is also an indication of two lobes of probability extending to the west, one to the west-southwest parallel to the orientation of the coastline in this area, and one to the west-northwest which roughly parallels the coast of Alaska.

b. Ice Draft

Statistics of ice draft are available only from the more northerly site, near the edge of the continental shelf, and only for the months of April and May. It can be seen from the survey line plotted in Figure 14 that the first 110 km of observations were obtained over a folded path within a relatively small area. Later in May, westerly drift moved ice over the sonar from an area east of the mooring site, and therefore closer to the edge of the landfast ice. At the same time, leads opened in the ice cover, thereby lowering its compactness and average thickness.

The mean drafts of ice over 40 km sections of the 348 km survey line are plotted in Figure 23. The error bars depict, parallel to the track axis, the spatial domain of the mean, and parallel to the draft axis, the estimated uncertainty in the mean, based on the standard deviation of ice draft and the number of degrees of freedom within the 40 km section. Over the first 120 km of the track, where observations were concentrated in a small area, the three independent estimates of mean

[2]This peak contains 47% of the variance in ice drift velocity.

Table 8: Ice Speed Statistics (Seasonal Breakdown)

Site 1 *ADCP-179*	Mean cm s^{-1}	Stnd Dev cm s^{-1}	Maximum cm s^{-1}	Duration days	Time Scale days
Apr - May '90	4.6 ± 1.2	6.4	33	51.4	0.8
Oct - Dec '90	15.3 ± 5.2	18.1	99	71.6	3.0
Jan - Mar '91	3.9 ± 1.0	7.5	47	70.9	0.6

Site 2 *ADCP-318*	Mean cm s^{-1}	Stnd Dev cm s^{-1}	Maximum cm s^{-1}	Duration days	Time Scale days
Apr - May '90	7.9 ± 2.9	8.6	41	56.4	3.1
Sep - Dec '90	13.6 ± 4.1	14.8	75	72.2	2.9
Jan - Mar '91	4.8 ± 1.1	7.9	41	71.9	0.7

draft agree within estimates of sampling error. The plotted diamonds show the values of mean draft calculated when open water and nilas are ignored (only draft values greater than 0.125 m were used). From the differences between the two estimates of the mean, it is evident that on the early part of the track, and on the track section immediately preceding the passage of the ice edge over the mooring, very little open water or new ice was present. In the first case this is because there was insufficient movement in the ice cover to generate leads. In the second case the margin of the ice field had been consolidated by the action of wind and waves on the upwind flaw lead, seen clearly in the satellite views of Figure 18. The inset plot illustrates that the standard deviation of ice draft increases in proportion to the mean draft.

The number of degrees of freedom within a 40 km section is derived from the autocorrelation function of ice draft. The autocorrelation function computed from this set of observations is displayed in Figure 24. The function is cusped at zero lag, drops rapidly over the first 250 m, and thereafter maintains a value near 0.1. The long tail in the autocorrelation function is a reflection of the regional scale of level seasonal ice in this area. The integral of the function, also plotted, is a measure of the distance over which draft values are correlated. The integral increases to a value of 75 m at 300 m lag, but fails to converge beyond this point because the autocorrelation function

Table 9: Ice Velocity Statistics (Seasonal Breakdown)

Site 1 *ADCP-179*	Mean cm s^{-1}	σ_{Major} cm s^{-1}	σ_{Minor} cm s^{-1}	Bearing of Major Axis
Apr - May '90	1.8 along 277°	7.1	3.0	107°
Oct - Dec '90	5.8 along 261°	20.1	11.2	89°
Jan - Mar '91	1.6 along 253°	7.7	3.1	101°

Site 2 *ADCP-318*	Mean cm s^{-1}	σ_{Major} cm s^{-1}	σ_{Minor} cm s^{-1}	Bearing of Major Axis
Apr - May '90	4.5 along 259°	9.1	5.8	98°
Oct - Dec '90	6.5 along 249°	16.1	10.1	85°
Jan - Mar '91	1.5 along 224°	8.3	3.9	102°

remains positive. For the purpose of estimating sampling uncertainties, the decorrelation scale has been assumed to equal the integral scale at a lag of 300 m, where the autocorrelation function levels off. This is an accurate reflection of the decorrelation scale of deformational features such as ridges and leads. Thus, within the 40 km sections of ice used for analysis it is estimated that there are 40,000/75, or 533 degrees of freedom.

Disregarding the open water and new ice, the overall mean draft of ice was 3.15±0.04 m. From Figure 25, which depicts the low-draft portion of the probability density function of ice draft, it is seen that this mean value is twice the 1.55 m draft of the most common ice along the survey path. Three separate statistics are plotted in this figure: the higher curve is computed from the entire 348 km survey by sonar; the lower curve is computed only for those sections of the survey which were classified as level[3]; the superimposed histogram is based on 34 draft values measured directly by augering first-year ice in late March. Comparison of the solid and dashed curves in Figure 25 indicates that 90% of the ice with draft between 1.15 and 1.875 m was level by the definition adopted. This ice forms the peak of the function and belongs to the first-year ice category. The fact that only about 30% of the thin ice (draft between 0.25 and 1.00 m) was level is an indication of the susceptibility of ice in this category to widespread deformation on small (<10 m) scales. On the other side of the peak, approximately 25% of the ice with draft up to 3 m was level. Four augered holes yielding drafts in the 2-3 m range confirm that this percentage is associated with rafting of ice from the predominant first-year ice category. Two holes which were augered in multi-year floes indicate that multi-year ice (not necessarily level) also makes a contribution over this range of draft. Where draft exceeded 3 m, almost all ice was heavily deformed and irregular in topography.

At the low end of the draft probability density function are found the open-water, young-ice and first-year ice categories. These are the components of the ice field which vary most dramatically on short time scales, in response to the opening and freezing of leads. For each of the 40 km sections of the survey, the fractions of open-water/nilas (draft < 12.5 cm), young/thin first-year ice (12.5 < draft < 112.5 cm) and medium/thick first-year ice (112.5 < draft < 187.5 cm) were calculated by integrating the probability density function of draft between the appropriate limits. The results are displayed in Figure 26. The coverage of thick first-year ice as a fraction of the area of the ice alone (that is the area which excludes recently formed open water and nilas) is plotted using symbols. For the first 80 km, surveyed between April 5 and May 9, there was almost no open water/nilas and very little young/thin first-year ice. Less than 40% of the ice field was undeformed medium/thick first-year-ice. Over the next 10 days (80-120 km), the ice cover diverged to create a 2% coverage of new leads. In the next two sections (120-200 km), the fraction of deformed ice increased. Between 160 and 200 km, 70% of the ice was deformed and only 26% was in the medium/thick first-year ice category. For this reason this section has the largest average draft (3.92 m). Subsequent sections, acquired while the ice was undergoing rapid westward drift over 23-30 May, had larger fractions of open-water/nilas (up to 30%) and smaller fractions of deformed ice. These changes reflect the fact that the survey path crossed from an area of 7/10 multi-year ice to an area of predominantly first-year ice (Weekly Composite Charts, Ice Centre Environment Canada). It is noted, however, that the sonar record consistently identifies the presence of a greater fraction of first-year ice (3/10-7/10) than indicated in the ice chart based on aircraft and satellite surveillance.

The horizontal extent of level sections of sea ice is equivalent to the distance which separates

[3] A section of the profile was classified as level if its draft varied by less than ±0.25 m and its length was 10 m or greater.

deformational features. Using level ice indentified through application of the definition quoted above, a probability density function for the extent of level areas was calculated (Figure 27). Note that leads are included as level ice of zero thickness, but that level ice in sections smaller than 10 m is not. The data match a truncated log-normal probability function with a 2.5 m median and a 10.9 m mean. The function is truncated at the 10 m cut-off of the level-ice discriminator. The fit provides an estimate of 20% for the fraction of all level-ice fragments which are of a dimension greater than the cut-off and therefore seen. Thus, if it is assumed valid to extrapolate the log-normal function to block sizes below the cut-off, about 80% of the level-ice fragments have not been detected by the level-ice criterion. These are the smaller fragments resulting from ice failure which have been tilted and piled into ice ridges.

Figure 28 displays the fraction of the ice cover which is level over distances greater than the abscissa value. Overall, 53% of the ice cover (including open water) is level over distances of 10 m or more. However, only 20% is level over distances exceeding 100 m!

Mean properties of the level component of the ice field are summarized in Table 10.

Table 10: Mean Draft of Areas of Level Ice

	Mean Draft	Standard Deviation
All Level Ice	1.47 m	0.82 m
Level ice, excluding leads and nilas	1.73 m	0.59 m
Level ice, excluding leads, nilas and rafted areas	1.55 m	0.31 m

The probability function of draft for the deformed portion of the ice field is displayed most effectively against log-linear axes (Figure 29). In this figure, symbols with error bars delineate the probability function for the entire record. Uncertainty has been computed using the equation,

$$\sigma = \sqrt{\frac{p\,(1-p)}{n}}$$

where p is the value of the function and n is the number of degrees of freedom given by the total path divided by the integral scale (*i.e.* 348409/75=4646). The solid curve is the function for the 40-km section of greatest average thickness, between 160 and 200 km along the path, and the dashed curve is that for that of least average thickness (280-320 km). The probability density function for level ice is overlaid to show the rapid fall-off of this function with draft increasing above 2 m.

For draft exceeding 3.5 m, the probability density function, *f(d)*, can be represented within sampling uncertainty by the exponential function (straight line on this plot):

$$f(d) = 0.258\ e^{-d/3.06}$$

The same function fits over the 2.5-25 m range in draft, if the contribution from level ice in this draft range (the light solid line) is subtracted from the overall draft probability density function[4]. It appears that different sections of the path can be fit by exponential functions having the same roll-off but different amplitudes. The *e*-folding scale is 3.06 m. The amplitude varies by a factor of 3 between the upper and lower curves plotted, reflecting a difference of the same magnitude in the proportion of ridged ice in these 40-km sections. Integrating the exponential function over draft, one obtains the result that 35% of the ice surface is occupied by rough ice of 2.5 m draft or greater. The remainder is occupied by level ice and leads (53%) and by rough ice of less than 2.5 m draft (about 13%). Integration over the deep-draft part of the domain reveals that only about 0.1% of

[4]The result of this subtraction is plotted using open circles in the figure.

the ice surface is occupied by ridged ice of 20 m draft or greater.

The finite decorrelation scale for ice draft (Figure 24) implies that similar values of ice draft are clustered. Thus, the recurrence distance between identifiable *features* reaching a particular draft will be much larger than the recurrence distance for that draft. Features of deep draft in this data set were identified using two different criteria. The first is the familiar Rayleigh criterion, used initally by WILLIAMS *et al.* (1975). By this criterion, a local maximum in draft is identified as a keel if it is bounded on both sides by ice whose draft beyond a reference level is less than half that of the maximum. The reference draft for keels in this application of the Rayleigh criterion was taken to be 2 m. Under the second criterion, a keel is identified if it is flanked on both sides by level ice as defined earlier. No choice of reference datum is required under the second criterion. The frequencies of keels identified by the two different criteria are plotted as a function of draft in Figure 30. Both criteria yield counts which are well fitted by exponential functions over a portion of their domain. For keels with draft of 20 m and more, the counts by both criteria are in agreement. However, as draft decreases towards 5 m the Rayleigh criterion identifies progressively more features than the level-ice criterion. For draft below 5 m, the Rayleigh criterion is not an effective discriminator, missing many features found by the level-ice criterion. Table 11 summarizes properties of the two keel populations.

Table 11: Summary of Keels Selections by the Rayleigh Criterion

	Selected by the Rayleigh Criterion			
Minimum Keel Draft (m)	9	5	3	0.5
No of Keels	551	1541	1910	-
Keels per km	1.58	4.42	5.48	-
Mean Keel Draft (m)	12.35	8.81	7.92	-

	Selected by the Level-Ice Criterion			
Minimum Keel Draft (m)	9	5	3	0.5
No of Keels	387	1071	1729	2329
Keels per km	1.11	3.07	4.96	6.68
Mean Keel Draft (m)	12.87	8.97	7.04	5.81

Pressure ridges are just one of several types of features which delimit level ice. Thus, the number of keels selected by the level-ice criterion is less than the number of sections of level ice identified. Level ice may also be delimited by steps, slopes and cracks. A step is an abrupt change in draft between one level section and another; such may occur at the edge of a refrozen lead. A slope is a more gradual but steady transition in draft; it may occur on the downwind side of a lead where a wedge of frazil ice has been driven by wind and waves. A crack is a section of locally reduced draft which could be either rough, or level if less than 10 m in width. Table 12 summarizes the occurrence frequency of features of each type.

The occurrence of very deep keels in this area may be predicted from the data set by extrapolation of the fitted functions plotted in Figure 30. The frequency function for Rayleigh-delimited keels is,

$$f(d) = 5.97\ e^{-d/3.46}$$

and that for level-ice-delimited keels is,

$$f(d) = 2.95\ e^{-d/3.85}$$

Recurrence distances are obtained simply by integration of these functions. Recurrence intervals are obtained by dividing the distances by the mean speed of ice motion over the observation period. Both distance and interval estimates are subject to cautionary remarks concerning the short duration of the data set, and its relevance to the late winter conditions only. In this area of the Arctic Ocean, where ice is absent or light for 3-5 months of the year, true recurrence intervals are likely longer. Table 13 summarizes the estimates. Note that the level-ice criterion predicts much shorter recurrence intervals for deep keels than does the Rayleigh criterion. The validity of these predictions is tentative until the frequency of rare deep keels in this area can be better established observationally.

Table 12: Incidence of Features Separating Sections of Level Ice

No of Features is 4181	Frequency of Occurrence
Ridges	55.9 %
Steps	25.0 %
Slopes	10.2 %
Cracks	8.8 %

Over the 348.4 km of ice profile from these observations, twenty-one features with draft exceeding 20 m, including two with draft exceeding 25 m, were detected. The maximum draft was just under 27 m. Cross-sections of these features, without coordinate distortion, are illustrated in Figure 31. It is clear that it is not possible to represent all these features by a single simple geometrical form. There is no typical shape which characterizes ridge keels.

Table 13: Predictions of the Recurrence of Deep Ice Keels

	Rayleigh Criterion		Level-Ice Criterion	
Keel Draft (m)	Distance (km)	Interval	Distance (km)	Interval
20	16	2.3 days	16	2.3 days
25	67	10 days	58	9 days
30	282	41 days	213	31 days
35	1197	5.7 months	781	3.7 months
40	5078	24.0 months	2863	13.5 months

c. Ice Thickness

How can one derive mean ice thickness from the draft data presented? Ideally, one applies Archimedes' Principle to relate the submerged volume of ice, represented by the mean draft, ***d***, to the overall volume (***f*** is mean freeboard), with allowance for the presence of a snow layer of mean thickness, ***s***. Material densities are represented by ρ:

$$\rho_w d = \rho_i (d + f) + \rho_s s$$

Although, over a long track it is correct to assume (as done here) that the ice is in overall isostatic equilibrium, there are other complications. Level ice and multi-year ice contain no voids on a macroscale, and their bulk densities are reasonably well known (900-920 kg m^{-3}). However, because new pressure ridges are piles of ice blocks which may enclose a significant volume of ice-free voids, the bulk density of ridge keels is higher than the density of sea ice, ρ_i, and the bulk density of ridge sails is lower. Equivalently, the draft and freeboard of ridges, if compressed to

solid sea ice, are less than the envelopes of draft and freeboard defined by their component blocks. Work by VEITCH *et al.* (1991) indicates that voids can occupy as much as 30% of first-year ridges. If it is assumed that the ratio of the void fractions within the draft and freeboard envelopes of first-year ridges is approximately one (MELLING *et al.* 1993), an envelope thickness, t_E, can be calculated which is approximately independent of the void fraction:

$$t_E \approx d + f + s_e \approx \frac{\rho_w}{\rho_i} d$$

The left side includes snow converted to an equivalent thickness of sea ice, s_e. When calculating the *volume* of ice (considered broadly as sea ice plus snow ice), however, the void fraction, υ, cannot be ignored. The equation above is modified to compute a thickness based on ice volume , t_V, as follows:

$$t_V \approx (1-\upsilon)(d+f)+s_e \approx (1-\upsilon)\frac{\rho_w}{\rho_i} d$$

When computing values averaged over distances which contain many ice features, deformed first-year ice, because of its high void fraction, should be considered separately from level and multi-year ice forms. Unfortunately, it is not possible at this time to use ice-profile data to discriminate between first-year and multi-year deformational features. Thus the fraction of the deformed ice observed in the present survey which is consolidated is not known. Thus only lower and upper bounds for the thickness representing ice volume can be derived. The lower bound is derived by assuming that all deformed ice is recently built and has a significant void fraction. The upper bound, based on the assumption that all deformed ice is old and contains no voids, is the same as the envelope thickness. Results of the calculations are listed in Table 14.

Table 14: Estimates of the Mean Thickness of Ice on the Profile

	Entire Ice Profile			Profile, excluding Leads & Nilas		
	Level Ice	Deformed Ice	All Ice	Level Ice	Deformed Ice	All Ice
Fraction of Profile	53.58%	46.42%	100%	49.70%	50.30%	100%
Mean Draft	1.47 m	4.55 m	2.90 m	1.73 m	4.55 m	3.15 m
Volume Thickness	1.67 m	4.15 m	2.82 m	1.97 m	4.15 m	3.06 m
Envelope Thickness	1.67 m	5.18 m	3.30 m	1.97 m	5.18 m	3.59 m

Assumptions:	*Water Density:*	*1025 kg/m^3*	*Ice Density:*	*900 kg/m^3*	*Void Fraction:*	*20%*

As indicated in the table, the amount of ice present might possibly be as little as 2.8 m (2520 kg m^{-2}), if 20% of the volume of all deformation features is void space. However, since ice reconnaissance charts from the Ice Centre of Environment Canada indicate a substantial presence of multi-year ice over most of the survey path at this time, the actual amount of ice present is probably closer to the envelope value of 3.3 m (2970 kg m^{-2})

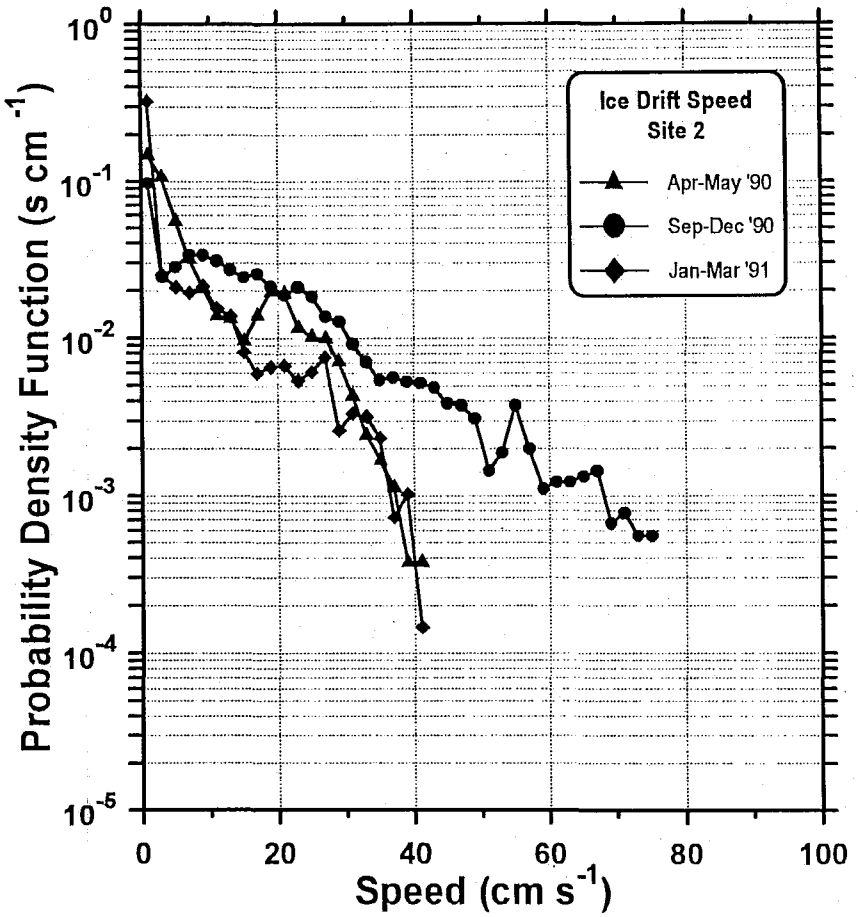

Figure 20: Variations with season of the probability density function of ice speed at Site 2.

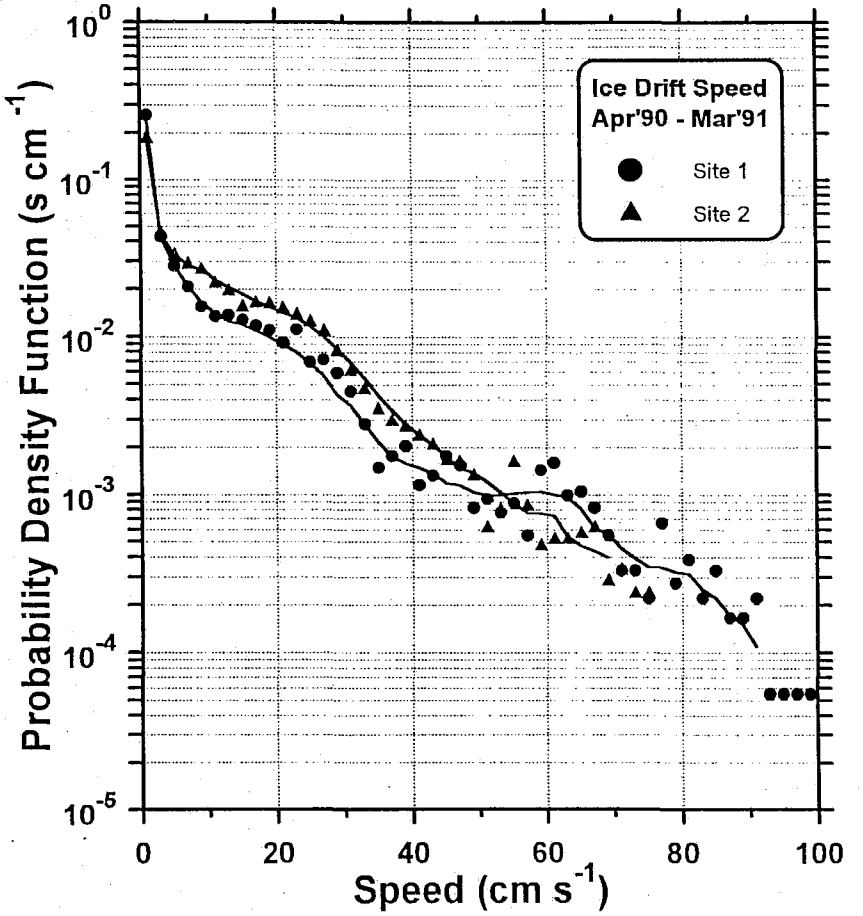

Figure 21: Comparison of the probability density functions of ice speed at the two sites, averaged over the three seasons for which data were obtained.

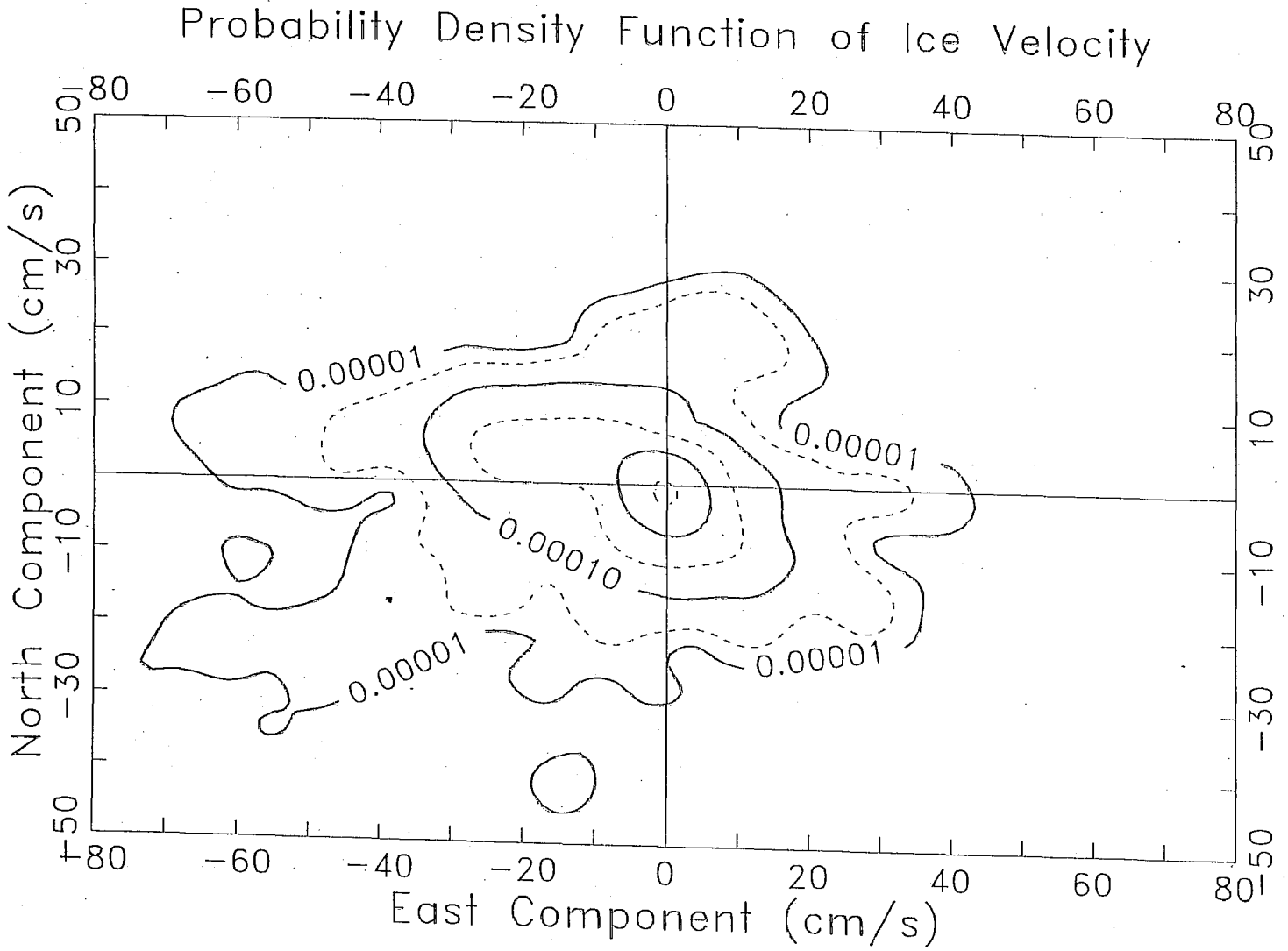

Figure 22: *Contour plot of the probability density function of ice velocity. The huge peak at speeds less than 4 cm* s^{-1} *has, for clarity, not been contoured. Units are* $s^2\ cm^{-2}$

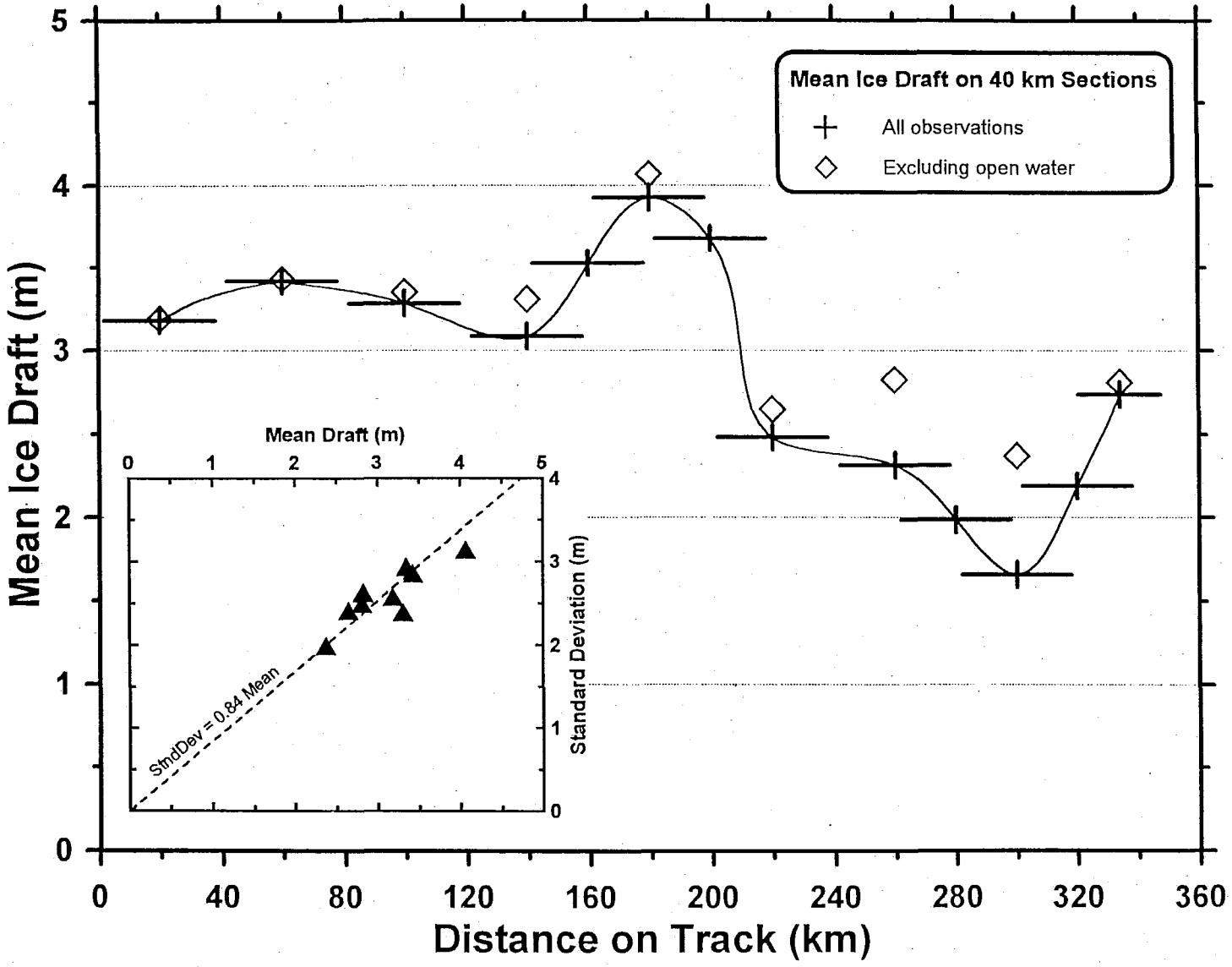

Figure 23: Mean drafts of ice over 40 km sections of the 348 km survey line. Error bars represent sampling error. Diamonds show means computed if open water and new ice (<0.125 m) are excluded.

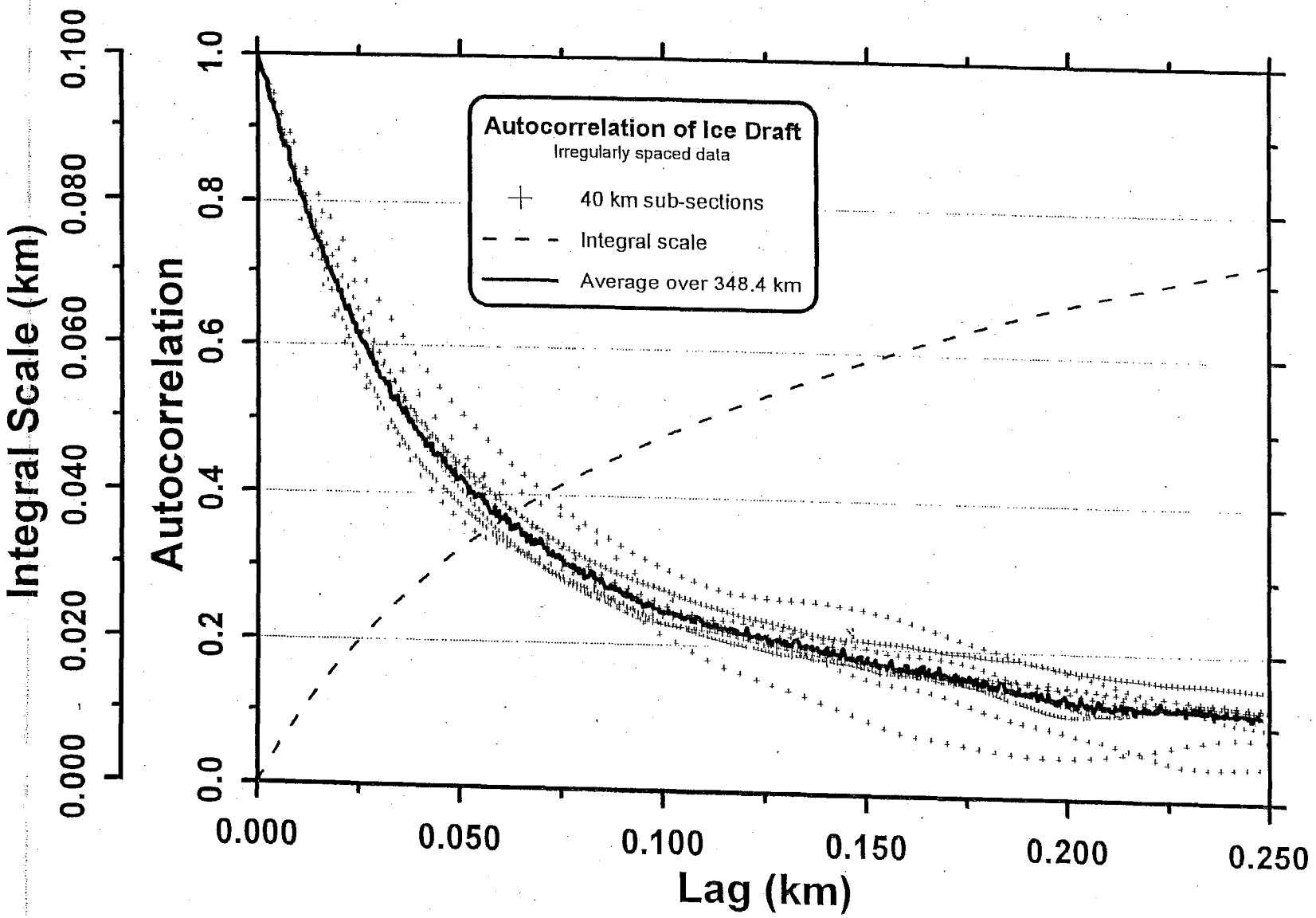

Figure 24: Autocorrelation function of ice draft. Symbols represent values computed from individual 40 km sections of track. The solid line is an average over the entire path and the dashed line is its integral.

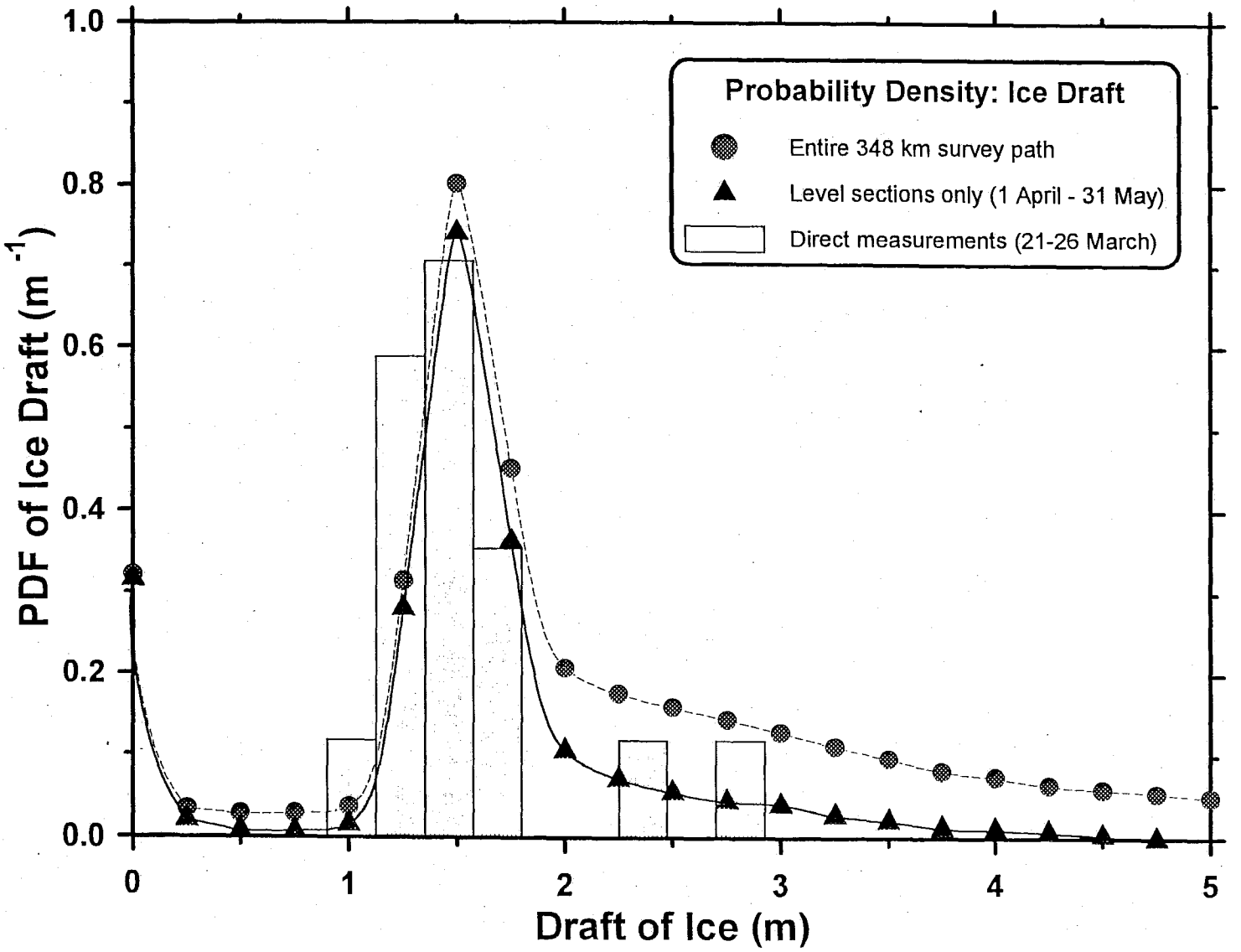

Figure 25: *Probability density functions of the draft of sea ice observed by sonar at Site 2 in April-May 1990. The superimposed histogram shows the distribution of 34 draft values measured by augering first-year ice in the same area in late March.*

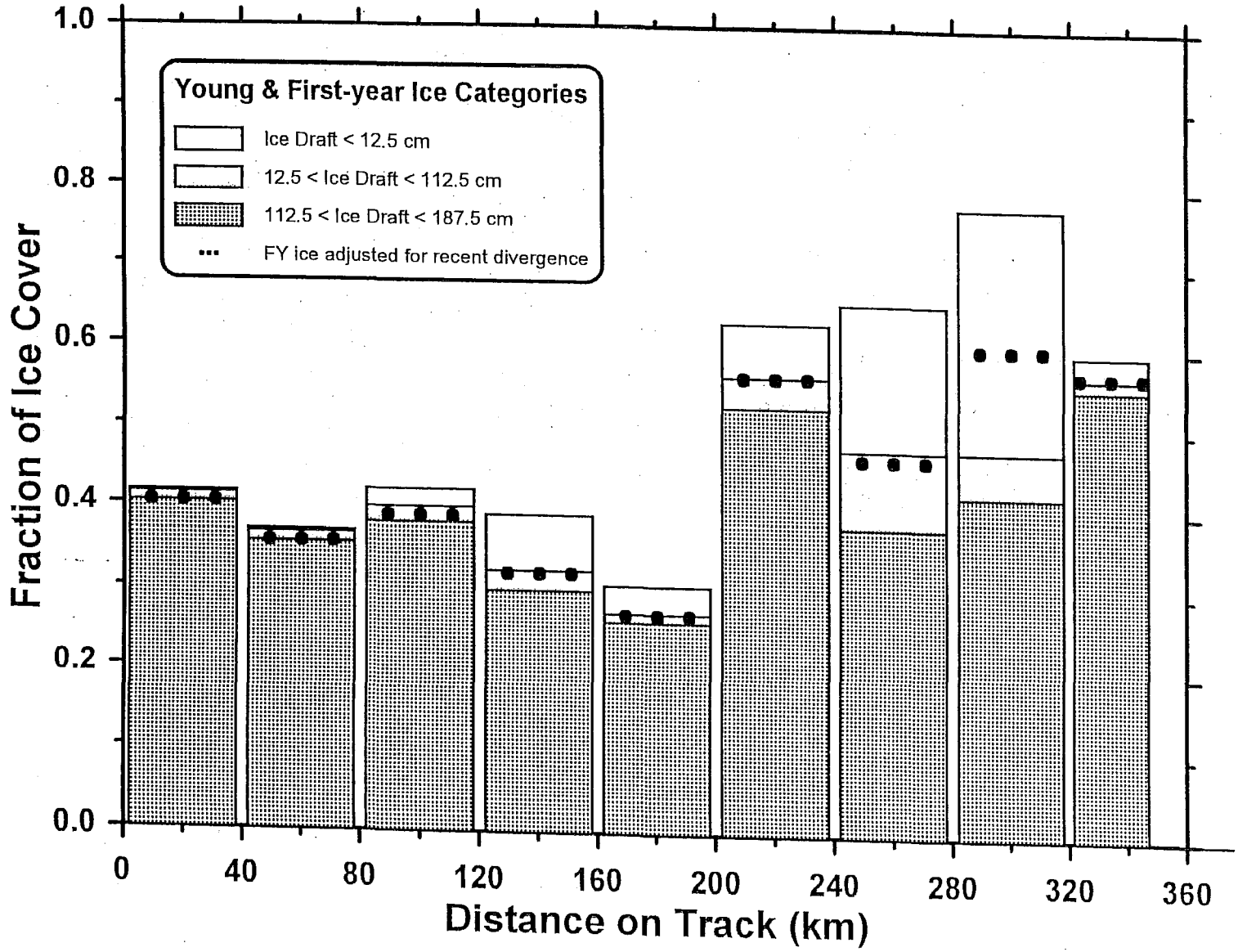

Figure 26: *Fractions of the survey path occupied by young and first-year ice categories. Histogram boxes are cumulative.*

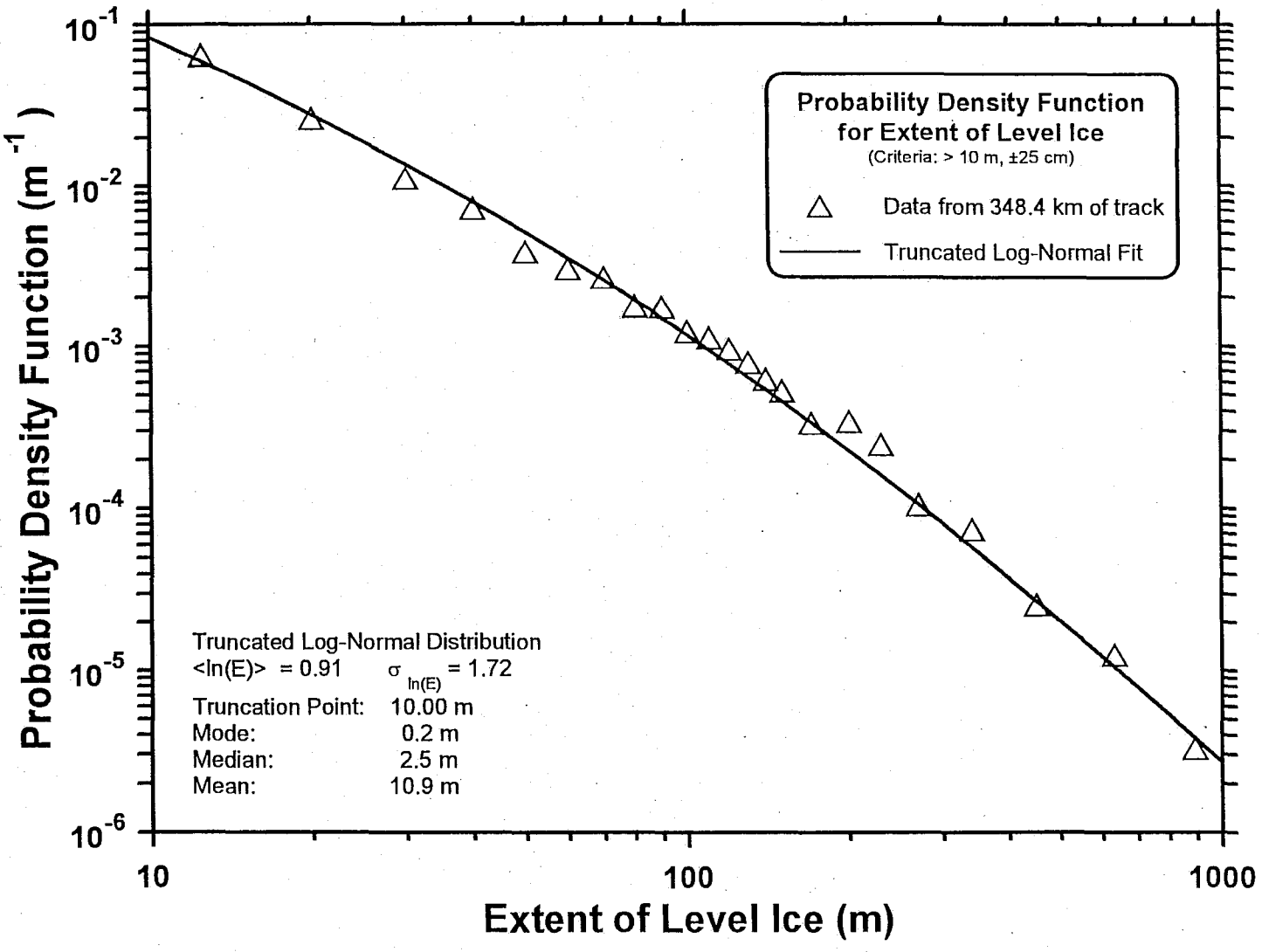

Figure 27: *Probability density function of the extent of sections of level ice which separate deformational features. Open leads are included. The curve is an empirical fit using a truncated lognormal probability function.*

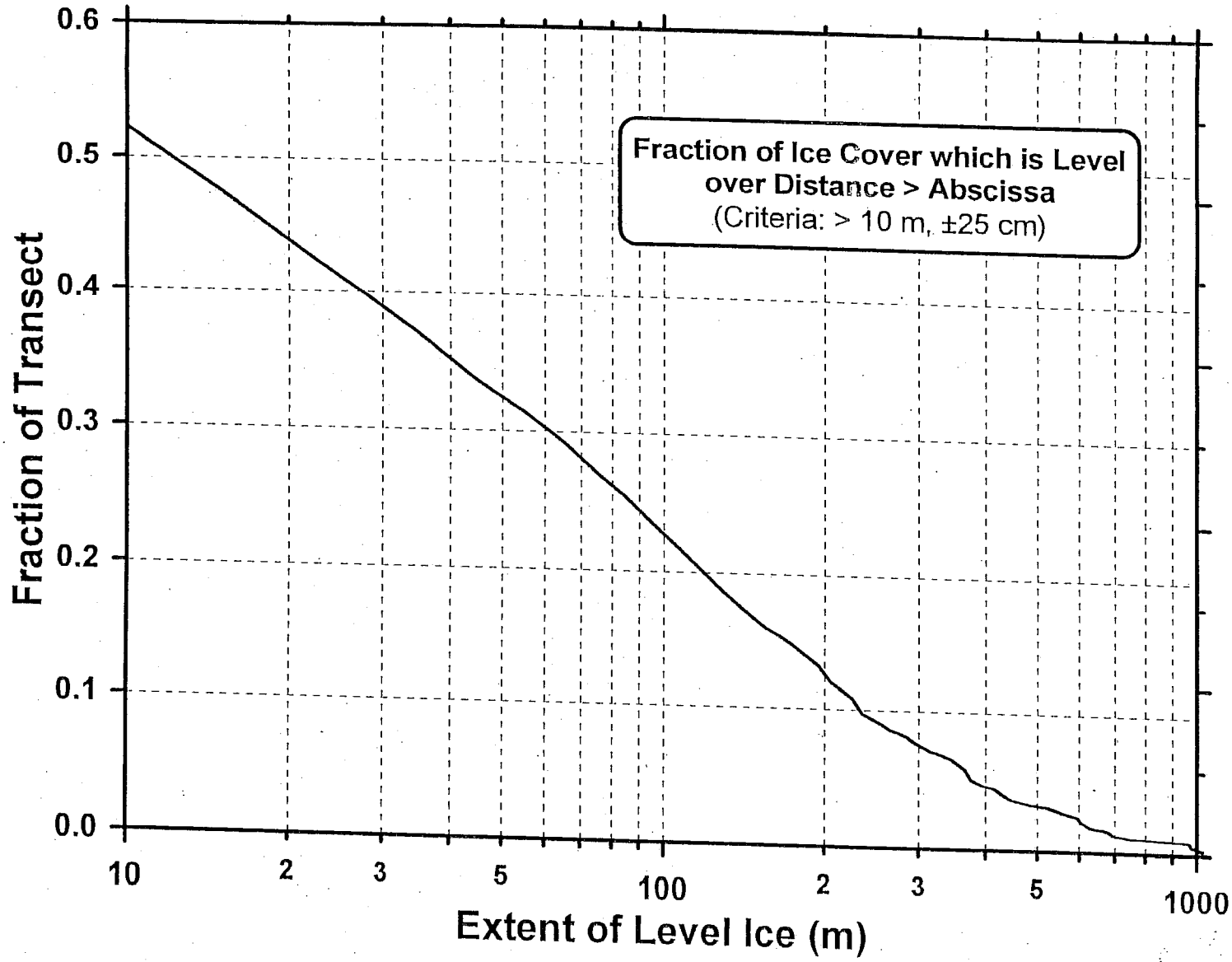

Figure 28: Fraction of the ice profiled at ISC90_2A which was level over distances equal to or greater than the abscissa. Open leads are included.

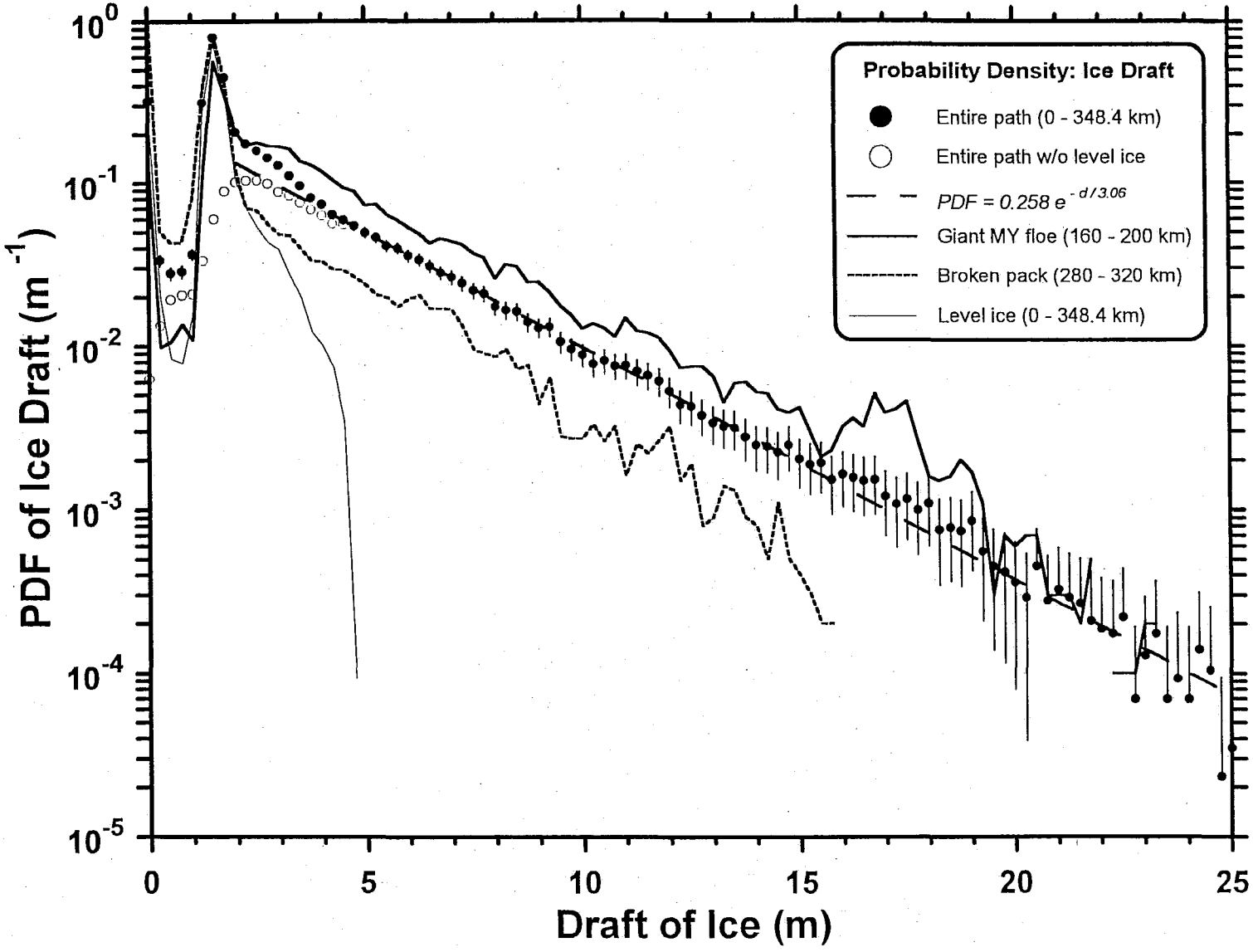

Figure 29: *Probability density functions of the draft of sea ice observed at ISC90_2A in April-May 1990, plotted on log-linear axes to display better the ridged component of the ice field.*

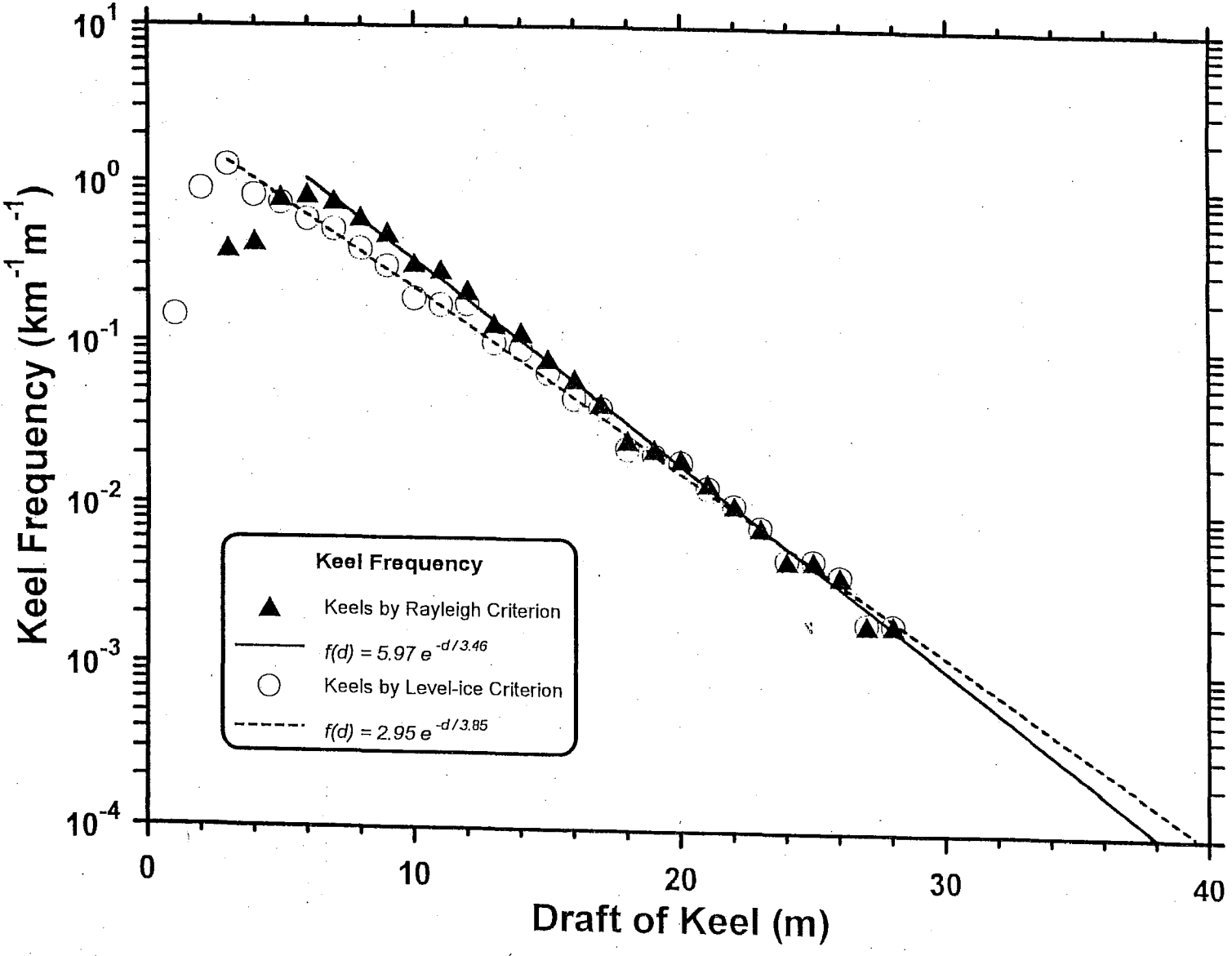

Figure 30: Frequency of ice keels derived using two selection criteria. Extrapolation of the fitted exponential curves permits estimation of the frequency of very deep keels.

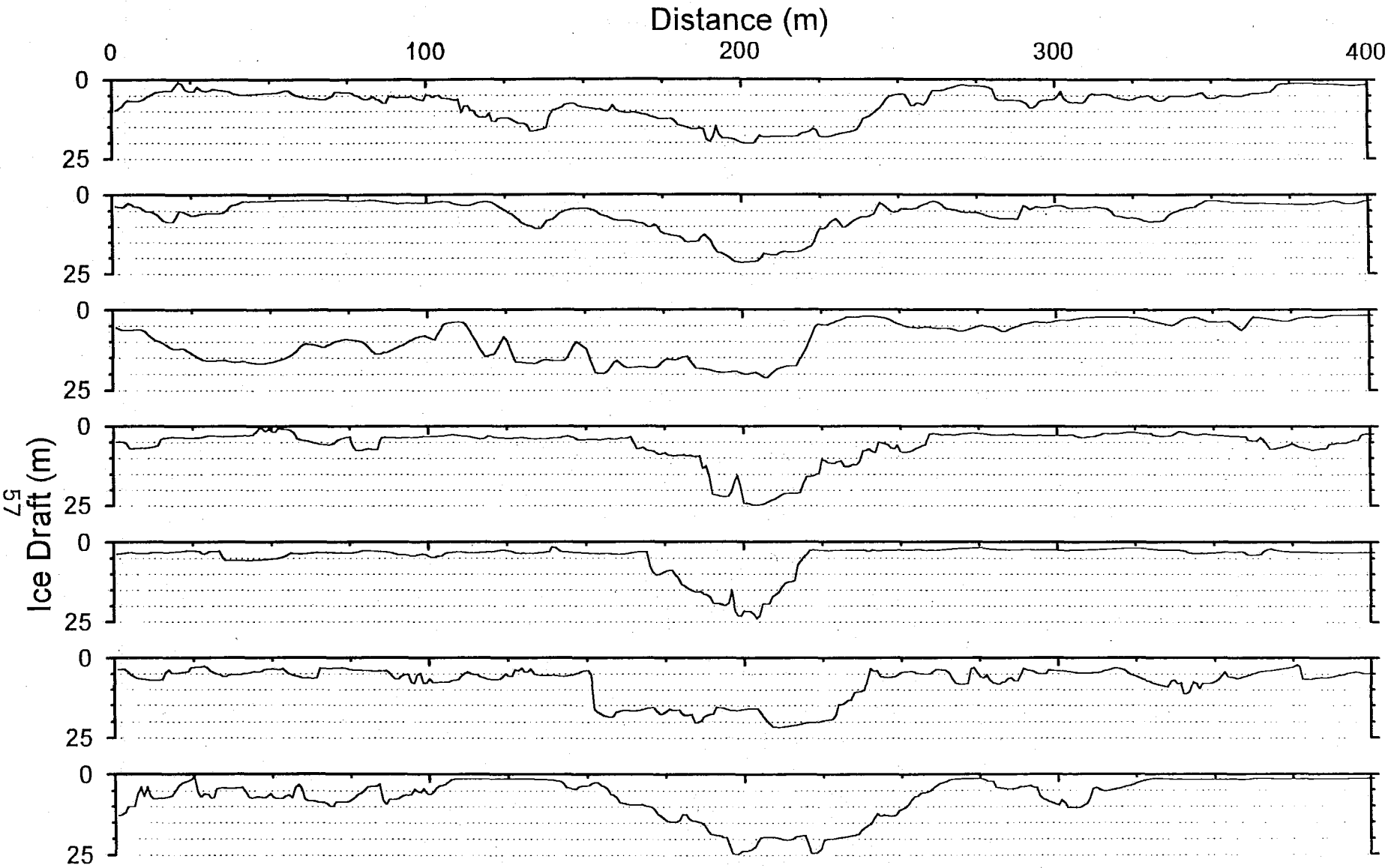

Figure 31: *Detailed cross-sections of the 21 keels observed to extend to a depth of 20 m or greater. Since the horizontal and vertical scales are equal, the features are displayed without distortion.*

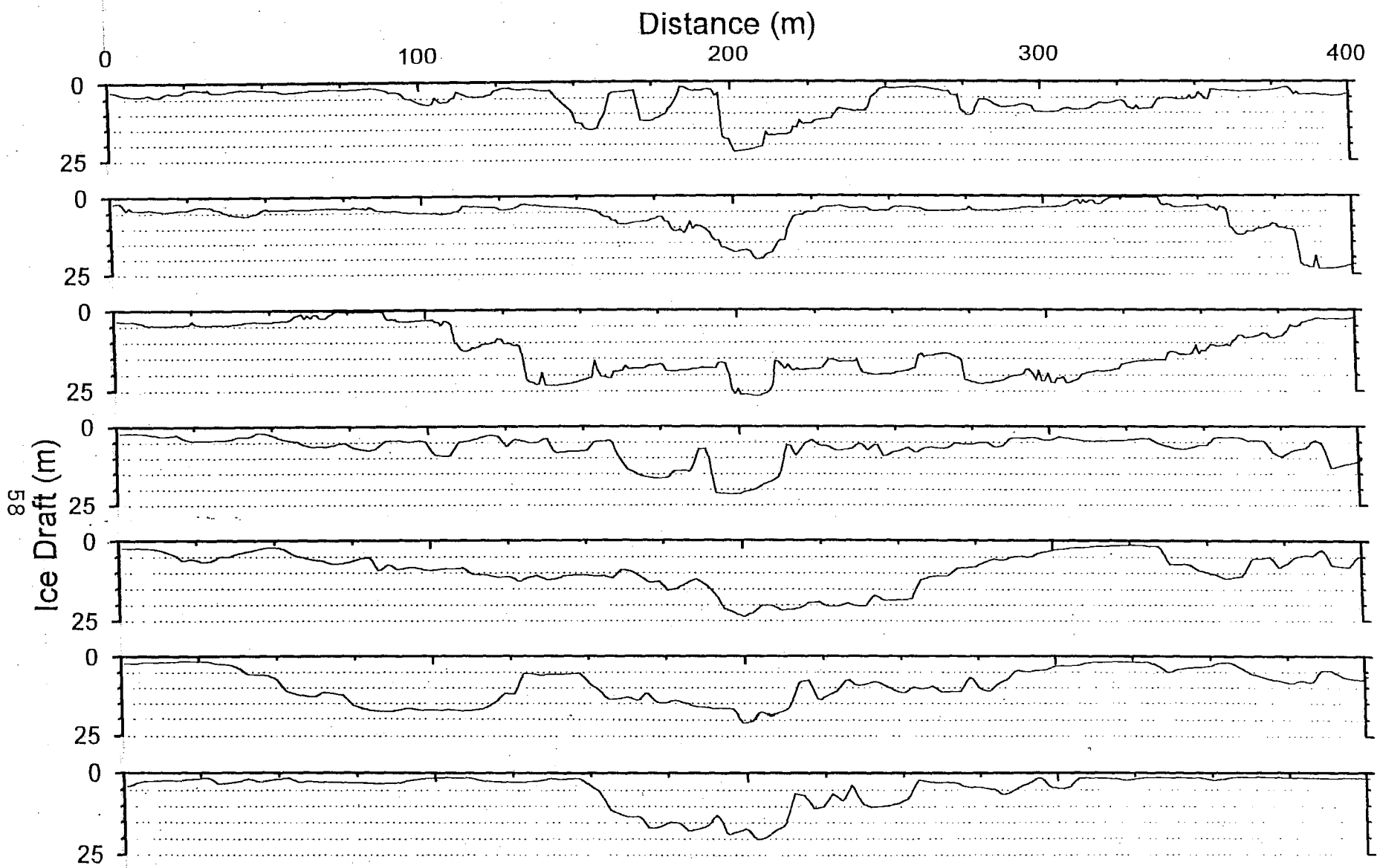

Figure 31 (continued): *Detailed cross-sections of keels displayed without distortion.*

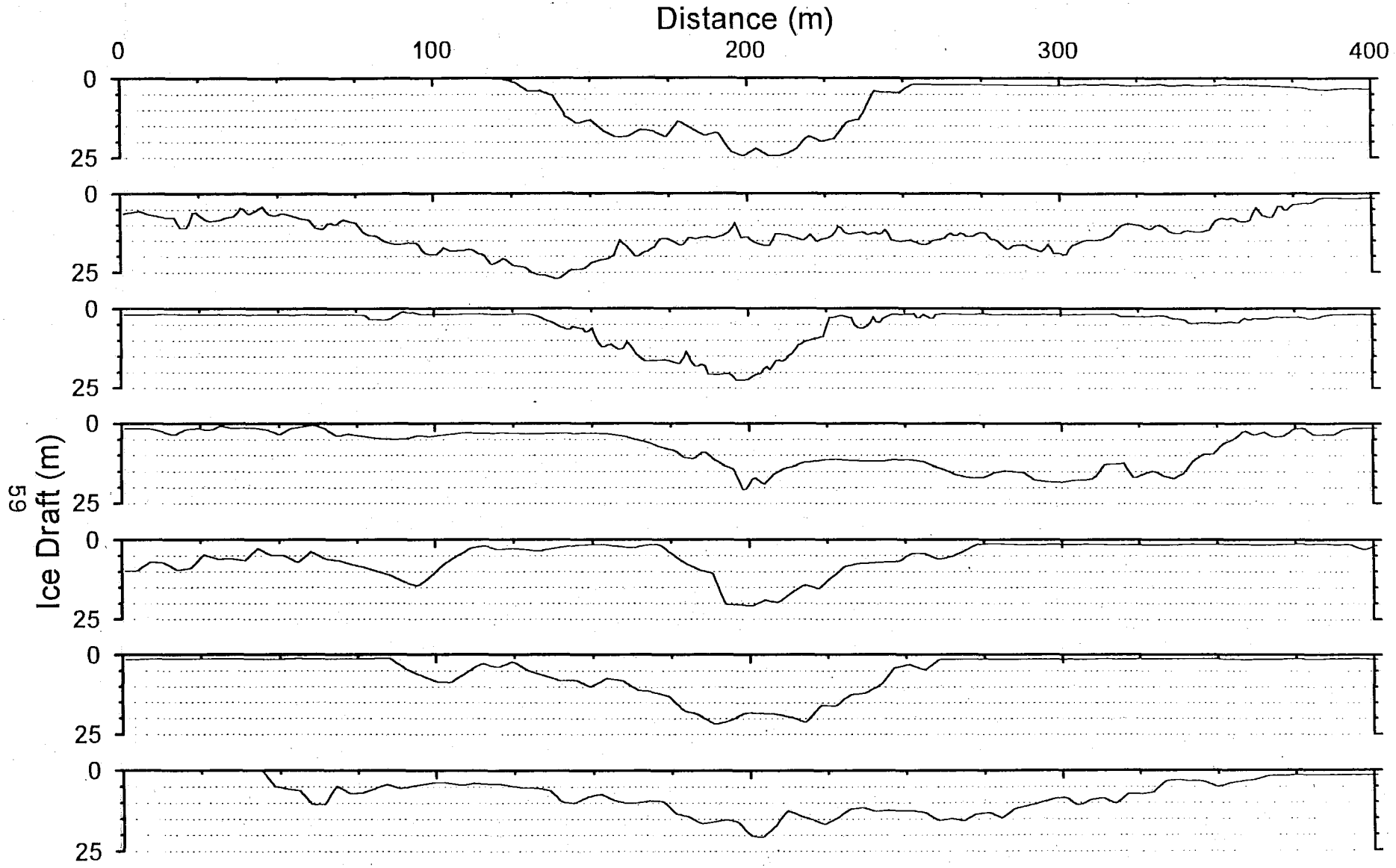

Figure 31 (continued): *Detailed cross-sections of keels displayed without distortion.*

References

BELLIVEAU, D.J., G.L. BUGDEN, B.M. EID and C.J. CALNAN (1990) Sea ice velocity measurements by upward-looking doppler current profilers. *Journal of Atmospheric and Oceanic Technology*, 7, 596-602.

BOURKE, R.H. and R.P. GARRETT (1987) Sea ice thickness distribution in the Arctic Ocean. *Cold Regions Science and Technology*, **13**, 259-280.

HUDSON, R.D. (1990) Annual measurement of sea-ice thickness using an upward-looking sonar. *Nature*, **344**, 135-137.

KOVACS, A., W.F. WEEKS, S. ACKLEY and W.D. HIBLER, III (1973) Structure of a multiyear pressure ridge. *Arctic* **26**(1), 22-31.

MAYKUT, G.A. and N. UNTERSTEINER (1971) Some results from a time-dependent thermodynamic model of sea ice. *Journal of Geophysical Research*, **76**, 1550-1575.

MELLING, H., P. JOHNSTON and W.R. GREEN (1992) *IPS3: Ice Profiling Sonar Model 3.* Unpublished user manual. Institute of Ocean Sciences, P.O Box 6000, Sidney, B.C. 52 pp. + appendices.

MELLING, H., D.R. TOPHAM and D. RIEDEL (1993) Topography of the upper and lower surfaces of 10 hectares of deformed sea ice. *Cold Regions Science and Technology,* **21**, 349-369.

PILKINGTON, G.R. and B.D. WRIGHT (1991) Beaufort Sea ice thickness measurements from an acoustic, under-ice, upward-looking ice keel profiler. *Proceedings of the First International Offshore and Polar Engineering Conference*, Edinburgh, U.K., 11-16 August 1991. pp. 456-461.

THORNDIKE, A.S., D.A. ROTHROCK, G.A. MAYKUT and R. COLONY (1975) The thickness distribution of sea ice. *Journal of Geophysical Research*, **80**, 4501-4513.

TUCKER, W.B. III, W.F. WEEKS and M. FRANK (1979) Sea ice ridging over the Alaskan continental shelf. *Journal of Geophysical Research*, **84**, 4885-4897.

VEITCH, B., M. LENSU, K. RISKA, P. KOSLOFF, P.KEILEY and P. KUJALA (1991) Field observations of ridges in the northern Baltic Sea. *Proceedings, 11th International Conference on Port and Ocean Engineering under Arctic Conditions*, St John's, Canada, 24-28 September 1991. pp 381-400.

WILLIAMS, E., C. SWITHINBANK AND G. DE Q. ROBIN (1975) A submarine sonar study of arctic pack ice. *Journal of Glaciology*, **15**, 349-362.

Appendix: Continuous Record of Sea Ice Draft

The topographic profiles of the underside of sea ice which are depicted on the following pages were acquired at Site ISC90_2A between 4 April and 31 May 1990.

The vertical scale of the plots is exaggerated by a factor of 27.

A trace approximating the elevation of the ice surface is plotted for artistic effect only, and has no physical reality. The elevation has been set equal to 1/5 of the draft.

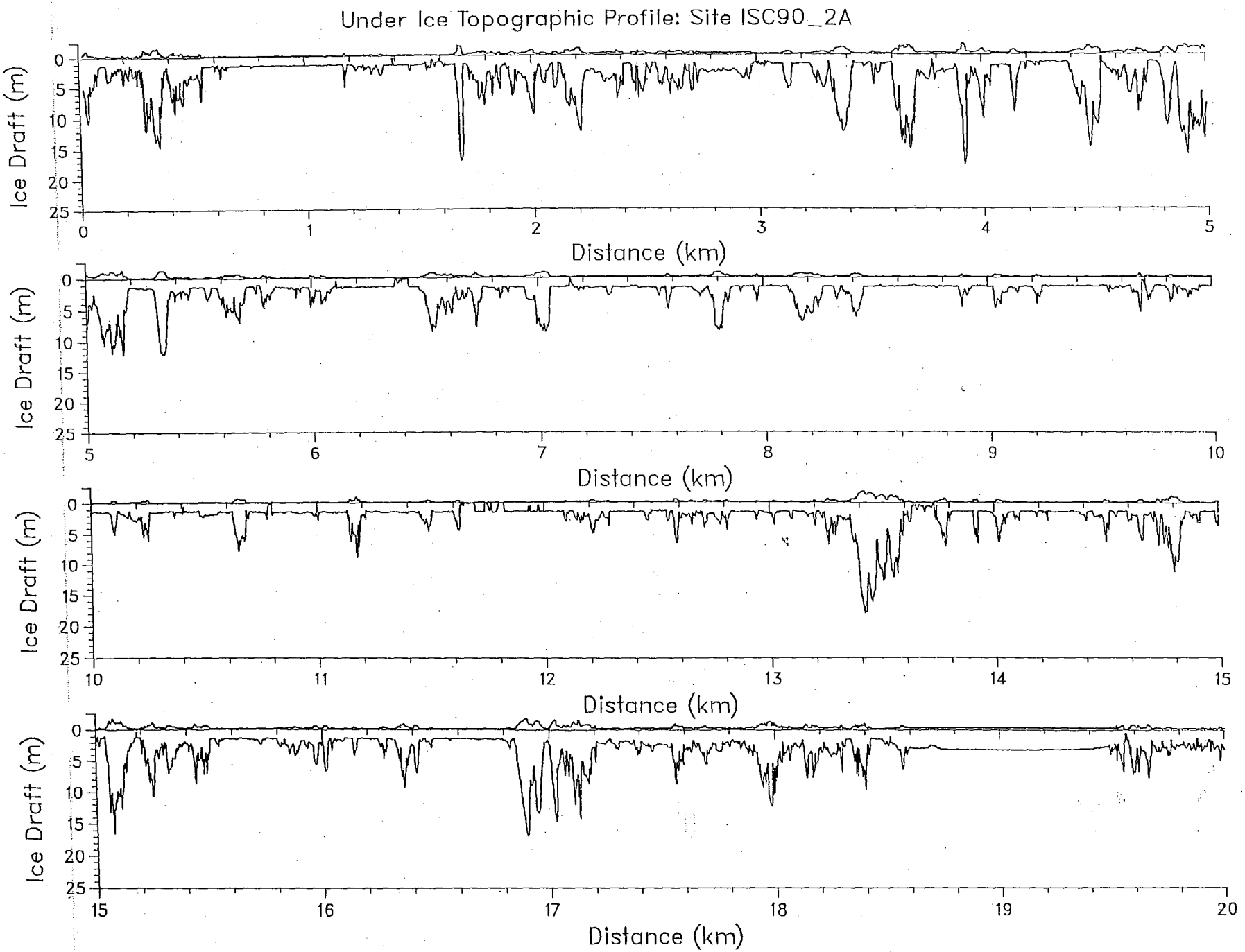
Under Ice Topographic Profile: Site ISC90_2A
Ice Draft (m)
0
5
10
15
20
25
0
1
2
3
4
5
Distance (km)
Ice Draft (m)
5
6
7
8
9
10
Distance (km)
Ice Draft (m)
10
11
12
13
14
15
Distance (km)
Ice Draft (m)
15
16
17
18
19
20
Distance (km)

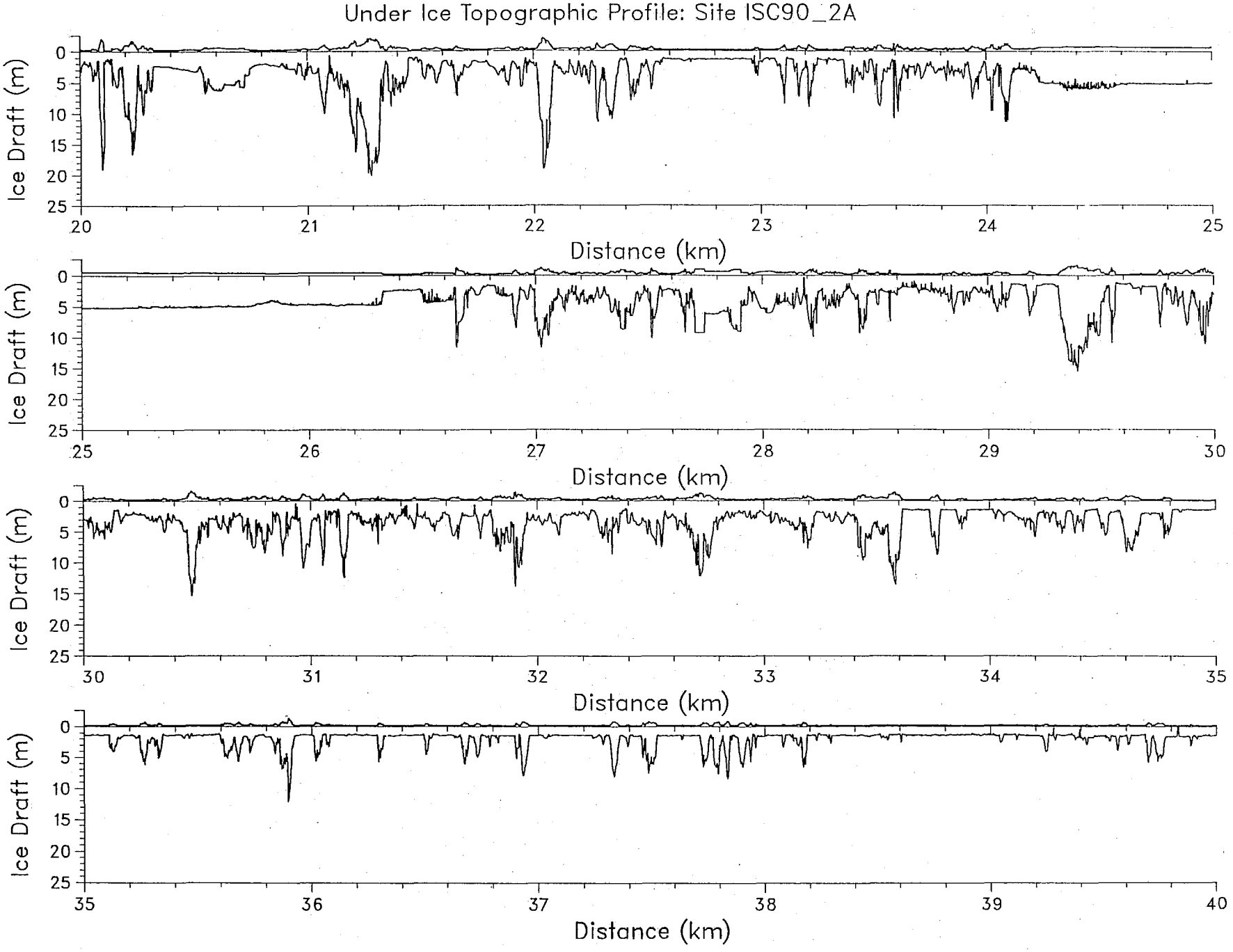
Under Ice Topographic Profile: Site ISC90_2A
Ice Draft (m)
0
5
10
15
20
25
20
21
22
23
24
25
Distance (km)
Ice Draft (m)
25
26
27
28
29
30
Distance (km)
Ice Draft (m)
30
31
32
33
34
35
Distance (km)
Ice Draft (m)
35
36
37
38
39
40
Distance (km)

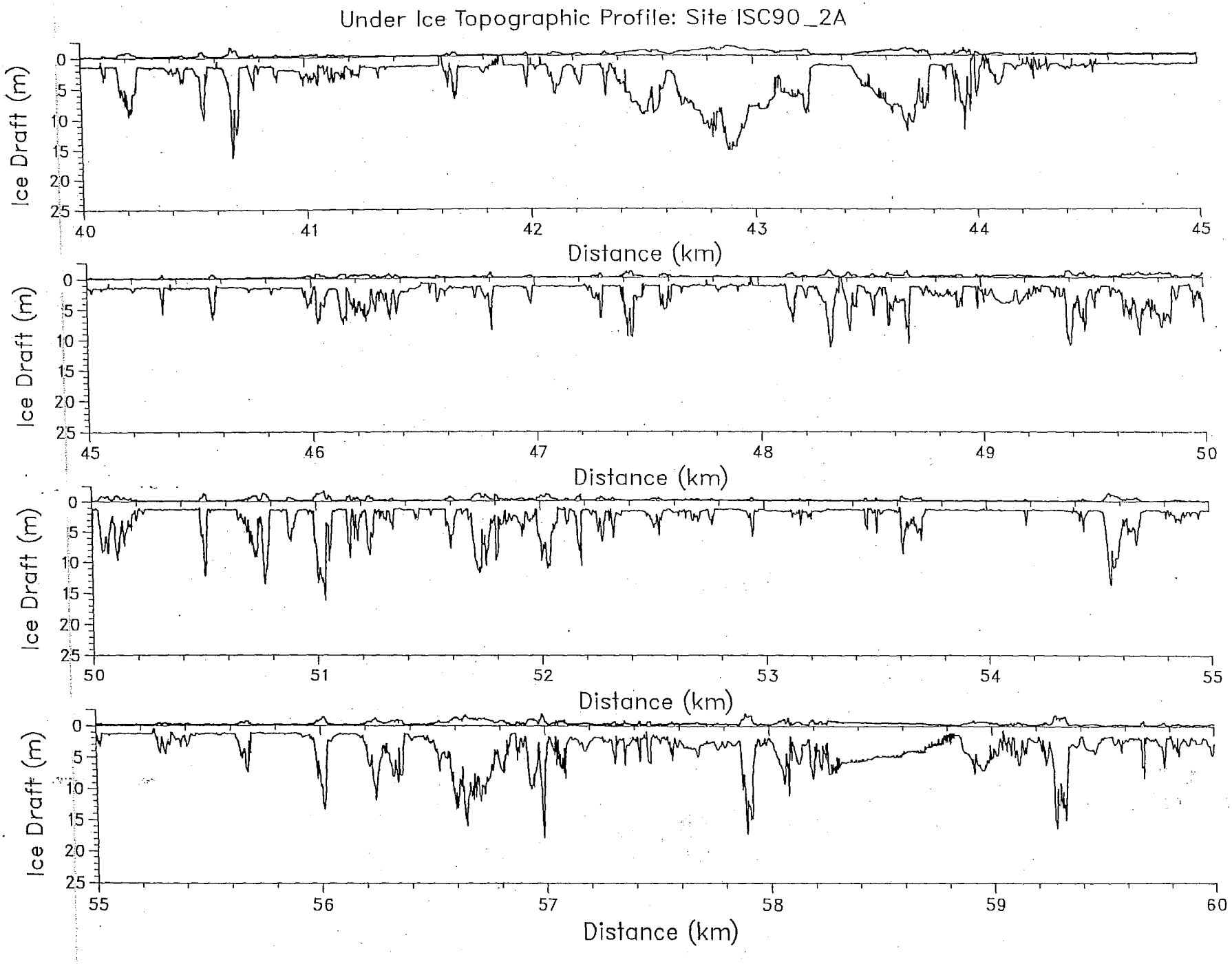
Under Ice Topographic Profile: Site ISC90_2A
Ice Draft (m)
0
5
10
15
20
25
40
41
42
43
44
45
Distance (km)
Ice Draft (m)
45
46
47
48
49
50
Distance (km)
Ice Draft (m)
50
51
52
53
54
55
Distance (km)
Ice Draft (m)
55
56
57
58
59
60
Distance (km)

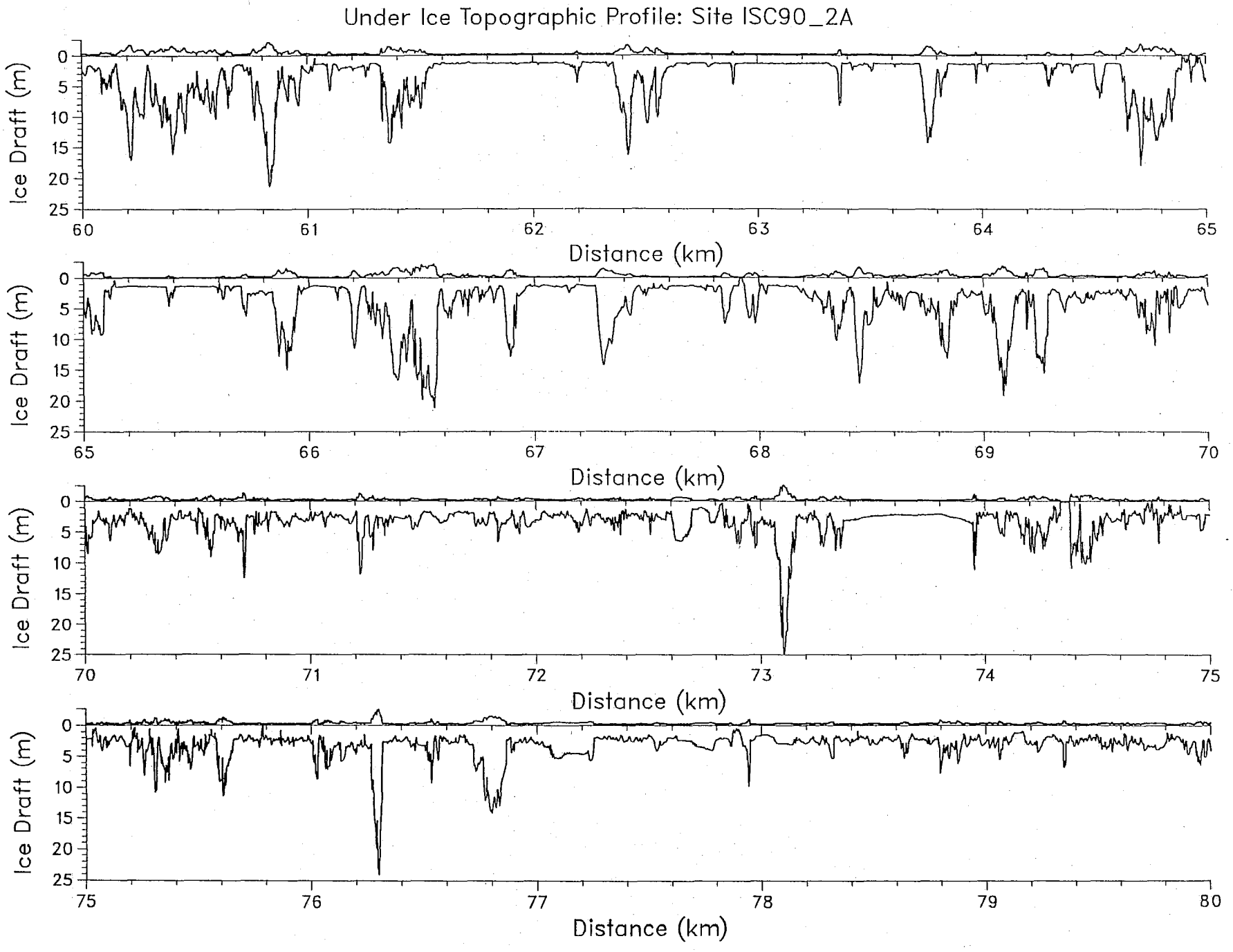
Under Ice Topographic Profile: Site ISC90_2A
Ice Draft (m)
0
5
10
15
20
25
60
61
62
63
64
65
Distance (km)
Ice Draft (m)
65
66
67
68
69
70
Distance (km)
Ice Draft (m)
70
71
72
73
74
75
Distance (km)
Ice Draft (m)
75
76
77
78
79
80
Distance (km)

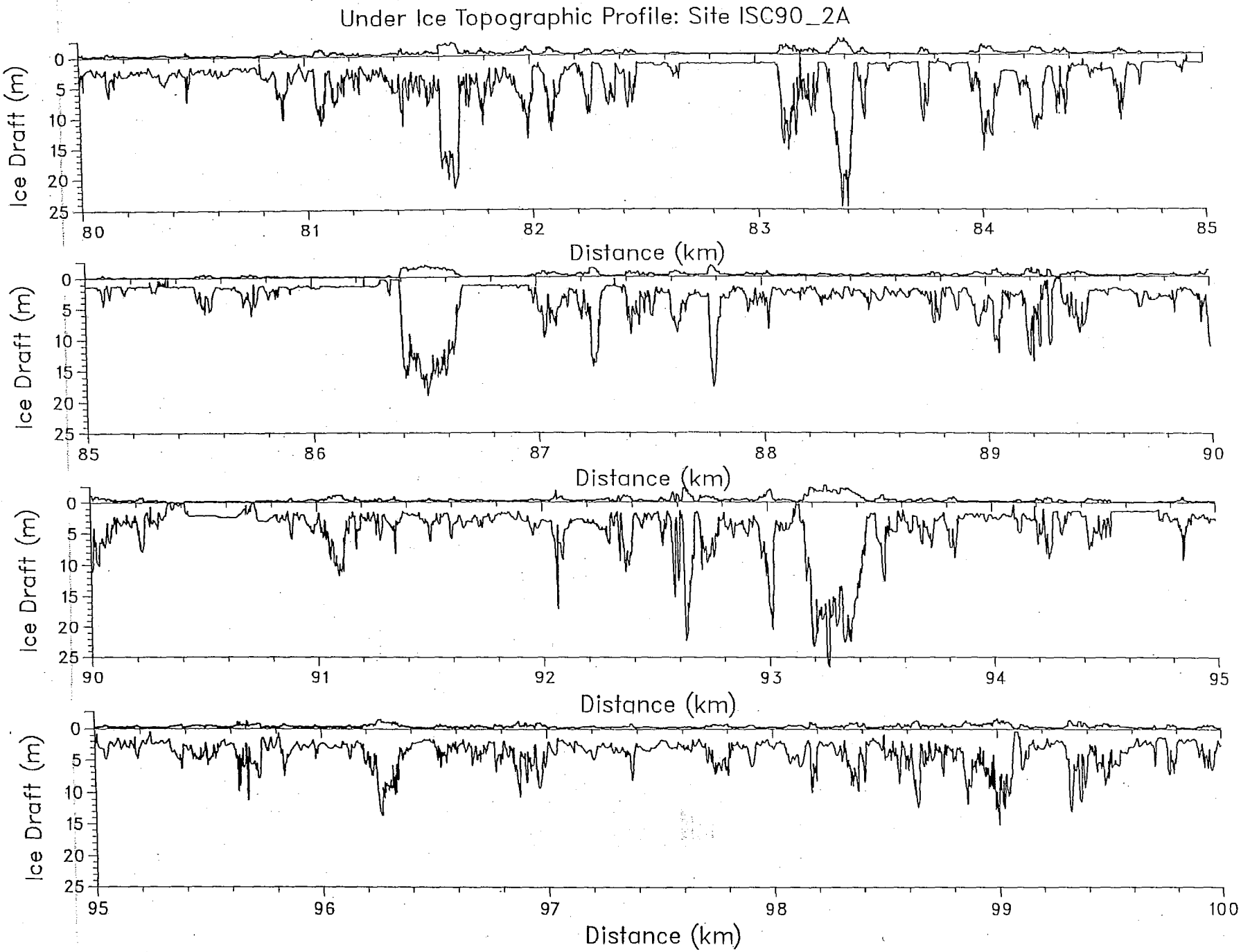
Under Ice Topographic Profile: Site ISC90_2A
Ice Draft (m)
0
5
10
15
20
25
80
81
82
83
84
85
Distance (km)
Ice Draft (m)
85
86
87
88
89
90
Distance (km)
Ice Draft (m)
90
91
92
93
94
95
Distance (km)
Ice Draft (m)
95
96
97
98
99
100
Distance (km)

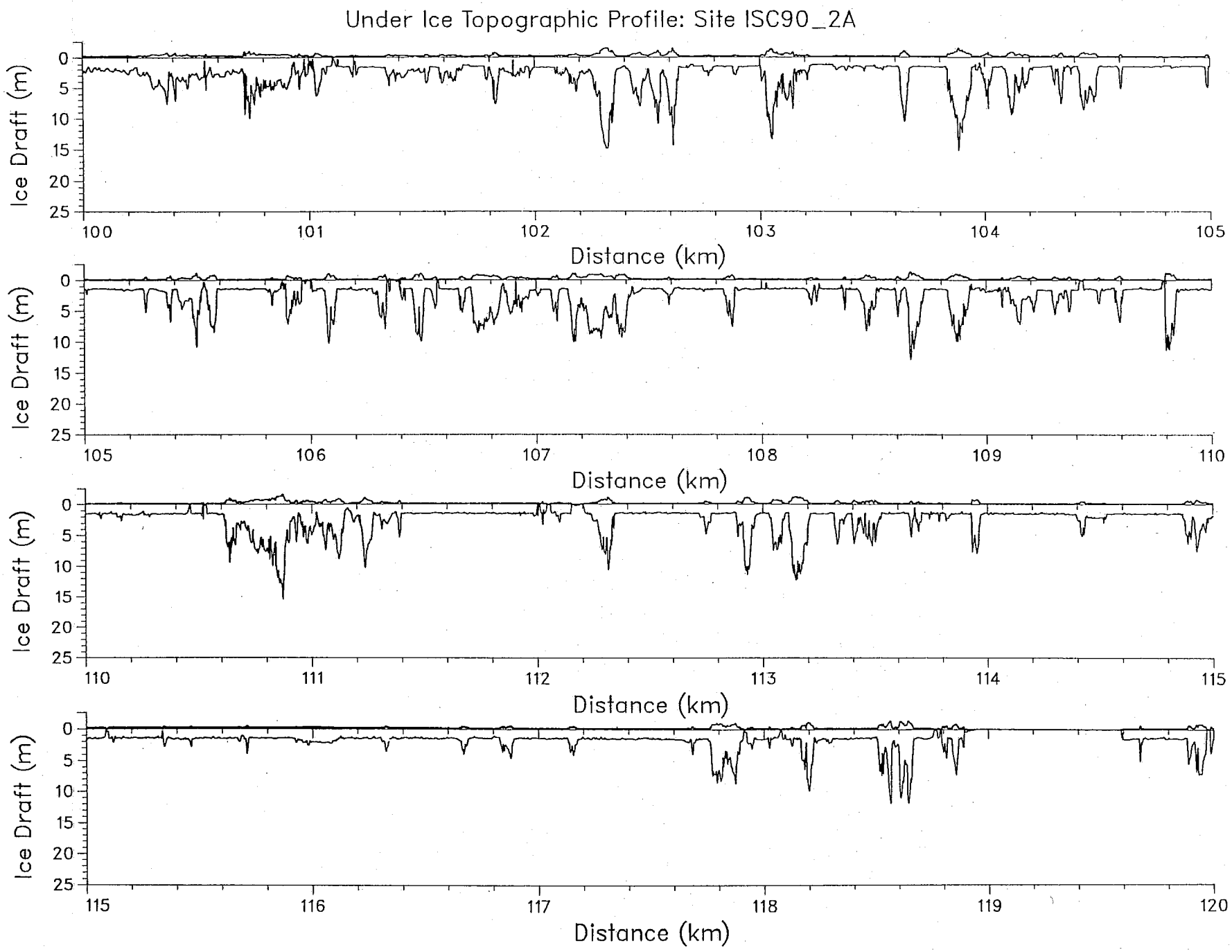
Under Ice Topographic Profile: Site ISC90_2A
Ice Draft (m)
0
5
10
15
20
25
100
101
102
103
104
105
Distance (km)
Ice Draft (m)
105
106
107
108
109
110
Distance (km)
Ice Draft (m)
110
111
112
113
114
115
Distance (km)
Ice Draft (m)
115
116
117
118
119
120
Distance (km)

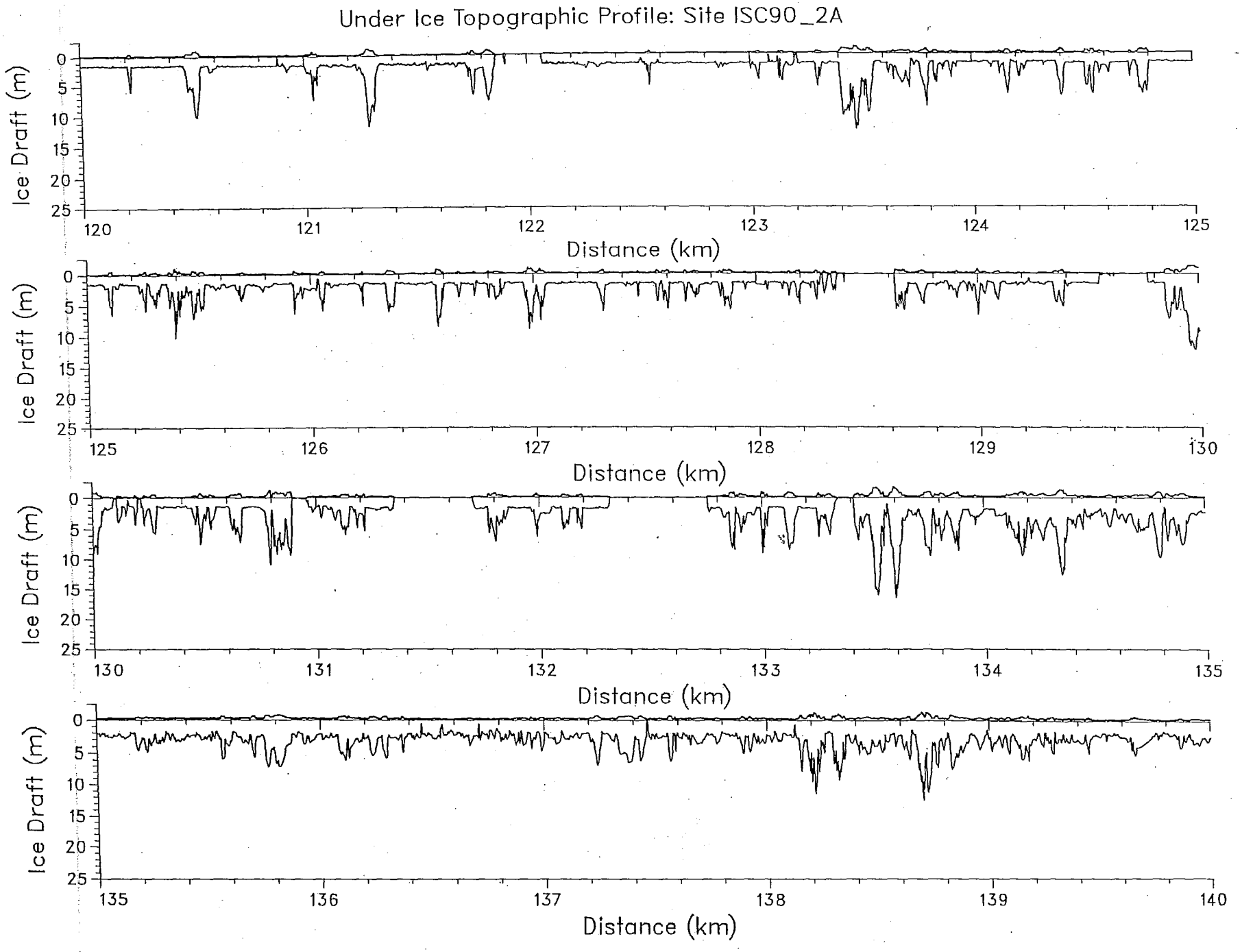
Under Ice Topographic Profile: Site ISC90_2A
Ice Draft (m)
0
5
10
15
20
25
120
121
122
123
124
125
Distance (km)
Ice Draft (m)
125
126
127
128
129
130
Distance (km)
Ice Draft (m)
130
131
132
133
134
135
Distance (km)
Ice Draft (m)
135
136
137
138
139
140
Distance (km)

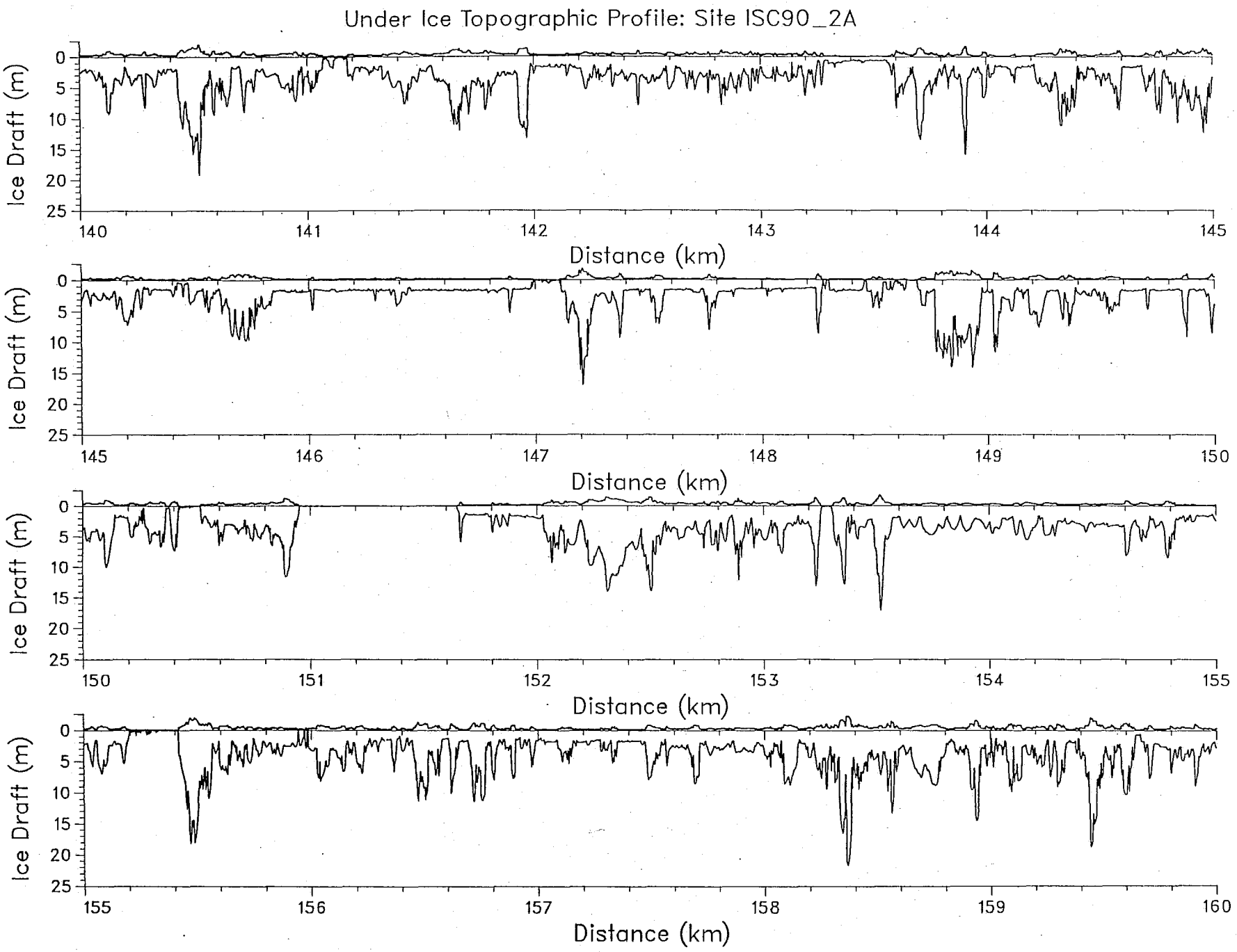
Under Ice Topographic Profile: Site ISC90_2A
Ice Draft (m)
0
5
10
15
20
25
140
141
142
143
144
145
Distance (km)
145
146
147
148
149
150
150
151
152
153
154
155
155
156
157
158
159
160

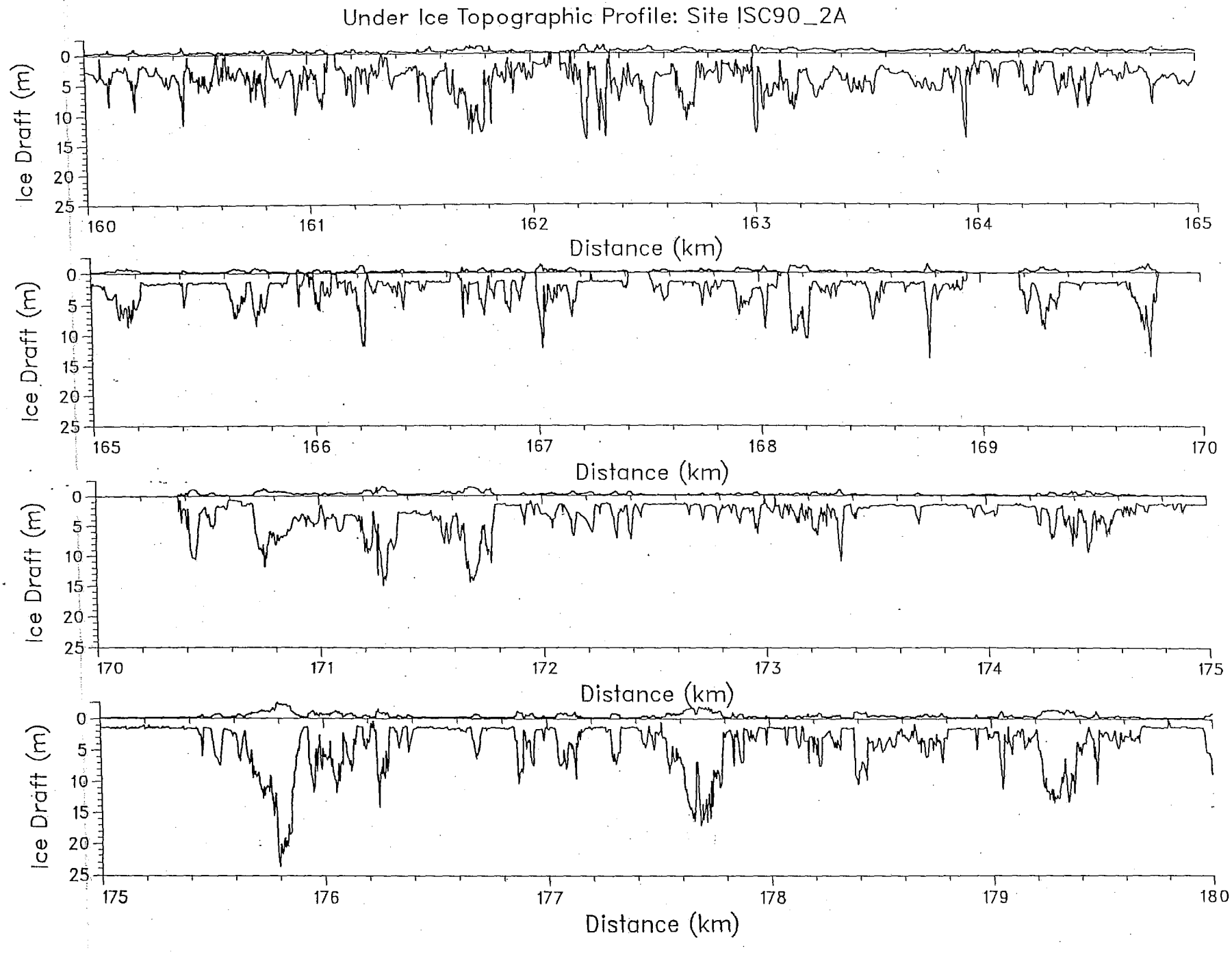
Under Ice Topographic Profile: Site ISC90_2A
Ice Draft (m)
0
5
10
15
20
25
160
161
162
163
164
165
Distance (km)
Ice Draft (m)
165
166
167
168
169
170
Distance (km)
Ice Draft (m)
170
171
172
173
174
175
Distance (km)
Ice Draft (m)
175
176
177
178
179
180
Distance (km)

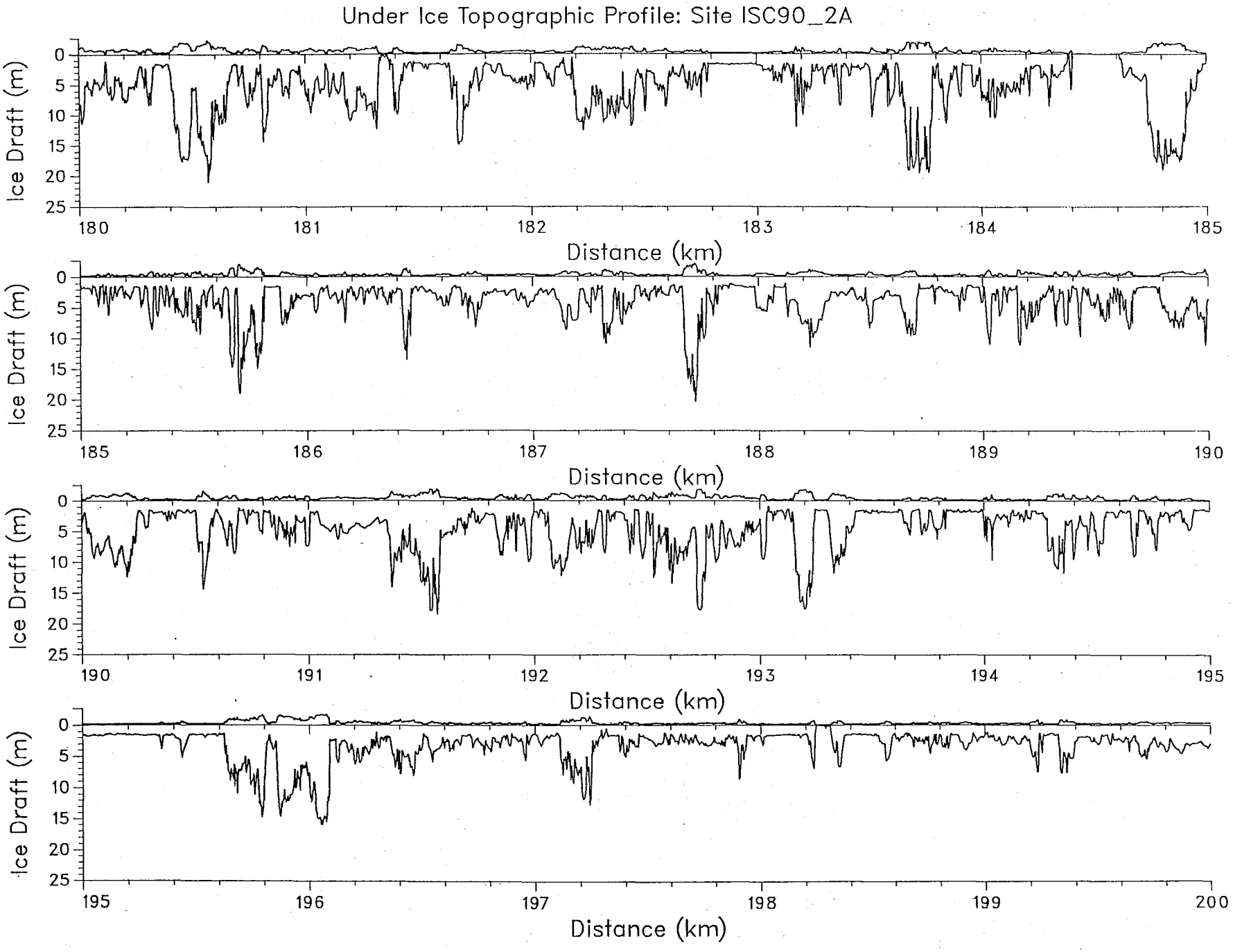
Under Ice Topographic Profile: Site ISC90_2A
Ice Draft (m)
0
5
10
15
20
25
180
181
182
183
184
185
Distance (km)
Ice Draft (m)
185
186
187
188
189
190
Distance (km)
Ice Draft (m)
190
191
192
193
194
195
Distance (km)
Ice Draft (m)
195
196
197
198
199
200
Distance (km)

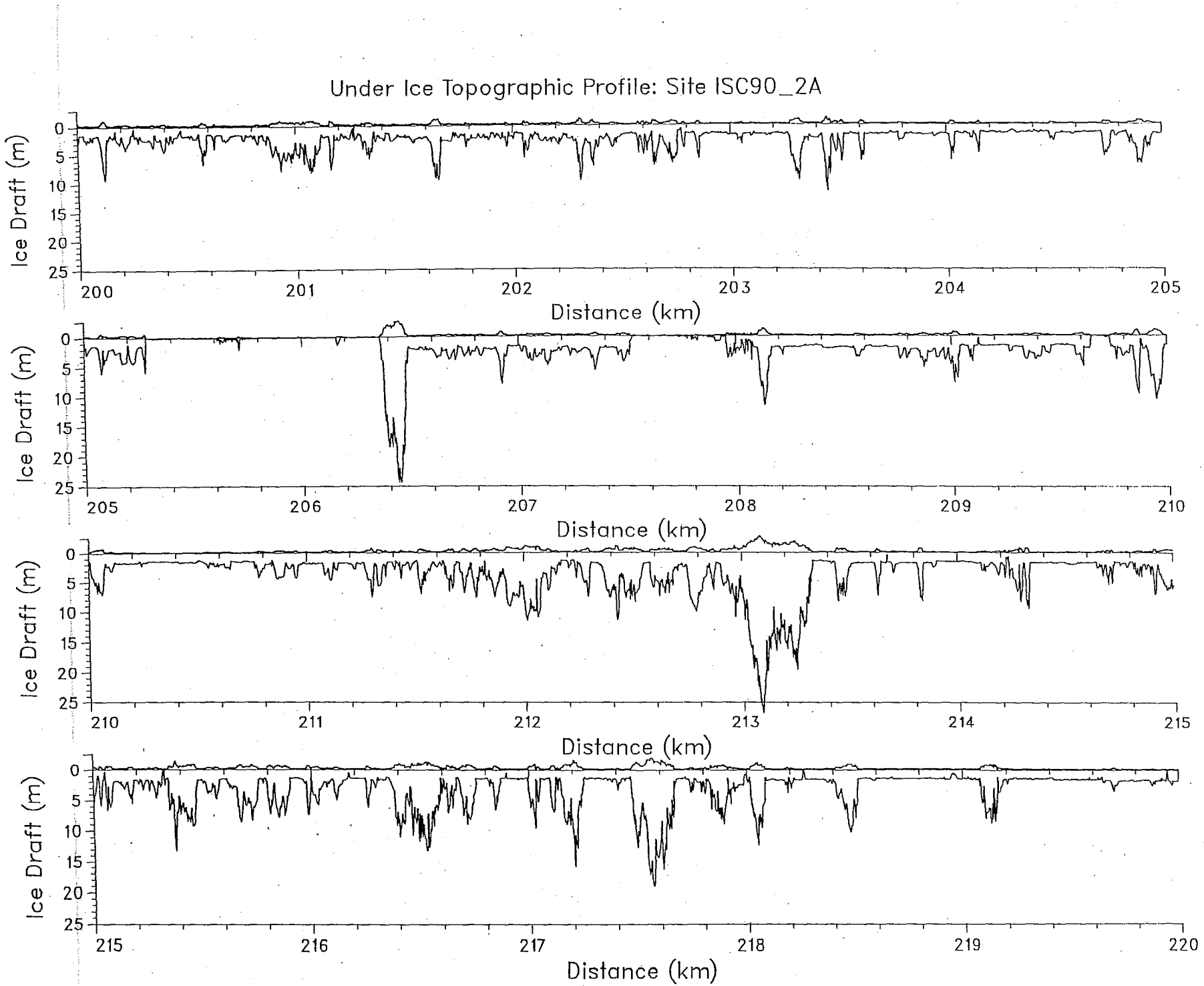
Under Ice Topographic Profile: Site ISC90_2A
Ice Draft (m)
0
5
10
15
20
25
200
201
202
203
204
205
Distance (km)
Ice Draft (m)
205
206
207
208
209
210
Distance (km)
Ice Draft (m)
210
211
212
213
214
215
Distance (km)
Ice Draft (m)
215
216
217
218
219
220
Distance (km)

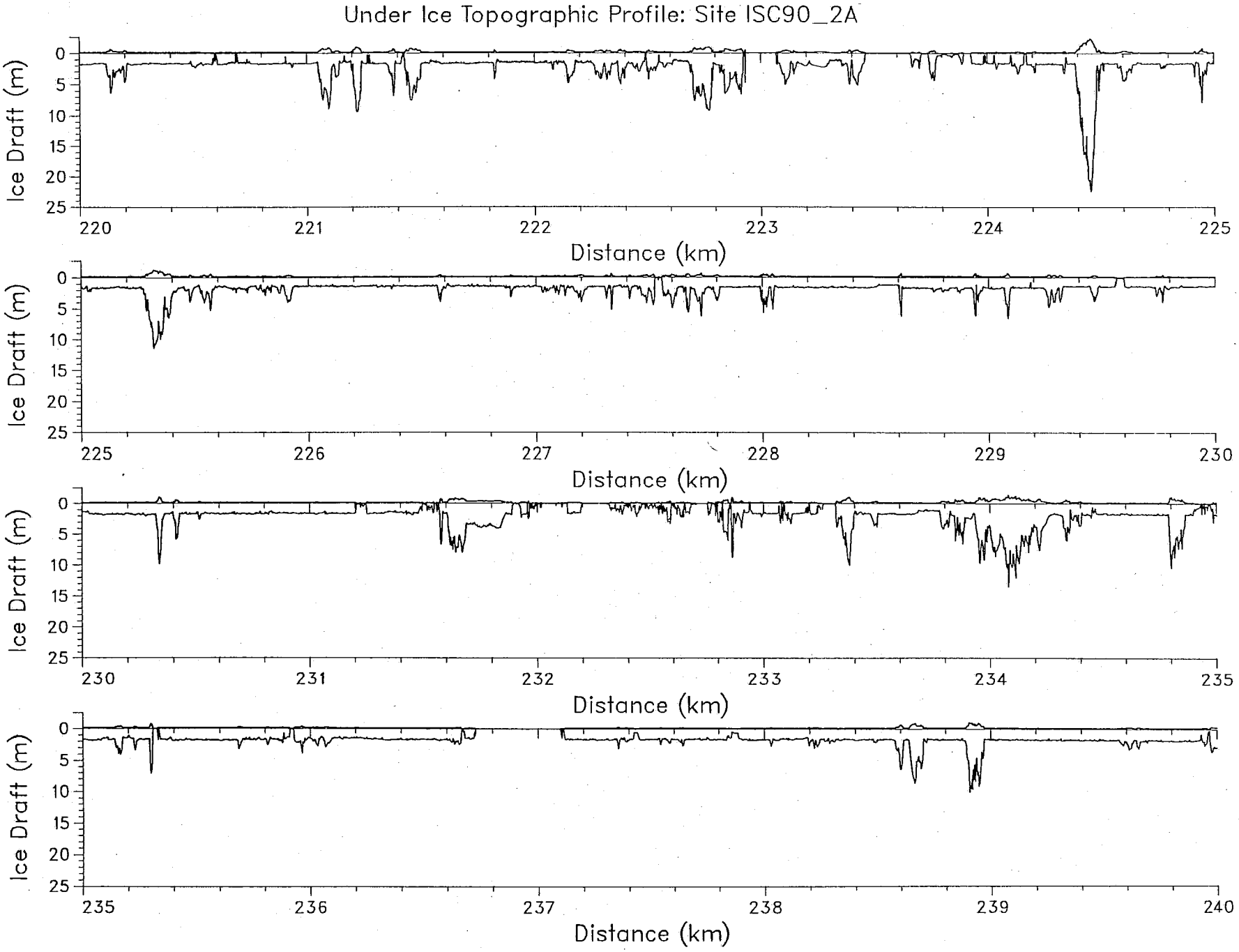
Under Ice Topographic Profile: Site ISC90_2A
Ice Draft (m)
0
5
10
15
20
25
220
221
222
223
224
225
Distance (km)
Ice Draft (m)
225
226
227
228
229
230
Distance (km)
Ice Draft (m)
230
231
232
233
234
235
Distance (km)
Ice Draft (m)
235
236
237
238
239
240
Distance (km)

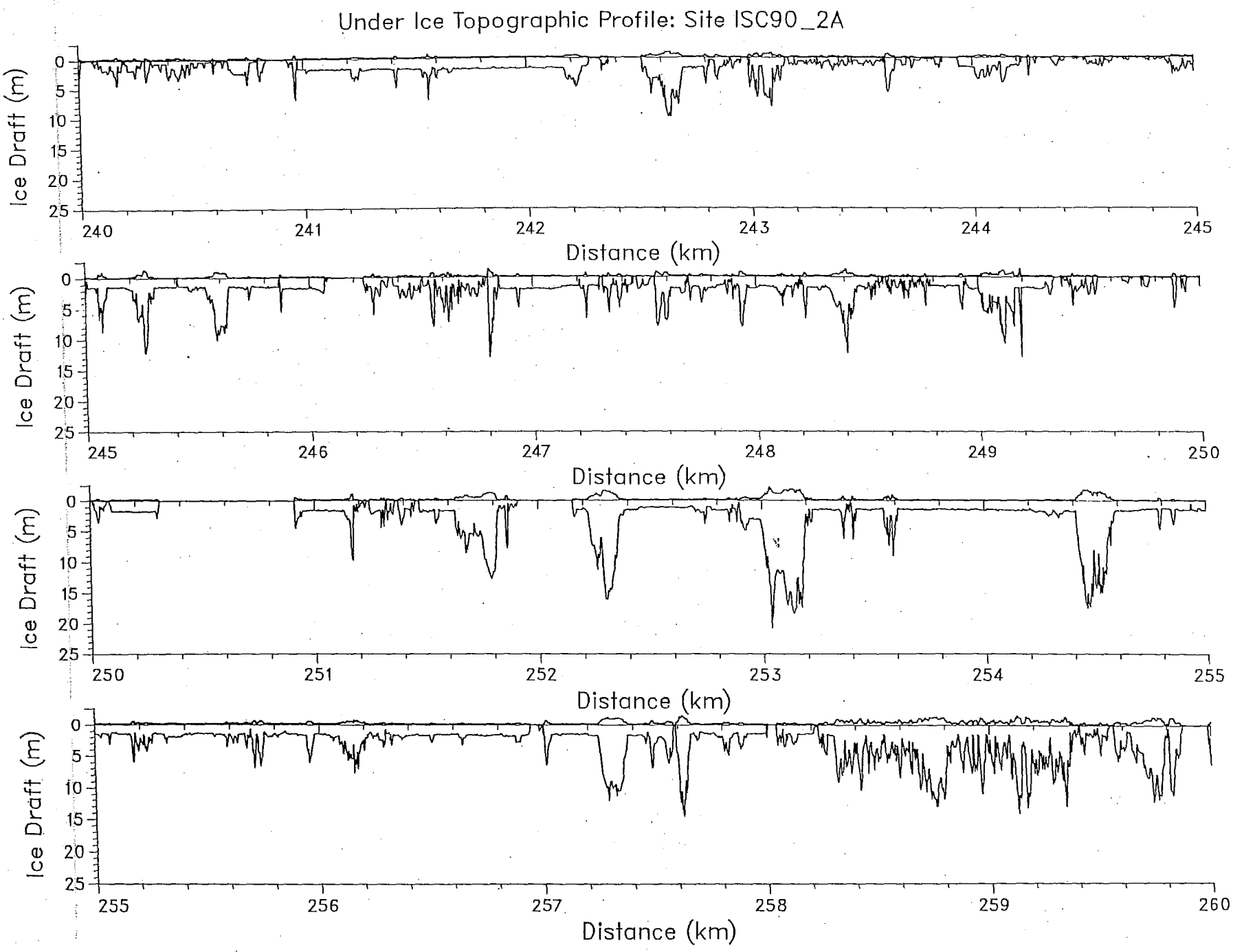
Under Ice Topographic Profile: Site ISC90_2A
Ice Draft (m)
0
5
10
15
20
25
240
241
242
243
244
245
Distance (km)
Ice Draft (m)
245
246
247
248
249
250
Distance (km)
Ice Draft (m)
250
251
252
253
254
255
Distance (km)
Ice Draft (m)
255
256
257
258
259
260
Distance (km)

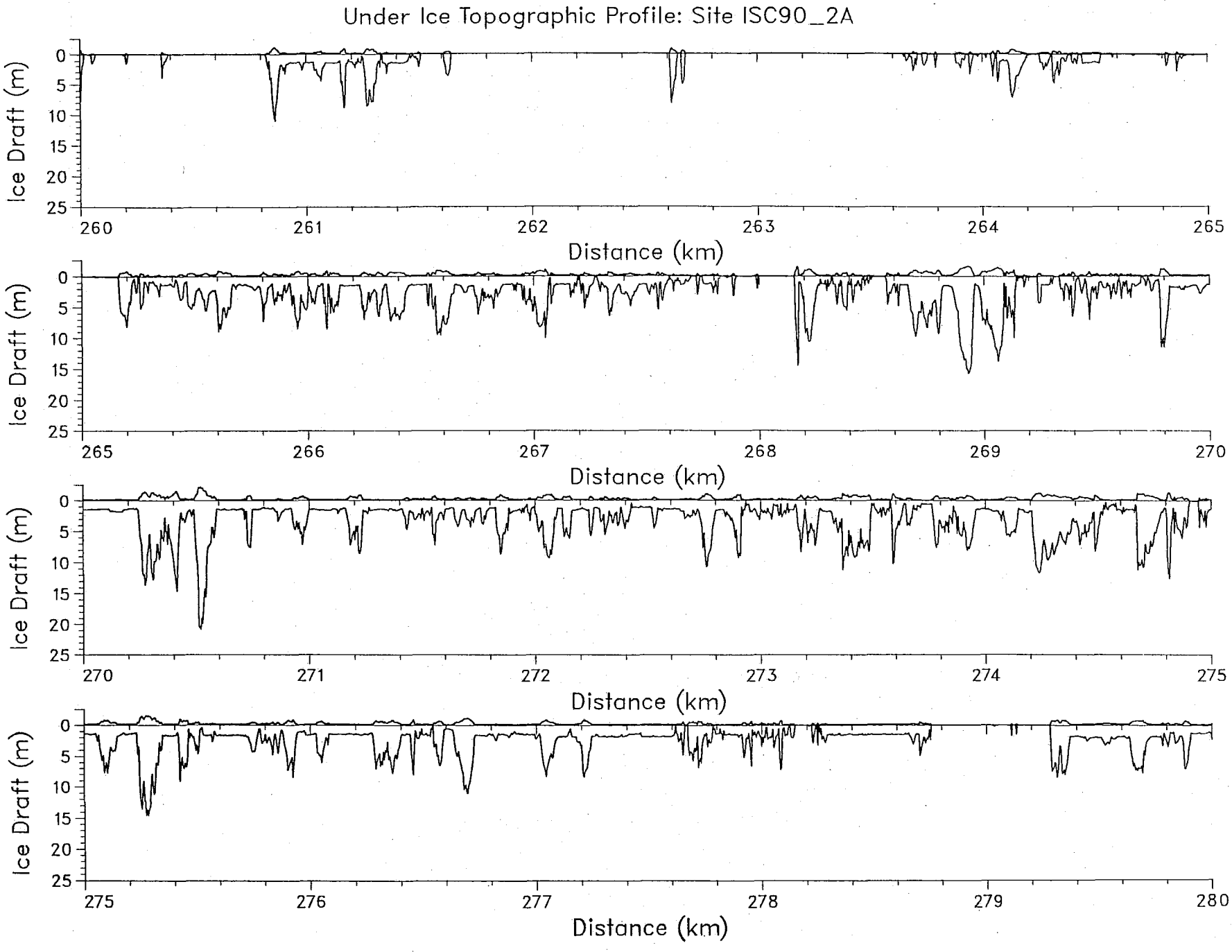
Under Ice Topographic Profile: Site ISC90_2A
Ice Draft (m)
0
5
10
15
20
25
260
261
262
263
264
265
Distance (km)
Ice Draft (m)
265
266
267
268
269
270
Distance (km)
Ice Draft (m)
270
271
272
273
274
275
Distance (km)
Ice Draft (m)
275
276
277
278
279
280
Distance (km)

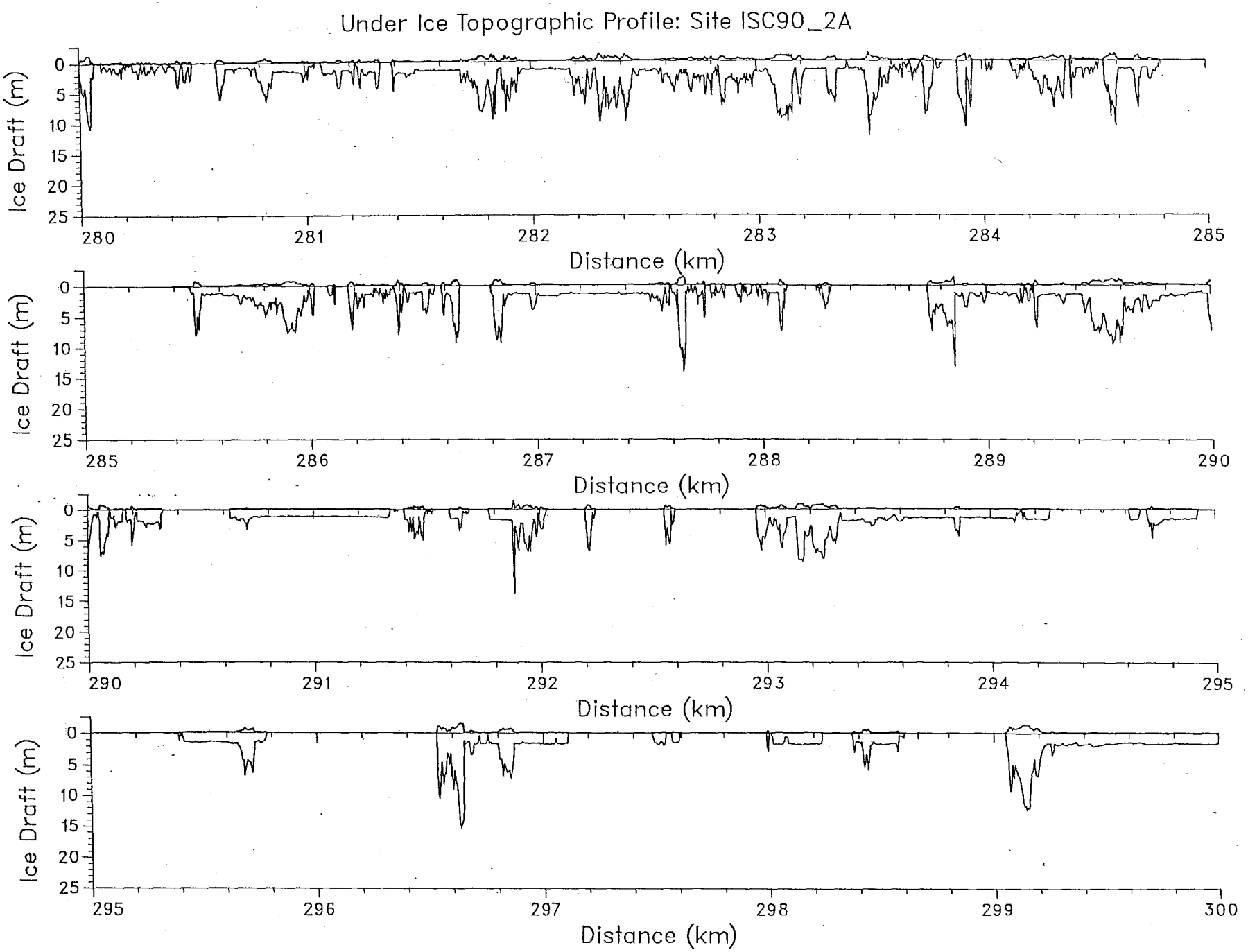
Under Ice Topographic Profile: Site ISC90_2A
Ice Draft (m)
0
5
10
15
20
25
280
281
282
283
284
285
Distance (km)
Ice Draft (m)
285
286
287
288
289
290
Distance (km)
Ice Draft (m)
290
291
292
293
294
295
Distance (km)
Ice Draft (m)
295
296
297
298
299
300
Distance (km)

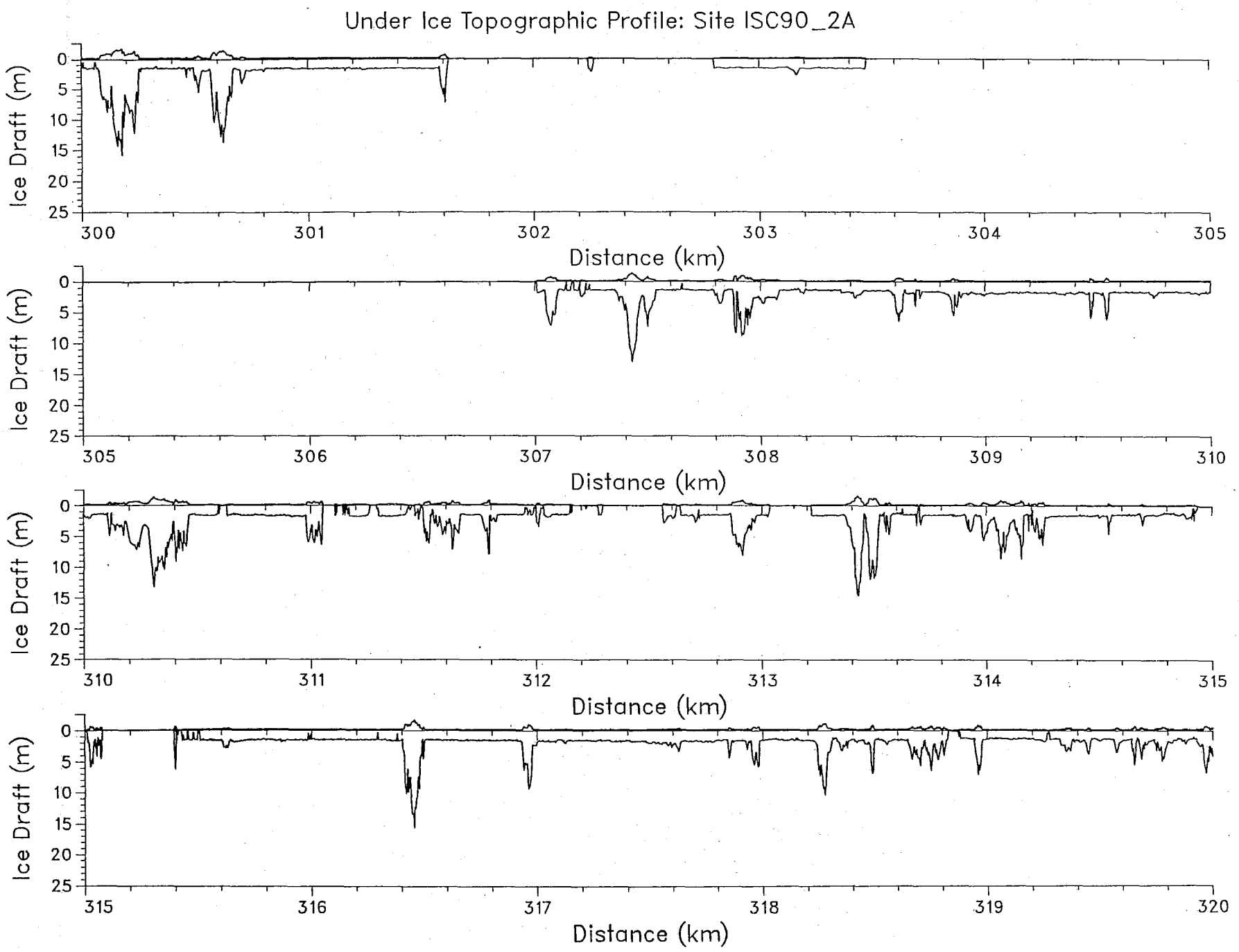
Under Ice Topographic Profile: Site ISC90_2A
Ice Draft (m)
0
5
10
15
20
25
300
301
302
303
304
305
Distance (km)
Ice Draft (m)
305
306
307
308
309
310
Distance (km)
Ice Draft (m)
310
311
312
313
314
315
Distance (km)
Ice Draft (m)
315
316
317
318
319
320
Distance (km)

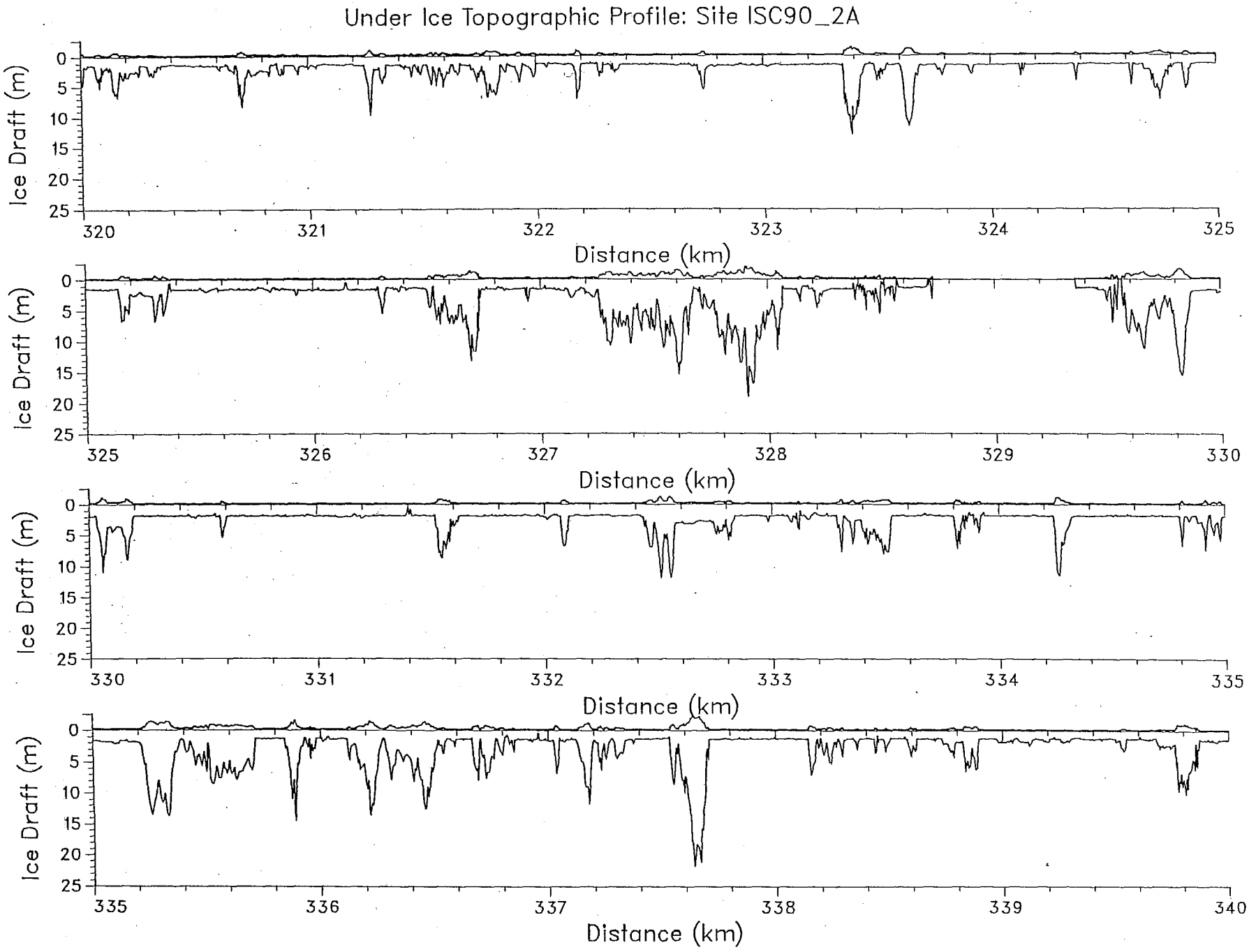
Under Ice Topographic Profile: Site ISC90_2A
Ice Draft (m)
0
5
10
15
20
25
320
321
322
323
324
325
Distance (km)
Ice Draft (m)
325
326
327
328
329
330
Distance (km)
Ice Draft (m)
330
331
332
333
334
335
Distance (km)
Ice Draft (m)
335
336
337
338
339
340
Distance (km)

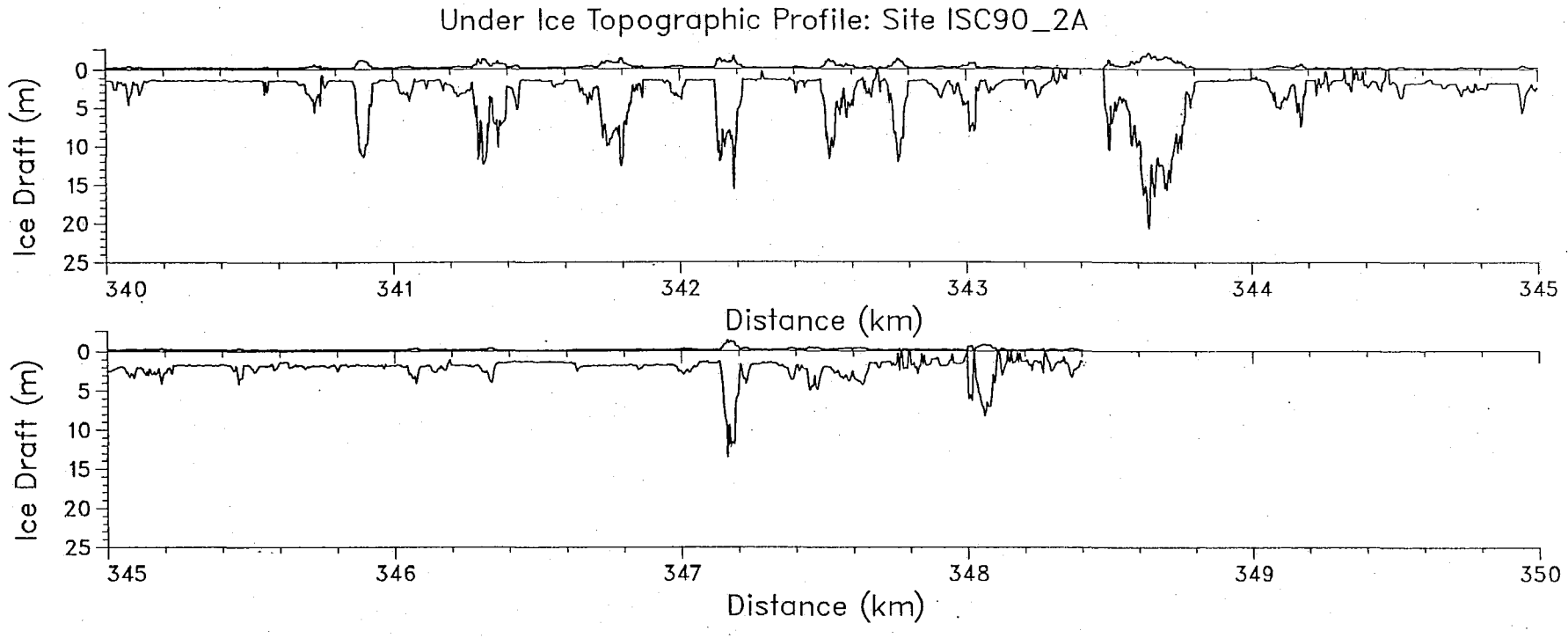
Under Ice Topographic Profile: Site ISC90_2A
Ice Draft (m)
0
5
10
15
20
25
340
341
342
343
344
345
Distance (km)
Ice Draft (m)
0
5
10
15
20
25
345
346
347
348
349
350
Distance (km)